THE UNIVERSITY OF MICHIGAN
COLLEGE OF ENGINEERING
Department of Nuclear Engineering

Technical Report

THE ABSORPTION OF MICROWAVE RADIATION
IN A SLIGHTLY-IONIZED GAS

L. H. Wald

ORA Project 07599

This report was also a dissertation submitted in
partial fulfillment of the requirements for the de-
gree of Doctor of Philosophy in The University of
Michigan, 1966.

ACKNOWLEDGMENTS

TABLE OF CONTENTS

LIST OF ILLUSTRATIONS

ABSTRACT

The purpose of this investigation was to study the absorption of microwave radiation in a slightly ionized gas as a function of electron density. Motivation was provided by the lack of interpretable microwave absorption data in the literature for the frequency range $.2 \leq \omega_p^2/\omega^2 \leq .8$ and the existence of three significantly different equations -- the Maxwell-Lorentz absorption equation, the classic Milne transport equation, and the Klevans-Osborn transport equation -- which have been used to predict microwave absorption in the above-mentioned frequency range.

The microwave absorption data was provided by measurement of the absorption produced in a collimated 12 GHz microwave beam passing along the axis of a pyrex cylinder containing ionized helium. The helium was ionized by an RF electric field of 7.1 mc frequency. Absorption data was taken for variations in electron density over the range $.2 \leq \omega_p^2/\omega^2 \leq .6$ and for variations in helium pressure over the range $.1 \leq p(\text{mm Hg}) \leq 17$. Data were taken from both afterglow and steady-state ionized gases and electron temperatures were taken

coincidently with the steady-state absorption data by
use of heated bi-polar Langmuir probes.

The absorption was found to be due partially
to refractive-defocussing effects, but it was possible to
measure and thus correct for these effects by use of a
combination of the steady-state and afterglow absorption
data. The corrected absorption data obtained were used
in each of the three absorption equations mentioned above
to calculate collision frequencies which were then cor-
rected for electron temperature changes and displayed
as functions of both electron density and helium pres-
sure. Only collision frequencies from one absorption equa-
tion -- those obtained from the Klevans-Osborn absorption
equation -- were found to be independent of electron
density to within probable error as required. The col-
lision frequencies were found to be independent of pres-
sure to within probable error. The value of the collision
probabilities of helium obtained from the collision fre-
quencies (20 $cm^{-1}mm$ Hg^{-1} @ kT_e = .0381 ev; 22 $cm^{-1}mm$ Hg^{-1}
@ 13 ev) is within probable error of the values obtained
by other experimental means given in the literature.

The correct interpretation of the absorption
data from this experiment should be given by Maxwell's
equations with current-source particle coupling as given
by the Boltzman equation. The poor agreement between
the experimental results and the Maxwell-Lorentz absorp-
tion equation is taken as an indication that the Maxwell-
Lorentz solution is too crude an approximation for the
experimental situation encountered to provide good agree-
ment. Although the Klevans-Osborn transport equation
is only an approximation to the situation studied, good
solutions are available, and the satisfactory agreement
observed between the K.O. absorption equation and the
absorption data is indicative that the approximations
inherent in the use of the transport equation are not too
severe. The poor agreement between the classic Milne
absorption equation and the observed absorption is assumed
to be an indication that dispersion was not adequately
taken into account during development of the equation.
All conclusions are tentative, however. More data from a
different system should be obtained before a definite
statement as to the relative validity of the different
absorption formulae can be made.

CHAPTER I

INTRODUCTION

This experiment was designed to measure absorption of microwave radiation by slightly ionized helium in the frequency range $.2 < \omega_p^2/\omega^2 < .8$. The work was done to fill a notable gap in the experimental data and to test two approximate calculational schemes.

Although a great deal of microwave-plasma interaction data exists, only two studies are known to the writer which give data on the frequency dependence of microwave absorption in a slightly ironized gas. Olte and Miller (1) reported measurements in the vicinity of the plasma frequency. Bachynski et. al (2) made measurements for $\omega_p/\omega < 1$, but had no independent electron temperature measurements, so the attenuation data obtained could not be interpreted accurately. Thus the need for absorption data in the frequency range $.2 < \omega_p^2/\omega^2 < .8$ for which electron temperatures are also measured is obvious.

It should be noted that although several experiments have been carried out which yield electron-neutral collision frequencies for helium (3, 4, 5, 6, 7), none have been done in which the collision frequency was obtained from absorption of unguided waves in a slightly ionized

1

gas. The experiment which came closest to this case was that of Anderson and Goldstein (3) in which the collision frequency was measured from absorption in a waveguide. In the experiment presented here, unguided waves were used and a collision probability was obtained from the absorption data.

It is interesting to compare the collision probability obtained in this experiment with those obtained in other experiments

Reference	p_c $(cm^{-1}mmHg^{-1})$ for Helium $(T_e \sim$ room temp$)$
3	24
4	19
5	19
6	22
7	28
This experiment	20

The collision probability from this experiment agrees with those from the other references to within probable error except for that from reference 7.

Two calculational schemes have been developed to interpret the absorption data obtained in experiments of this type. The Maxwell equations with appropriate source-particle coupling and correct description of the source-particle distributions provide the most accurate and the most appropriate approach. This is because the Maxwell

equations are specifically designed to describe measurements

of the quantity measured-the electric field of the microwave.

However, the most commonly used solution for the experiment

performed is too crude to be realistic and gives poor

agreement with the data.

Two transport equations have been developed which

presumably apply to absorption experiments of this type.

Among other approximations is the requirement that the

beam intensity be large enough so that there is no signifi-

cant difference between photon number and the square of

the electric field. This requirement proved to be no

problem for this experiment. Although these equations are

approximate, realistic solutions are readily available

and so an advantage over the Maxwell-Lorentz approach is

obtained.

The dispersion of the medium is treated differ-

ently in the two transport equations and, as a result, they

differ significantly in the range of frequencies where

dispersion is important ($.2 < \frac{\omega_p^2}{\omega^2} < .8$). The most recent

equation (8) was found to give the best agreement with the

absorption data obtained in this experiment.

The data were obtained by measuring the absorption

of a collimated beam of 12 G Hz radiation as it passes

along the axis of a 5 inch diameter by 5 inch long cylinder

of ionized helium. The ionization was produced by a

7.1 MHz electric field.

CHAPTER II

DEVELOPMENT OF THE RADIATION ABSORPTION EQUATIONS

Three methods of analysing radiation absorption experiments will be briefly discussed here. The main intent is to delineate the basic assumptions and to explore the range of validity of each approach. For greater detail, the reader is referred to the references cited and Appendices A, B, and C.

Borrowing from Milne (9) and Woolley (10), the writer has constructed a transport equation for dispersive media by use of a phenomenological argument. Several aspects of the construction are ambiguous, so no suggestion as to the validity of the equation will be given. In non-dispersive media, however, the equation reduces to that given by Milne for non-dispersive media. The equation obtained is as follows.

$$1 \qquad \frac{d}{ds}\left[\frac{I_\nu(s)}{\mu^2}\right] = -\frac{I_\nu}{\mu^2}\left(\frac{ck}{\omega}\sigma\right) + \frac{2\pi h\nu}{c}\frac{S_\nu}{\mu^2}$$

where

$I_\nu(s)\, d\Omega d\nu da$ = the amount of energy passing through da at s which is in $d\Omega$ about Ω and which has frequency in $d\nu$ about ν

$x_j = \Omega_j s + x_{jo}$

$\sigma = \dfrac{\alpha - \varepsilon}{c^2 k/\omega}$ = the absorption coefficient

4

$$\frac{2\pi h\nu}{\mu^2 c} S_\nu(s)d\Omega d\nu = \frac{2\pi h\nu}{\mu^2 c} \varepsilon\rho d\Omega d\nu =$$ the amount of radiant energy emitted in $d\Omega$ about $\underline{\Omega}$ which has frequency in $d\nu$ about ν

$\varepsilon =$ probability per unit time for emission of a photon with direction in $d\underline{\Omega}$ about $\underline{\Omega}$ and frequency in $d\nu$ about ν.

$\alpha =$ probability per unit time for absorption of a photon traveling in a direction in $d\Omega$ about $\underline{\Omega}$ and with frequency in $d\nu$ about ν.

$\rho = k^2/(2\pi)^3 =$ density of states

$\underline{k} =$ wave vector

Equation 1 will be referred to hereafter as the classic transport equation.

In 1962, another transport equation was developed by Klevans and Osborn (8). They arrived at the equation by deductive rather than phenomenological means. The equation differs significantly from the classic equation only for dispersive media. The equation is as follows.

2    $$\frac{d}{ds} G_k(s) = -G_k\sigma + S$$

where

$$G_k(s) = \frac{I_\nu(s)}{ch\nu}\frac{d\nu}{dk}$$

$$S = \varepsilon\rho$$

Note that in free space, $\mu = 1$ and

$$G_k(s) = I_\nu(s)/ch\nu(2\pi)$$

Equation 2 will be referred to hereafter as the K.O. transport equation.

The solutions to equations 1, 2 are

$$3 \qquad T = \frac{I_\nu(A)/\mu^2}{I_\nu(o)/\mu_0^2} = \exp\left[-\int_0^S \mu(s')\, \sigma(s')\ ds'\right]$$

$$4 \qquad T = \frac{G_k(s)}{G_k(o)} = \exp\left[-\int_0^S \sigma(s')ds'\right]$$

where

T = transmission through the medium.

In the development of the transmission formulae 3, 4, two assumptions are implied which limit their applicability. First, the transport equation is based on the assumption that distances over which the photon distribution function is expected to vary greatly are much larger than the wave length of the radiation. Thus reflections at boundaries and diffraction effects cannot be accounted for. Second, the solutions assume weak absorption and negligible spontaneous emission.

In order to complete the transport theory presentation, it is necessary to obtain the absorption coefficient σ. A suitable model for the absorption process must be chosen to make this calculation. For electron temperatures of interest in this thesis (a few ev) the electron energy of the majority of the electrons is insufficient to ionize the neutral molecules in the system. If the neutral molecules are monatomic, the electrons will not have enough energy to excite line radiation either. Thus it is assumed

that the absorption-emission process of interest is

Bremsstrahlung. The calculation of the absorption coeffi-

cient σ is carried out in some detail in (11). The result

of this calculation is the absorption formula which follows.

5 $\qquad \sigma = \dfrac{32\,\pi}{3}\sqrt{\dfrac{2}{\pi}}\ \dfrac{e^2}{m_e^{3/2}}\ \sigma_{sc}\ \theta_e^{1/2}\ Nn_e\ \dfrac{1}{ck\omega_k}$

where

$\theta_e = kT_e$

T_e = electron temperature

N = neutral density

n_e = electron density

ck = photon momentum

ω_k = photon energy

σ_{sc} = total electron-neutral scattering cross
section

Several restrictive assumptions have been made in developing

formula 5. As a calculational convenience, it was assumed

that the scattering cross section was slowly varying with

electron speed. For this experiment, the assumption was

no problem since only electron-neutral collisions are

important, and the scattering cross sections for the gasses

used (helium and neon) are slowly varying with electron

speed. Only the first term of the expansion of the exact

results in powers of $\hbar\omega/\theta_e$ has been retained in equation

5. This approximation is justified for the frequency used

in this experiment as long as the electron temperature

is equal to or greater than room temperature. Formula 5
neglects induced dipole radiation and exchange radiation
effects. This approximation is acceptable only if the
electron temperature is a few electron-volts or smaller,
and if the radiation frequency is in the microwave range.
These restrictions are not a problem for this experiment,
however. The neutral gas density was assumed to be small
enough so that the average distance between molecules
was greater than the DeBroglie wavelength of the electrons
in the ionized gas. This condition is satisfied as long
as pressures are maintained at less than ~175 mm Hg and
thus is no problem. Finally, it was assumed in the de-
rivation that the electron energy distribution is Maxwellian.
This condition is not always easy to achieve with the ionizing
means generally available. The problem of the electron
energy distribution will be discussed again later.

Formula 5 requires a dispersion relation to
connect k and ω_k. The K.O. theory (8) yields such a relation
which for the temperature (Te $\leq$ 10ev), collision frequency
(ν^2/ω^2 << 1), and plasma frequency ($\omega_p^2/\omega^2 \leq .6$) ranges of
this experiment is simply

6 $$\omega_k^2 = c^2k^2 + \omega_p^2$$

This relation is the same as that obtained from the Maxwell-
Lorentz theory for the same range of plasma parameters.

The main advantage of the transport theory is

its simplicity, which is easily seen in absorption formulae
3 and 4. If the path direction and the electron density
profile along the path are known, the attenuation of the
ray may easily be calculated by an integration procedure.
It will be seen later, however, that the solution of a
partial differential equation is required for each different
electron density profile in using the Maxwell-Lorentz theory.

A radiation absorption formula may be obtained
from the solution to Maxwell's equations and the Boltzman
equation. The argument by which the formula is obtained is
briefly reviewed here.

The principles of the use of Maxwell's equations
in a conductive medium to account for radiation absorption
are given in (12). For the case of no space charge separ-
ation, Maxwell's equations yield the wave equation

7 $\qquad (\nabla^2 - \frac{1}{c^2} \frac{\partial^2}{\partial_t^2}) \underline{E} = - \frac{4\pi}{c^2} \frac{\partial}{\partial_t} \underline{J}$

where

$\underline{E}$ = electric field

$\underline{J}$ = current density.

The current density is usually approximated by the formula

8 $\qquad \underline{J} = \rho_c \underline{E}$

where

ρ_c = scalar conductivity of the medium.

The use of equation 8 in 7 and the assumption of a harmonic wave of the form $e^{-i\omega t}$ yields

9 $\qquad \nabla^2 \underline{E} + (\frac{\omega}{c})^2 \left[1 - i (\frac{4\pi}{\omega}) \rho_c \right] \underline{E} = 0$

Equation 9 must be solved with suitable boundary conditions for each ionized gas of interest. It is easily seen that if ρ_c is a function of position, the solution of equation 9 becomes a formidable task. In fact, solutions for only two non-uniform medium configurations are known to the writer. Given the space dependence of ρ_c, a simpler, approximate solution may be obtained by use of the WKB method which is valid as long as ρ_c varies slowly with position. It has the same form as equation 3, but has a different absorption coefficient. This coefficient will be given here for the case of plane waves passing through a homogeneous medium in which boundary effects are negligible. The plane waves are attenuated according to the formula.

10 $\qquad E = E_o \exp \: i\underline{k}\cdot\underline{x} - i\omega t$

where $\underline{k}$, the complex propagation coefficient is defined by

11 $\qquad k^2 = \frac{\omega^2}{c^2} (1 - i (\frac{4\pi}{\omega}) \rho_c)$

It is convenient to define the refractive index μ and absorption constant χ as follows

$$12 \qquad \frac{ck}{\omega} = \mu - i\chi$$

It will be noticed that a knowledge of the conductivity will make it possible to calculate the refractive index and absorption coefficient.

The complex conductivity is calculated by the use of the Boltzman equation. It is usually referred to as the Lorentz conductivity. The result of this calculation is

$$13 \qquad \rho = \frac{1}{4\pi} \omega_p^2 \left[\frac{\nu_{eff} - i\omega}{\nu_{eff}^2 + \omega^2} \right]$$

where

$$\nu_{eff} = \nu_{eff\ n} + \nu_{eff\ i}$$

$\nu_{eff\ n} \equiv$ electron-neutral collision frequency

$$\cong \frac{8}{3} \sqrt{\frac{2}{\pi}} \sigma_m N \sqrt{\frac{kT_c}{m}} \qquad \omega^2 >> \nu_{eff}^2$$

$$\sigma_m = \sigma_S \int (1 - \cos \Theta) I_S (\Theta) d\Omega_{cm}$$

$\sigma_S =$ total electron-neutral scattering cross-section

$I_S (\Theta) d\Omega_{cm} =$ elastic scattering frequency function

$\Theta \qquad =$ scattering angle in CMCS

$\nu_{eff\ i} \equiv$ electron-ion collision frequency

$$= 3.6 \frac{n_i}{T_e^{3/2}} \ln \frac{3.7 \times 10^3}{n_i^{1/2}} T_e \left(\frac{2T_e T_i}{T_e + T_i}\right)^{1/2}$$

n_i = ion density (ions/ec)

T_e = electron temperature

T_i = ion temperature

The electron-ion collision frequency is taken from (4).

Values of σ_m for several noble gasses of interest in this experiment are given in (13).

The use of equation 13 in 11, 12 yields

14a $$\mu = \left[\frac{1}{2}(1 - \frac{\omega_p^2}{\omega^2 + \nu_{eff}^2}) + \frac{1}{2}\left\{ (1 - \frac{\omega_p^2}{\omega^2 + \nu_{eff}^2})^2 + (\frac{\omega_p^2}{\omega^2 + \nu_{eff}^2} \frac{\nu_{eff}}{\omega})^2 \right\}^{1/2} \right]^{1/2}$$

14b $$\chi = - \frac{1}{2} \frac{\nu_{eff}}{\omega} \frac{\omega_p^2}{\omega^2 + \nu_{eff}^2} \frac{1}{\mu}$$

Restrictive assumptions have been made in developing equations 10, 14 which should be investigated briefly. First, plane wave propegation was assumed. Thus, as in the case of transport theory, effects which distort wave fronts must be avoided. A homogeneous medium in which boundary effects are negligible was assumed, but this assumption is not necessary. It will be shown later that effects (such as boundaries) which occur within a wavelength can easily be treated with Maxwell-Lorentz theory.

Several assumptions were made in connection with the calculation of conductivity which are similar to those made in the calculation of the absorption coefficient for the transport equations. For example, the scattering cross section was assumed slowly varying with electron speed, the electrons were assumed non-relativistic, the neutral density was assumed small enough to avoid interference effects between two molecules, and the electron energy distribution was assumed Maxwellian.

It is interesting to note in passing that a type of transport equation may be obtained from Maxwell's equations for the case of plane waves, namely

15 $$\frac{d}{ds} H_\nu(s) = 2\frac{\omega}{c}\chi H$$

where

$$H_\nu(s) = vU$$

v = speed of energy propagation in the medium

U = time averaged energy per unit volume contained in the electric and magnetic fields.

The solution to equation 15 is

$$T = \frac{H_\nu(s)}{H_\nu(o)} = \exp\left[\int_o^s 2\frac{\omega}{c}\chi\, ds\right]$$

Equation 15 lacks the spontaneous emission source term. This term was lost when $\underline{J}$ was approximated by $\rho_c\underline{E}$. Since

this source term is small for the experiment of interest,
the loss is not important, but the loss of this term does
illustrate what can happen as a result of the approximation
$\underline{J} = \rho_c \underline{E}$. Equation 15 is not valid if ρ_c changes rapidly
with s (as at medium boundaries) since in these zones the
averaging procedure used to define $H_\nu(s)$ has no meaning.

It is enlightening to compare the results of the
transport equations and the Maxwell-Lorentz equations as
given in equations 3, 4, 5, 10, 14, and 16 for the case of
a microwave beam passing through a homogeneous volume of
ionized gas in which boundary effects are negligible.
For this case, all of the attenuation equations may be
written in terms of the transmission T as follows

17    $T = \exp\left[-Kd\right]$

where

$$T = \frac{I_\nu(s)/\mu^2(s)}{I_\nu/\mu^2\big|_o} = \frac{G_k(s)}{G_k(o)} = \frac{E^2(s)}{E^2(o)} = \frac{H_\nu(s)}{H_\nu(o)}$$

K = absorption coefficient

d = distance between transmitter and receiver

In equation 17, the absorption coefficient will be different
for each theory. If the transport absorption coefficient
is expressed in terms of the "effective transport collision
frequency"

18    $\nu_{eff\ tr} = \frac{8}{3}\sqrt{\frac{2}{\pi}}\ d_s c^N \sqrt{\frac{\Theta_e}{m}}$

the absorption coefficient K may be written as follows for the various absorption equations

Classic Absorption Equation

$$K \equiv \mu\sigma = \frac{\nu_{eff\ tr}}{c} \frac{\omega_p^2}{\omega^2}$$

K.O. Absorption Equation

$$K_{Ko} \equiv \sigma = \frac{\nu_{eff\ tr}}{c} \frac{\omega_p^2}{ck\omega_k}$$

Maxwell-Lorentz Equation

$$K_{ML} \equiv -2\frac{\omega}{c}x = \frac{\nu_{eff}}{c} \frac{\omega_p^2}{\omega^2 + \nu_{eff}^2} \frac{\omega}{ck_\omega}$$

Transport Equation developed from the Maxwell-Lorentz Equation

$$K_{TML} \equiv \frac{4\pi\rho_1}{c\mu_1} = \frac{\nu_{eff}}{c} \frac{\omega_p^2}{\omega^2 + \nu_{eff}^2} \frac{\omega}{ck_\omega}$$

For the experimental conditions of interest here, $\nu_{eff}^2/\omega^2 \ll 1$ and $\frac{\omega_p}{\omega} < 1$.

Thus one may write

19 $$K = \frac{\nu_{eff\ tr}}{c} \frac{\omega_p^2}{\omega^2}$$

20 $$K_{KO} = \frac{\nu_{eff\ tr}}{c} \frac{\omega_p^2}{ck\omega_k}$$

21 $$K_{ML} = K_{TML} = \frac{\nu_{eff}}{c} \frac{\omega_p^2}{\omega ck_\omega}$$

where from equations 6 and 14 a,

22a $\qquad \omega_k = ck(1 + \dfrac{\omega_p^2}{c^2 k^2})^{1/2}$

22b $\qquad ck_\omega = \omega (1 - \dfrac{\omega_p^2}{\omega^2})^{1/2}$

It should be noted here that the $\nu_{eff\ tr}$ and ν_{eff} differ by the amount

$$\frac{\nu_{eff}}{\nu_{eff\ tr}} = \frac{\sigma_m}{\sigma_S} = \int (1 - \cos\Theta)\ I_S\ (\Theta)\ d\Omega_{cm}$$

This ratio is so close to unity for conditions of interest in this experiment that the difference cannot be measured by the data taken.

It is clear from equations 19, 20, 21, that the main difference in the theories is in the term $c\ k\ \omega$. Only those frequencies (or electron densities) for which $ck\omega/\omega^2$ differs noticeably from unity will provide information on the zones of applicability or inapplicability of the three theories. It will be seen from equations 22, that $ck\omega/\omega^2$ differs noticeably from unity only when the radiation frequency is within an order of magnitude of the plasma frequency.

CHAPTER III

INTERPRETATION OF DATA

In the previous chapter, a development of three absorption equations was given which is valid for a homogeneous volume of ionized gas in which boundary effects are negligible. Obviously this model is not valid for any realistic laboratory plasma. This chapter is devoted to the treatment of effects which arise in laboratory plasmas that may affect the interpretation of experimental data in terms of radiation absorption due to collisions. Also a section is devoted to the analysis of the phase shift method of determining electron densities.

Microwave Measurements of Electron Density

The dispersion relation can be used to determine electron density from the phase shift due to passage of a wave through the ionized gas. For the case where $\nu_{eff}^2/\omega^2 \ll 1$ and $\omega_p/\omega < 1$ and for electron density configurations which vary only along the direction of wave propegation, it may be shown that

$$- \Delta\phi = \int_o^d \left\{ 1 - \left[1 - \frac{n_e(x)}{n_c} \right]^{1/2} \right\} \frac{2\pi}{\lambda}\ dx$$

where

$\Delta\phi$ = phase shift

d = thickness of the ionized gas

n_c = electron density at which the plasma frequency is equal to the radiation frequency

λ = free space wavelength of the radiation

$n_e(x)$ = electron density as a function of position along the path of wave propegation.

It is convenient to define an average electron density by the equation

$$23 \quad \left[1 - \frac{\bar{n}_e}{n_c} \right]^{1/2} = 1 - \frac{\lambda \Delta \phi}{2 \pi d}$$

It has been shown by Bachynski et al (2) that the phase is quite insensitive to the shape of the density profile but depends almost entirely upon the total electron content even for densities corresponding very near to the plasma frequency. Thus $\bar{n}_e$ is a function only of $\int n_e(x) dx$ as long as $\omega_p^2 / \omega^2 \lesssim .8$. Finally, one may see that the effect on $\bar{n}_e$ of electron density variation perpendicular to the direction of wave propegation is small by noting that the portion of the incident wave most affected by the density change (the outer portion) is eliminated by the refractive defocusing effect to be discussed later.

The Effect Of Reflections At Medium Interfaces

Laboratory sources of ionized gas are usually bounded by dielectric plate-ionized gas and vacuum (air)-dielectric interfaces. Each of these interfaces will cause reflections. The reflections generated will have two effects on the attenuation of the ionized gas. First, the mean

attenuation due to the ionized gas will be increased slightly

due to the energy reflected back into the wave generator.

Second, interference between incident and reflected waves

within the ionized gas will cause undulations around the mean

attenuation. These two effects will be studied briefly

in this section.

It is of interest to obtain the power transmission

and reflection coefficients for plane waves impinging

upon a semi-infinite region of ionized gas and an infinite

slab of ionized gas. The calculations are given in (14).

Only the results will be shown here.

The transmission coefficient t and the reflection

coefficient r for a plane wave traveling from a vacuum

to an ionized gas is,

$$24a \qquad r = \frac{(1 - \mu)^2 + \chi^2}{(1 + \mu)^2 + \chi^2}$$

$$24b \qquad t = 1 - r = \frac{4\mu}{(1 + \mu)^2 + \chi^2} \quad ,$$

where μ and χ are given in equations 14. The power trans-

mission and reflection coefficients for a plane wave traveling

from an ionized gas to a vacuum are the same.

The transmission and reflection coefficients T

and R for an infinite uniform slab of ionized gas of thick-

ness d are given by the following equations.

25a $\quad R = \dfrac{r\left[1 - \exp(-2\alpha d)\right]^2 + 4\exp(-2\alpha d)\sin^2(\beta d)}{\left[1 - r\exp(-2\alpha d)\right]^2 + 4r\exp(-2\alpha d)\sin^2(\beta d - \psi)}$

25b $\quad T = 1 - R = \dfrac{(1 - r)^2 + 4r\sin^2\psi\ \exp(-2\alpha d)}{\left[1 - r\exp(-2\alpha d)\right]^2 + 4r\exp(-2\alpha d)\sin^2(\beta d - \psi)}$

where

α = absorption coefficient = $\dfrac{\omega}{c}x$

β = phase constant = $\dfrac{\omega}{c}\mu$

ψ = phase angle of $\breve{\rho} = |\breve{\rho}|\ \exp(i\psi)$

$r^{1/2}\sin\psi = \dfrac{2\chi}{(1 + \mu)^2 + \chi^2}$

$r^{1/2}\cos\psi = \dfrac{1 - \mu^2 - \chi^2}{(1 + \mu)^2 + \chi^2}$

In a real experimental situation, the slab of ionized gas is usually bounded by dielectric plates. This situation complicates the expressions for T and R considerably, but Jahn (15) has shown that if the dielectric plates are matched for minimum reflection in free space the complex expressions for the slab of ionized gas bounded by dielectric plates reduce to the simple expressions for the slab of ionized gas in free space. In this thesis, the simple slab expressions will be used and the dielectric plates used in the experiment will be matched for minimum reflection in free space.

If one suppresses the oscillations in equation 25 due to interference between incident and reflected waves,

the following equations result.

26a $\qquad R = r + \dfrac{r(1 - r)^2 \exp(-4\alpha d)}{1 - r^2 \exp(-4\alpha d)}$

26b $\qquad T = t' \exp(-2\alpha d)$

where

t' = transmission coefficient of the two boundaries to the ionized gas region

$\qquad = \dfrac{(1 - r)^2}{1 - r^2 \exp(-4\alpha d)}$

Heald and Wharton (14) show numerically that the reflection and transmission of equations 25 oscillate around the mean given by equations 26.

It is important to note that for $.1 \leq \dfrac{\omega_p^2}{\omega^2} \leq .7$ and $\nu_{eff}^2 \ll \omega^2$, r is dependent mainly on μ which in turn is dependent mainly on electron density. Thus the transmission term due to reflection t' is the same for a given density regardless of the attenuation of the ionized gas.

The Effect of Density Variations Along The Direction of Propagation of The Wave

The treatment of electron density variations along the direction of propagation of the wave in an exact fashion is impractical. An approximate treatment using the Maxwell equations (equation 9) and the Lorentz conductivity has been attempted for a few electron density profiles (12), but this technique is very difficult also. However, an approximation scheme exists which should be valid for most experimental electron density profiles. Suppose that the electron

density profile can be approximated by a rapid rise in density at the chamber wall and then a slow variation within the ionized gas. Under these circumstances, the mean transmission coefficient for all of the different absorption theories is given by

27    $T = t´(0+) \exp \left[- \int_o^d K(s) \, ds \right]$

where

  $t´(0+)$ = boundary transmission coefficient (equation 26) evaluated for the electron density just inside the ionized gas.

  $K(s)$ = absorption coefficient as defined by equations 19, 20, 21, 22 for each of the absorption theories.

The reflection coefficient which could be calculated with the use of this approximation scheme, namely

$$R = r + \frac{r(1 - r)^2 \exp(-4\alpha d)}{1 - r^2 \exp(-4\alpha d)}$$

where

$r = r(0+)$

$\alpha = \alpha(0+)$

would not be expected to be a very good approximation to the observed reflection coefficient since reflection depends strongly on the shape of the density profile.

Insofar as equation 27 is valid, Bachynski et al (3) have shown that the shape of the density profile is not important to the transmission T as long as $\omega_p^2/\omega^2 \leq .8$. In fact, one may calculate ν_{eff} from given values of T and

$\Delta\phi$ by use of formulae 19 and 23 and get a negligibly small
difference from the value of ν_{eff} calculated by using the
more exact formula, 27, as long as $\omega_p^2/\omega^2 \leq .8$ and
$\nu_{eff}^2/\omega^2 \leq .01$.

The Effect Of Density Variation Perpendicular
To the Direction of Wave Propagation

If a microwave beam is incident upon a plasma
slab that has an electron density variation in a direction
normal to the direction of wave propagation, the beam will
be either focussed or defocussed. If the density profile
is such as to defocus the beam, part of the incident beam
will miss the receiving horn and the effect of the defocussing
will be an apparent attenuation. The attenuation observed
from this effect may be large enough to completely over-
whelm the attenuation due to collisions.

It is enlightening to consider a simple model
which will give an analytical expression for the attenu-
ation due to refractive defocussing. Consider a plane wave
incident upon the axis of a cylindrical column of ionized
gas of radius r and length d. Assume that the electron
density is constant along the axis of the cylinder, but
depends upon the distance from the axis. That is, the
electron density $n_e(r)$ varies in the direction normal to
the direction of propagation of the wave. Assume further
that the incoming wave is a uniform beam of circular cross-

section with radius a and that the receiving horn aperture

is determined by a diaphragm of radius A situated a distance

R from the far face of the cylinder of ionized gas. With

this model Bachynski et al (2) develops an expression for

the power transmission coefficient η where attenuation is

due to refractive defocussing. This expression is the

following

$$\eta = 1 + \frac{dR}{2A} \frac{\left[\partial n_e(r) / \partial r\right] r = a}{\sqrt{1 - n_e(a)}}$$

Now for a diffusion limited cylinder of ionized gas, the

radial density profile function is

$$n_e(r) = n_0 J_0 \left(\frac{\Gamma r}{r_0}\right)$$

so

$$\eta = 1 - \frac{d}{2r_0} \frac{R}{A} \frac{\Gamma n_0 J_1(\Gamma a/r_0)}{\sqrt{1 - n_e(a)}}$$

The experimental apparatus actually used closely approxi-

mates the above model except in four particulars

1) The above mentioned development does not take into account

   the refraction of the beam by the dielectric plates of

   the chamber containing the ionized gas.

2) The geometrical optics type of refractive defocusing

   considered to obtain the above result has not taken

   into account the phase difference between the various

   rays (from different radii) as they reach the receiving

   antenna.

3) The electron density does vary considerably along the axis of the cylinder.

4) The microwave beam is probably not completely uniform throughout its cross-section.

Thus the simple expression given above would not be expected to give a good representation of η over the full range of electron densities achieved in this experiment.

It has thus been shown that as long as attenuation due to refractive defocussing is small compared to that due to collisions, the mean transmission through a finite ionized gas with a non-uniform electron density profile may be adequately expressed in terms of the formula

$$29 \qquad T = t'(0+) \exp\left[-K(\bar{n}_e)d\right]$$

where $t'(0+)$ is defined in equation 27 and $\bar{n}_e$ is defined by equation 23.

It is clear from the relation between formulae 25 and 26 that formula 29 will only represent the mean transmission around which an experimentally determined transmission coefficient would oscillate.

CHAPTER IV

INSTRUMENTATION

The purpose of this chapter is to discuss the
problems encountered in the design, construction, and cali-
bration of the equipment used in the experiment.

A great deal of effort was expended on the experi-
mental equipment to reduce the number of effects which would
cloud the interpretation of the data. The limitations
implied in the development of the absorption formulae of
Chapter II determine the effects most likely to reduce
interpretability. These limitations were treated briefly
in Chapter II, but for convenience they will be restated
here. The effect these considerations had on equipment
design is discussed later in this chapter.

The two main requirements implied in the develop-
ment of the transport absorption formulae are that the wave-
like effects (diffraction, interference of reflections,
etc.) of the medium be small and that the photon mean-
free-path be large compared to a wavelength. These require-
ments were the main considerations in the design of the
microwave system. Practical considerations, such as the
conditions necessary to obtain measurable attenuation,
were also important. The methods used to meet these demands
on the microwave equipment are given in the section on
design of the microwave system.

26

The limitations implied in the development of
the absorption coefficient provided the main considerations
in the design of the ionized gas source. They are:

1) The electron energy distribution must be at least approxi-
   mately Maxwellian.

2) Electron neutral collision cross-section should vary
   slowly with electron speed.

3) The average electron energy should be low enough so that
   the electrons are non-relativistic and the majority of
   the electron-neutral collision do not excite line radi-
   ation.

4) The neutral gas pressure should be held within two limits.
   a) The lower limit is determined by the condition that
      attenuation of the beam be large enough to be measurable.
   b) The upper limit is determined by the most stringent
      of two factors.
      i) Electron wavelength must be less than the average
         distance between molecules.
      ii) The collision frequency should be such that
         $$\omega^2 \gg \nu^2.$$

In addition to these requirements, strictly practical
considerations demand that the source supply an unobstructed
path for the microwave beam and a means of varying the
electron density. The methods used to meet these demands
are given in the section on the design of the ionized gas source.

A. The Microwave System

Design of the Microwave System

The first step in the design of the microwave system was the choice of the frequency. Large changes in the frequency after the construction of the system were impractical because of the matching necessary for each component of the microwave system.

The useful frequency range for this experiment was limited by two considerations. First, the frequency had to be low enough to keep dispersion effects important for obtainable electron densities. Investigation of the absorption formula indicated that dispersion is important in the range $.2 < \omega_p^2/\omega^2 < .6$. It was determined by experiment and calculation that the maximum plasma density that could be obtained with the plasma generators used was $n_e \sim 10^{12}/cc$. Thus, the frequency had to be $\nu \le 12 \times 10^9$ cps.

The lower limit to the useful frequency range was determined by diffraction. It was found to be very difficult to construct and mount an ionization chamber which was larger than a cylinder 5 inches in diameter and 5 inches long. It has been noted that a good experimental test of the theory requires that diffraction effects be small and path lengths be large. These requirements can

be met by making the ratios of path length to wavelength
and beam diameter to wavelength large. This means that
the highest frequency possible should be used. The fre-
quency chosen was 12 x 10^9cps. This gave a path length
to wavelength ratio of five and a ratio of diameter to
wavelength of five. Tests showed that these ratios were
sufficient to avoid diffraction and short path length
problems.

In order to avoid diffraction around the edges
of the plasma chamber, to insure the flattest possible
density profile in the plasma, and to provide plane wave
fronts it was necessary to use lens corrected horns and
diaphragms to shape the beam and limit its size. The
microwave horn-lens system was designed and constructed
by the DeMornay Bonardi Company according to the specifi-
cations given in Figure 1. The dimension A was chosen to
be as small as possible. The dimensions F and T were
chosen to fit the size of the plasma chamber and its sur-
rounding aluminum can (Figure 2). The diaphragms used to
limit the diameter of the beam were made of microwave
absorber to avoid problems due to reflected waves.

A microwave bridge (16) was used to measure
phase shift and attenuation. It gives excellent accuracy
and reproducibility when the attenuation is low (less
than 15 db). If larger attenuations must be measured,

either a microwave source with output power greater than
the standard klystron must be used, or a different system
of measurement must be devised. A system designed specifi-
cally to measure large attenuations is given in (2). It
will be seen, then, that measurements of attenuation close
to the plasma resource frequency where attenuation is large,
were impossible with the bridge used in this experiment.

A standard reflectometer was used to measure
reflection coefficients from the ionized gas. No attempt
was made to measure the phase of the reflected signal.

Description, Calibration, and Performance
Of The Microwave System Used

A schematic diagram of the microwave bridge used
in this experiment is given in Figure 3. It is a standard
configuration except for the ferrite isolators in each arm
of the bridge, the attenuators in each arm of the magic
tee, and an extra phase shifter and attenuator. The
reasons for these additions will be indicated later in
this section.

One of the phase shifters and one of the attenu-
ators indicated in Figure 3 came from the factory with
calibration sheets. These pieces of equipment were re-
calibrated with all the equipment in place in the fol-
lowing manner. They were placed in series with another

phase shifter and attenuator which will be called the standard
phase shifter and attenuator. The calibration for either
the phase shifter or the attenuator then proceeded as
follows. The phase shifter (attenuator) was set at an
initial low value, the standard phase shifter (attenuator)
was set at the highest set point and the bridge was bal-
anced with a third uncalibrated phase shifter and attenu-
ator. Then the standard phase shifter (attenuator) was
reduced to the low set point and the amount of phase shift
and attenuation required to balance the bridge again was
noted. The standard was reset on the high set point,
the change compensated with the third uncalibrated phase
shifter and attenuator and the process repeated. Thus
it was possible to obtain, inch-worm fashion, a total cali-
bration curve in terms of the interval between set points
on the standard. Comparison of these calibration curves
with those supplied by the manufacturer showed agreement
to within 1% for both the phase-shifter and the attenu-
ator except in the very low attenuation region of the
attenuator. In the experiment, this region was never
used, however, so the discrepency was of no consequence.
This calibration procedure also revealed that the attenu-
ator supplied some phase shift and the phase shifter
supplied some attenuation. By using several set point

intervals on the standards it was possible to determine just how much of the attenuation (phase shift) was supplied by the standard and how much by the phase shifter (attenuator) to be calibrated. In this way it was possible to make a correction curve which was used in calculation of data.

Three sets of matched crystals were purchased for the reflectometer and were calibrated using the calibrated attenuator (16). The two crystals which were closest to being square low and which matched each other best were used in the reflectometer. The calibration curve was used in correcting reflection coefficient data.

All components of the bridge were tested for high VSWR before insertion into the bridge system. All were found to be well within manufacturer specifications and thus within the needs of the system.

It was found that if the high field arm of the matched magic tee was not carefully tuned and padded, it provided a rather large reflected wave which reduced the accuracy of reflectivity measurements obtained with the reflectometer. For this reason, two variable attenuators were placed in the arms of the matched magic tee. The attenuator in the maximum field arm was always placed at a maximum to reduce reflection and the attenuator in the

balancing arm was placed at a minimum to maximize sensitivity.

The reflection from the two types of microwave absorber used for limiting the beam was measured to insure that no large reflections would occur at their faces. It was found that one absorber gave a reflected wave intensity about 20 db down from the incident wave. The other absorber gave a reflected wave intensity about 15 db down from the incident wave. The diaphragms were constructed so that the 20 db absorber did the majority of the beam limiting job.

The diameter of the microwave beam at different points between the two inner diaphragms was measured in different ways and the results are presented in Figure 4. The "reflection beam" diameter was obtained by passing an aluminum plate in toward the beam until the reflection coefficient changed. The "attenuation beam" diameter was obtained by passing the aluminum plate in toward the beam until the bridge became unbalanced. It will be noted that the beam is always within the outer walls of the chamber so diffraction around the outer edges of the chamber should be negligible.

After the bridge components were tested separately, the system as a whole was tested with solids of known

refractive index. It was found that in order to insure
a correct refractive index the beam limiting diaphragms
had to be placed at least 4 inches from the end of the
microwave horn if it was smaller than 4-1/2 inches in
diameter. Furthermore, the diaphragm diameter had to be
at least 2 inches to obtain agreement with the literature
values of refractive index. These conditions might be
expected since their violation will spoil the plane wave
fronts of the microwave beam provided by the lens cor-
rected horns.

After the correct diaphragm diameter, material
and position was determined, the refractive index of
plexiglas and pyrex was determined. The refractive index
of plexiglas as determined by the bridge was $1.67 \pm .17$
and the literature value (17) was 1.61. The refractive
index of pyrex was $3.84 \pm .10$. The literature gave no
data for this particular kind of Borosilicate glass.
Phase shift and reflection data were taken for plexiglas
while the thickness was increased by adding 1/16" thick
pieces. The refractive index was found to increase
properly with thickness and the reflection coefficient
was found to minimize at thicknesses of $T_{1/2} = \frac{N\lambda}{2\mu}$ (1/2
wave plate) and maximize at thicknesses of
$T_{1/4} = \frac{(2N + 1)\lambda}{4\mu}$ (1/4 wave plate) in agreement with theory.

Calculation of the thicknesses of pyrex required for minimum reflection shows that for N = 4, T = .51 inch. The 1/2 inch plates used for the ends of the ionization chamber were tested and found to be very close to minimum reflection (1/2 wave) plates as expected. Thus it was not necessary to use any further matching techniques to insure that the chamber and plates were 1/2 wave plates as required by the theory.

The final preliminary test of the bridge system was made with the bridge, horn, diaphragms, and chamber set up in the final configuration. The chamber was filled with carbon-tetrachloride and the refractive index measured. The experimental value was 1.38 ± .05. The value given in the literature is 1.47.

For all of the above calibration tests, the attenuation did not change enough to be measured accurately so no attenuations are reported here.

After the system was completed and an ionized gas generated, three tests were made to check the sensitivity of the system to potential sources of error. First, the position of the horns was changed a distance of about 3 cm (more than one wavelength) to see if the position affected the phase, attenuation, and reflection measured from the plasma. The position was found to have

no measurable effect upon the phase and attenuation measured but did effect the reflection measured as much as 30%. Second, the reflection coefficient of the beam-limiting diaphragms was changed by inserting small pieces of metal in front of the absorbing material. Changes in phase and attenuation were noticed, the magnitude depending upon the area of absorber covered by metal. It was also noted that the phase and attenuation measurements became less reproducible. A maximum of 30% change was noted in the attenuation at a given phase with the absorber of one diaphragm one-half covered with metal. Reproducible measurements of reflection coefficient became impossible when only 20% of one diaphragm was covered with metal.

It should be mentioned that the "tracking" in attenuation for this system was not very good. The phase shifter was calibrated for only 190° of phase shift. If more phase shift than this was obtained from the plasma it was necessary to switch from one arm of the magic tee to the other. In this switching operation, a certain amount of attenuation was either added to or subtracted from the attenuation measured for the equivalent phase shift on the other arm. The phase shift "tracking" proved to be excellent, however. It was not difficult to correct for this defect in the system. Attenuation

measurements for equivalent phase shift on both arms of the
magic tee were taken. The observed attenuation difference
was then subtracted from all readings taken on that particu-
lar arm of the tee.

The reflection coefficient of the ionization
source was measured as x db down from the reflection due
to an aluminum plate placed at the same position as the
front face of the source. It was found that the system
was not perfectly matched even after the pains taken in
matching each component of the system. A reflection
coefficient of -24 db was observed. In order to achieve
the final matching, a tuner was inserted in front of the
primary horn and was tuned to give a reflection coefficient
too small to be measured (< -35 db). Very little tuning
was required at room temperature but when the chamber
and high temperature microwave absorbers were heated to
230° c, more tuning was required due to the changed charac-
teristics of the absorber and the pyrex at high temperature.
In order to insure that this tuner did not affect the
measurement of phase and attenuation, measurements were
taken both with and without the tuner present. No difference
in either phase or attenuation was noted.

B. The Ionized Gas Source

Design of the Ionized Gas Source

Three ionization techniques were attempted as possible means of generating an ionized gas. The first was the so-called "glow discharge" generated in a noble gas by a DC electric field. The second was an ionized gas produced in cesium vapor by ultra-violet radiation and the third was an "RF discharge" generated in a noble gas with a high-frequency electric field. Only the last source of ionized gas proved fruitful for this experiment but it is interesting to see why the first two sources were unsatisfactory.

The glow discharge source was rejected after some investigation. First, it tends to become unstable and break down into an arc in the high electron density region ($n_e > 10^{11}$ /cc) where the difference between the absorption equations is the largest. Second, there is reason to believe (19) that the electron energy distribution is not Maxwellian as the theory requires. Third, the impurity problem is increased by bombardment of the cathode.

The ultra-violet (UV) ionized cesium source looked very promising at the start. Because the UV photons provide very little extra energy over that required to ionize the cesium, the electron temperature should be nearly

chamber temperature and the energy distribution should be
Maxwellian. If the ionizing cesium were used as a seed
in a chamber filled mostly with helium or neon, the majority
of the electron-neutral collisions would be with atoms
which have cross sections which vary slowly with electron
speed. The noble gas should not impede the ionization
mechanism in any way but instead should augment the electron
density, and flatten the density profile by decreasing
electron diffusion to the walls without increasing the
recombination coefficient appreciably. If the noble gas
pressure is kept below 175 mm Hg, the electron wavelength
should always be less than the average distance between
collisions. Thus, it can be seen that all the require-
ments of the absorption formulae are satisfied. However,
the UV-cesium source was incapable of producing high enough
electron densities to be of interest in this experiment
(Appendix D).

The RF discharge proved to be the means needed
of generating an ionized gas which satisfies the require-
ments of the theoretical model. Cahn shows (19) that the
RF discharge used should have a Maxwellian electron energy
distribution. The electron temperature observed in the
most interesting pressure zone is about 2ev. This temper-
ature is low enough to insure that the majority of the

electrons are non-relativistic, they lack the energy re-
quired to generate line radiation, and the electron neutral
cross sections are slowly varying with electron energy.
The maximum pressure of use in this discharge was 20 mm
Hg which is small enough to insure that $\nu_{eff}^2/\omega^2 \ll 1$
and that the average distance between atoms was greater
than the electron wavelength.

On an experimental level, the RF discharge proved
to be an excellent means of generating an ionized gas.
Impurities were less of a problem since no inside electrodes
were required. Two methods were available to provide varying
electron density. The first was to vary the RF electric
field within the gas. The second was to take measurements
in the decaying ionized gas after the RF had been cut off.
An unobstructed path for the microwave beam was easily
supplied since no electrodes are required within the chamber.
Finally, higher electron densities were possible than with
a glow discharge and the UV cesium source. Some troubles
were encountered, however, and they will be discussed later
in this chapter.

Description, Calibration, and Performance of the Equipment Used to Generate an Ionized Gas

1. Vacuum System

The vacuum system consisted of a high vacuum pump, a noble gas source, a cesium vapor source, and a pyrex ionization chamber. A schematic diagram of the whole system is given in Figure 5.

The noble gas souce was a small tank of "Reagent Grade" noble gas from Matheson Company with a maximum impurity level of 8 ppm for argon, 59 ppm for neon, and 10 ppm for helium. In order to control the filling rate of noble gas for the system and to avoid over-pressure accidents, small vacuum valves were placed on either side of the needle valve. An oil manometer was placed in the noble gas system along with the thermocouple gauge to measure pressures from 1 mm Hg to 35 mm Hg and to calibrate the thermocouple gauge.

The thermocouple gauge was calibrated against the oil manometer for each of the noble gasses used. The method used is as follows. The small-volume noble gas system was closed off and filled to a high pressure (approximately 20 mm Hg). The cesium manifold and chamber was then closed off from the vacuum system and the noble gas system valve opened. Pressures were read on the manometer both before and after opening the valve and from these pressures the volume ratio of the whole system to the noble gas system was calculated. Then, using much lower starting pressures, the process was repeated and the final

pressure was read on the thermocouple gauge. Thus with

the known initial pressure and the volume ratio, the

correct final pressure could be calculated and compared

with the thermocouple gauge reading. This process was

repeated at several room temperatures to get temperature

dependence.

Impurities were no problem for the RF discharge.

The vacuum pump was capable of obtaining a vacuum of approxi-

mately 2×10^{-7} torr. When the vacuum valve between

the pump and the rest of the system was closed, the pressure

was found to rise to about 2 to 3×10^{-6} torr and level

off. The impurity level in the gas was very small, as

has been mentioned. The system was operated closed, so

there was a potential for the impurity rise indicated above

to be important. For this reason, phase and attenuation

data was taken with the system closed for a 3 hour period.

No measurable change in these data was observed, however.

A scale drawing of the pyrex chamber is shown

in Figure 4. The two end plates were matched for minimum

reflection of 12×10^{9} cps microwaves. It will be noted

that the probes were extended into the chamber as far as

possible without intersecting the microwave beam.

2. The Langmuir Probe System

Bi-polar probes were used to determine electron temperatures (18). The probes themselves were of the "hairpin" type to allow them to be run at red temperature. The circuit diagram for the probes is given in Figure 6.

Two separate 12 volt auto batteries were used to provide current for heating the probes. The current was limited by the transistor circuit shown.

The power supply consisted of the potentiometer circuit shown in Figure 6. A potentiometer circuit was chosen to insure smooth voltage variation from -45V to +45V. The potentiometer was driven by a slow-speed, reversible synchronous motor to insure smooth and easy data taking. The power to run the circuit was supplied by 45 and 90V radio batteries.

When probe data were taken from the RF discharge, both probes were grounded through capacitors to insure that no RF voltages from the RF field reached the probe measuring devices. All probe circuitry was also carefully shielded to eliminate noise pick up.

It will be noted that the probe current went directly from the probes, through the resistance box to the power supply to insure maximum accuracy in measurement. The "probe voltage" was taken directly off the power supply and differs from the actual probe voltage by the IR drop of the probe-current resistance box.

This IR drop was calculated and found to be negligible for any operating conditions of interest in this experiment. The probe-current resistance box consisted of a series of switchable precision (1%) resistors connected in parallel. The voltage across these resistors was placed across the y input of an x-y recorder. The voltage across the power supply was placed across the x input of the x-y recorder. Then by running the synchronous motor, probe curves were automatically traced out. This system was calibrated against a high impedance-high sensitivity Simpson multimeter which had been previously calibrated to better than 1% accuracy. The system was found to give readings within 2% of the Simpson readings.

It will be noted that the potentiometer carries 45 mA and so the power supply will be overdriven if more than about .45 mA is drawn by the probes. This maximum current rating was never exceeded.

3. The RF discharge.

The RF discharge was excited with RF energy supplied from a Barker and Williamson 100 watt transmitter. The frequency used was 7.1×10^6 cps. Some tests were made to see the effect of changing frequency on the discharge generated and no effect was noted over a frequency range of 6.8×10^6 to 8.0×10^6 cps. Higher frequencies were not used because the output power of the transmitter was reduced and control of the power output was more difficult.

The LC resonant circuit used to couple the trans-
mitter output into the gas is shown in Figure 7. The vari-
able position inductive link shown provided an excellent
means of controlling power into the gas and thus con-
trolling electron density generated in steady-state operation.

The keying circuit in the transmitter provided
a means of obtaining and measuring the properties of a
transient ionization source. A square wave generator was
used to trigger a transistor switch (Figure 7) which was
hooked up to the keying circuit of the transmitter.
When the switch was on, the RF power was on. When off,
the RF power was off and the ionized gas started to decay.
By varying the width and repetition rate of the square
pulse, it was possible to vary the on and off time of the
RF energy in such a fashion as to maximize peak electron
density and insure that the ionized gas had time to decay
between pulses.

The method used to obtain phase and attenuation
data is best given in terms of Figure 8. The signal from
a detector on the magic tee was displayed on the scope and
the microwave bridge nulled with no ionization in the chamber.
A decay curve appeared on the scope when the repeating
transient ionization source was turned on. When the
phase shifter was changed, a dimple appeared in the decay

curve. The dimple pointed at the time at which the electron

density reached the value indicated by the phase shifter.

The attenuator was then used to lower the dimple to the

null line and this was the attenuation of the source at

the electron density previously noted.

Thus, with the RF discharge, two methods were

available to obtain the attenuation versus electron density

data desired.

The maximum electron densities obtainable from

an RF discharge were of critical importance in testing

the theories. It has been noted that the quantity

$ck\omega/\omega^2$ must be measurably different from unity in order

to differentiate the theories. The effects of $ck\omega/\omega^2$

are clearly discernible for frequencies of 12×10^9 cps

if electron densities of the order of 60×10^{10}/cc can

be obtained. Attenuations at low ($n_e < 7 \times 10^{10}$) electron

densities can only be used to measure collision frequencies

ν_{eff}. These values are also of theoretical importance

however.

Since maximum electron densities are so important,

curves of maximum obtainable electron density versus pressure

for helium and neon are given in Figures 9, 10. It will be

noted that both neon and helium reach the required density

range for differentiating the theories. Plots of the

average electron temperature of the electron gas as deter-
mined by probe measurements versus gas pressure for helium
and neon are given in Figures 11, 12. A quick calculation
of collision frequency shows that for the electron temper-
atures measured and for the pressures of maximum electron
density for neon, the attenuation due to collisions is too
small to be measured accurately. Thus the helium RF
discharge was the only one of interest in this experiment.

Gaps will be noted in Figures 9, 10 in the .5
to 7 mm Hg range. These gaps represent pressures at which
high luminosity disks and balls were formed in the RF dis-
charge. Photographs of them are given in Figure 13.
The attenuation versus electron density curves showed
strange behavior while these disks and balls were present.
There was even some amplification of the microwave beam.
The amplification is believed to be due to a combination
of beam focussing and interference effects between incident
and reflected waves caused by the strange density profiles
associated with these balls. In any case, data in the
.5 to 7 mm Hg pressure range were found to be useless for
the problem of interest here.

The position of the RF electrodes was changed
to determine its effect on the electron density profile

and thus on the phase and attenuation measured. No effect
was noted on phase and attenuation data taken in the high
and low pressure ranges.

When a disk was present, as in helium at 4 mm Hg
pressure, reduction of the distance between electrodes caused
a similar reduction of the thickness of the disk with an
increase in the amplification of the beam. This increase
in amplification of the beam continued until the electrode
spacing could no longer be reduced because of the neck
on the chamber.

In an effort to improve maximum obtainable den-
sities in the high pressure region (5 - 20 mm Hg), a
Penning mixture (26) of neon and argon was tried in the
RF discharge. No measurable increase in maximum density
was observed. A cesium ionization seed was also tried.
With this mixture a considerable improvement was noted.
The maximum density is given in Figure 9 for the cesium-
helium mixture.

CHAPTER V

EXPERIMENTAL RESULTS

The results of the Langmuir probe curves and
the microwave phase and attenuation measurements will be
presented in this chapter. These results are conveniently
analyzed in terms of certain neutral-gas pressure ranges
which determine the type of discharge observed. For con-
venience, the pressure range which yielded strange attenu-
ation data will be referred to as the "medium pressure
range" (see Figure 9). All pressures below the medium
range will be referred to as belonging to the "low pressure
range". All pressures above will be in the "high pressure
range". It will be noted that the largest change in ioni-
zation characteristics takes place in the medium pressure
range.

A. Langmuir Probe Results

Typical high and low pressure range probe curves
are given in Figures 14, 15. The low pressure curves are
seen to be symmetrical and pass through the origin. The
ratio of the saturation currents for each probe is approxi-
mately the same as the ratio of probe areas as theory would
demand. The high pressure curves, however, are seen to
be shifted considerably from the origin on the current axis.

49

It is important to note the experimental con-
ditions extant while probe measurements were being made.
Conditions were different for high and low pressure measure-
ments. Typical photographs of the glow under high and low
pressure conditions are given in Figure 16. It will be
noted that the probes are out of the glowing region under
high pressure conditions, but are not out of the glow
under low pressure conditions. This may indicate that high
pressure probe curves are not typical of the electron gas
seen by the microwaves but that the low pressure curves
are.

The probe curves obtained without heating the
probes to dull red temperature were unsymmetrical and
sloppy and tended to indicate very high electron temperatures
(10-15 ev) and very low electron densities (3 to 4 orders
of magnitude less than the values observed by phase shift
measurement). However, higher probe temperatures (up to
cherry red) had no effect on the probe curves. For this
reason, all probe curves were taken with the probes at
dull red temperature.

The method used to obtain electron temperatures
and densities was the same as that used by Johnson and
Malter (18). Sample calculations of electron temperatures
and densities for both high and low pressure curves are
given in Appendix E-1.

The average electron temperatures obtained under
steady-state operating conditions for high pressure helium
are given in Figure 18 as a function of helium pressure.
It was found that the electron temperature did not vary
much as a function of electron density over the small
density range obtainable at these high pressures, so the
average value of electron temperature is given at each
pressure indicated.

The electron temperatures obtained under steady-
state operating conditions for low helium pressures are
given in Figures 24, 25, 26. The electron temperatures
are plotted against electron densities which were observed
when the probe curve was taken. Three plots are given
corresponding to three pressures in the low pressure
range.

B. Microwave Results from the High Pressure Discharge

Phase-attenuation data were taken for helium
both in the steady-state and in the transient modes of
operation. These data were used to calculate effective
collision frequency ν_{eff} which was corrected to a stan-
dard neutral density by the formula ν'_{eff} $(T_{n_0}P_0T_c)$ =
$\dfrac{T_n}{T_{n_0}} \dfrac{P_0}{P} \nu_{eff}$ and plotted against pressure in Figure 17.

A sample calculation of v'_{eff} is given in Appendix E-2.
No attempt was made to plot attenuation versus electron
density because the maximum density obtainable in this
pressure range was small even when augmented with cesium
seed. However, curves for two electron densities are
shown in Figure 17. The electron temperature corresponding
to the steady-state values of v'_{eff} in Figure 17 are given
in Figure 18.

Some uncertainty in the neutral pressure and
temperature measurement was encountered. It was found that
the neutral pressure increased about 8-12% upon turning
on the RF transmitter. The neutral temperature as indicated
by the chamber wall temperature, on the other hand, increased
only about 3-7%. If the pressure increase were due solely
to the heating of the neutral molecules by the RF field,
compensating temperature and pressure changes would be
expected to keep neutral density constant. Obviously this
did not occur, so other effects must be investigated.
One possible way to explain the discrepancy is to note
that adsorbed noble gas may have been driven out of the
walls of the chamber to account for the extra gas. It
is known from the outgassing time required after filling
with noble gas that some noble gas was adsorbed on the
surface of the vacuum system or in the neoprene and teflon
seals of the noble gas system. Another way to explain

the discrepancy is to note that the chamber wall temperature
may have been different from the temperature of the gas
within the chamber. The gas was probably dense enough
to support a temperature gradient. The neutral molecule
mean-free-path was never more than .2 mm for experimental
conditions of interest. Also, the heat transfer process
from the outside of the chamber was more efficient than
transfer from the noble gas to the chamber walls because
of the higher gas pressure outside of the walls. The pro-
cedure used for calculation was to assume that the pressure
and chamber wall temperatures were correct and then a
possible error of 5% (difference between pressure and
temperature increases) was assigned to the neutral density
results over and above the errors in measuring the thermo-
couples and the manometer. The whole error bar calculation
is given in Appendix E-2.

In order to test for the effects of attenuation due to
refractive defocussing, measurements of attenuation were
taken with several different diaphragm sizes on both the
primary and secondary horns. The results were calculated
as if the entire attenuation were due to collisions and
plotted in Figure 19.

C. Microwave Results From the Low Pressure Discharge

Phase and attenuation data were taken for helium both in the steady-state and in the transient modes of operation for four pressures in the low pressure range. The phase data were used to calculate electron density n_e and then plotted in the electron density versus attenuation plots shown in Figures 20, 21, 22. In order to correlate reflection coefficient oscillations with attenuation oscillations, a sample curve of reflection versus electron density is shown in Figure 23. The electron temperature corresponding to the electron densities and neutral pressures shown in figures 20, 21, 22 are plotted in figures 24, 25, 26. A sample calculation of ν_{eff} from these data is given in Appendix E-2. It will be noted that the electron densities achieved in this pressure range are large enough to be of interest in differentiating between the three absorption equations.

The uncertainty found in measuring the neutral gas pressure in the high pressure region was not found in the pressure measurements in the low pressure region. No measurable change was noted in the neutral pressure when the RF field was turned on. A small (1-2%) increase in temperature of the chamber was observed, however. It is believed that the reason a smaller pressure change

due to RF was observed is that the ionization process
itself is more efficient in this pressure range and so
less of the RF energy was expended in heating the neutral
molecules and in knocking gas out of the chamber walls.

Again in the low pressure region, measurements
of attenuation at a certain phase were taken for several
different beam-limiting diaphragm sizes. The results
were calculated as if the attenuation was due to collisions
and plotted in Figure 27.

CHAPTER VI

DISCUSSION OF RESULTS

Two tests are required to evaluate the three absorption formulae of Chapter II. First, values of effective collision frequency and corresponding electron temperature are required to test the relation between collision frequency, electron temperature and scattering cross section. Second, the dependence of radiation absorption on electron density for a constant collision frequency is required to test which treatment of the dispersion of the medium is correct.

It was discovered that a sensitive means of carrying out both tests was to calculate collision frequency using each of the three absorption equations, reduce these collision frequencies to a common value of neutral density and electron temperature, and then plot ν_{eff} versus electron density. The correct theory should then give no dependence of ν_{eff} on electron density. This procedure has been carried out and the method used to obtain the results is presented here. Also, an evaluation of the data for error is presented.

A. Discussion of Langmiur Probe Results

The electron temperatures obtained from the Langmuir probes are potentially subject to several systematic experimental and theoretical errors as well as the obvious random errors in current and voltage measurement. These systematic errors will now be discussed.

The experimental problem which gives the most drastic and the most easily observed error in the electron temperature measured by Langmuir probe curves is oxide and impurity contamination of the surface of the probes. Even after chemical cleaning, degreasing, and outgassing, the probe curves obtained were uneven, sloppy, and gave high electron temperatures (~12 ev) until operated at dull red temperature. When the probes were heated, however, the curves were improved (Figure 15). There is no way to guarantee that high temperature operation is sufficient to completely eliminate the impurity problem. Experience with low temperature operation indicates that if the probe temperatures are still in error from surface impurities, they will be too high. It is possible that the adsorption of gas on probe surfaces causes the odd probe curves obtained in high pressure RF discharge. This is not thought to be too likely, however, since adsorption is expected to occur on both probes equally and thus should not give the asymmetric probe curves observed.

Another problem which could be important in this experiment comes from the position of the probes with respect to the chamber walls. Probe temperature data taken with a mono-polar probe in a glow discharge indicate that electron temperatures observed for probes positioned in or near the boundary sheath are considerably higher than temperatures observed in the core of the discharge. Temperatures taken in profile across the core, however, are independent of position. Thus, although the source used was not a glow discharge, there is some reason to believe that probes positioned within the boundary sheath will give too high a temperature, while probes anywhere else will give a good average temperature for the plasma. The probes used in this experiment were positioned near the edge of the chamber to avoid microwave reflections, but visual observation of the probe position with respect to the glowing gas showed that the probe was not within the sheath for low pressure discharges (Figure 16). For the high pressure discharge, the probe was not within the glow, so some doubt is cast upon the measurements made there.

In any experiment using Langmuir probe techniques, it is important to determine if the current drawn by the probes is enough to disturb the ionized gas significantly. If the current drawn is too large, the region around

the probes is depleted of electrons and the electron and
ion currents entering the probe sheath will not be indepen-
dent of the voltage across the probes. This problem is
usually not significant for equal-area bi-polar probes,
however, because the ion current rather than the much larger
electron current is the limiting factor in the current drawn.

There are several design parameters which will
affect the accuracy of the electron density determined
by a bi-polar probe but have little effect on the electron
temperature determined. These parameters affect only the
effective area of the probe sheath for absorbing electrons
and ions. It will be noted from Figure 4 that the two
wires of the hairpin probe are very close together.
If the sheaths are large enough, they may merge into one
sheath and the effective area calculated on a basis of
unmerged sheaths will be too large. Another possibility
is that whether the sheaths merge or not, one wire may
"shadow" the other wire. In either case, the effect on
the electron density calculated would be to lower it,
but the electron temperature should be uneffected. Cal-
culations indicate that the sheaths should not interfere
for conditions of interest in this experiment but the
accuracy of the sheath diameter calculations is not very
good, so the densities obtained from the Langmuir probes
may be somewhat low.

Care must be taken to insure that current due
to leakage, photoelectric emission, and thermo-electric
emission is small compared to current from the ionized
gas, or erroneous electron densities and temperatures will
result. The current from these sources was small for
the RF discharge. Both calculations of the magnitude of
the effects and measurement of the current-voltage curve
without the ionization present showed a negligible
effect.

The most important theoretical consideration
in the use of the Johnson and Malter theory to interpret
bi-polar probe curves is the electron energy distribution
function. If the distribution is Maxwellian, the theory
applies; if not, the theory does not apply. Bi-polar
probe theory is critically dependent upon this consider-
ation since only the highest energy electrons are sampled
to make the curve, and the high energy region is the first
to show the breakdown of the conditions which create a
Maxwellian distribution. For example, it has been shown
(19) that the energy distribution of a glow discharge is
not Maxwellian. In fact, there is even some experimental
indication that a high energy group forms in glow discharge.
Thus bi-polar probe measurements in a glow discharge may
be expected to be in error. Measurements done here on a

glow discharge indicate that electron temperatures measured
by bi-polar probes do indeed differ from temperatures ob-
tained by other methods and may be as much as an order of
magnitude too high.

Theory shows finally that the Johnson and Malter
technique for obtaining probe curves is valid only if an
average of one electron-neutral collision or less takes
place within the sheath volume surrounding the probe.
If many collisions take place within the sheath, diffusion
processes control the absorption of current by the probes
and equations used by Johnson and Walter are no longer
valid. Calculations (see Appendix E-1) show that only one
collision or less will take place within the sheath for
the low pressure discharge but at high pressures
(~ 10 mm Hg) about three collisions will take place.
Diffusion effects would be expected to reduce the amount
of current reaching the probe at saturation which, in turn,
would decrease the electron density and increase the elec-
tron temperature given by the probe curves. Thus the high
pressure discharge temperatures are again in doubt.

Finally, the electron densities obtained from
the probe curves are a little more than an order of magni-
tude below the average electron density as determined by
phase measurements for both the low and high pressure

discharges. The low density values for the low pressure discharge would be expected since a peaked density profile is expected in this pressure range and the probes are near the edge of the chamber. However, the low electron density observed in the high pressure discharge is not expected since recombination controls the discharge and the profile should be flat. Thus there is evidence that the previously mentioned problems in connection with the determination of electron temperatures in the high pressure discharge do operate to make the observed values erroneous. On the other hand, there is no reason to doubt the low pressure electron temperatures.

B. Discussion of Microwave Data from the High Pressure
   RF Discharge.

The value of ν'_{eff} for this steady-state RF discharge given in Figure 17 are notably oscillatory. The oscillations may be due only to random scattering of the observed attenuation or they may be due to interference of incident and reflected waves, but the latter possibility is thought to be more likely. In either case, the steady-state mean line shown should represent the pressure variation of the collision frequency for a pressure variation of the electron temperature given in Figure 18. The effective collision frequency ν''_{eff} corrected to a standard

neutral density and electron temperature by the formula

$$\nu'_{eff}(T_{n_0}P_0T_{e_0}) = \sqrt{\frac{T_{e_0}}{T_e}} \frac{T_n}{T_{n_0}} \frac{P_0}{P} \nu_{eff}$$

using the mean ν'_{eff} of Figure 17 and the electron temper-
atures of Figure 18 is given in Figure 28 as a function
of pressure.

The electron temperature corresponding to each
value of ν'_{eff} for the afterglow ionized gas in Figure
17 was taken to be chamber temperature since the electron
thermalization time is of the order of microseconds while
the decay times observed are on the order of milliseconds.
The values of ν'_{eff} corrected for changes in chamber
temperature with pressure are given in Figure 18.

A check of the magnitude of the electron-ion collision
frequency indicates that it is always small compared to
the electron-neutral collision frequency in the high pres-
sure range. Also, the collision frequency of the electrons
with the chamber walls is small compared to the electron-
neutral collision frequency because the mean-free-path
of the electrons in the gas (< 1 mm) is much less than
the distance from the beam edge to the walls
(> 1 cm).

With respect to the plot of ν'_{eff} versus beam-
limiting diaphragm diameter (Figure 27), two things should
be noticed. First, no measurable difference in collision
frequency is apparent for diaphragm diameters greater than
2 inches. Second, some oscillation and a dramatic fall-
off in collision frequency is measured for diaphragms
of diameter less than 2 inches. Since simple theory
indicates that attenuation of a beam due to refractive
defocussing should be linearly dependent upon primary
and secondary diaphragm diameter, the first observation
is taken as evidence that refractive defocussing is small
in the high pressure region. This might be expected since
recombination controls the discharge in this pressure
range and the density profile would be expected to be
nearly flat. The second observation is taken as evidence
that diffraction effects on the beam become important
when the diaphragm diameter is reduced to less than 2
inches. This conclusion is justified when one recalls
that the wave length of the 12×10^9 cps waves used is
about one inch. Thus at 2 inches, the diaphragm diameter
is nearing the wave length which is the condition for
diffraction to become important.

A cursory look at the discharges of Figure 16
might lead one to believe that the discharge has a bright

disk at each end of the chamber which, in turn, may indi-
cate a high density zone near the boundary. This is not
actually true. The bright areas which appear near the
ends of the chamber are caused by the nearby RF electrodes
and are only about 1/8 inch thick. The volume of gas
that the microwave beam passes through is of a uniform
color and light intensity. This is at least one indi-
cation that even if the density profile is peaked, the
variations are smooth from boundary to center for dis-
charges in the low and high pressure ranges.

The main contribution to the probable error for
data in the high pressure range are from the measurements
of attenuation and pressure. The probable error in the
attenuation was determined by taking several attenuation
measurements for a given neutral pressure and electron
density. The maximum scatter in the data was used as the
probable error. The largest portion of the probable
error in the pressure measurement came from the anomalous
increase in pressure observed after the discharge was turned
on. This error has already been discussed.

C. Discussion of Microwave Data from Low-Pressure RF
   Discharges.

It is the attenuation-electron density data given
in Figures 20, 21, 22 that supply the means to test which

treatment of the dispersion of the medium is correct.
It will be shown later that some of the attenuation in
these plots is due to refractive defocussing and some
of the attenuation is due to collisions. If the electron
density profile in the direction perpendicular to the cylinder
axis is the same for equal electron densities regardless
of whether the data was taken under steady-state conditions
or in the afterglow, then the observed difference between
the steady-state and the transient curves must be due
to the lower electron temperature in the afterglow ioni-
zation. A simple subtraction of attenuation for the two
modes of operation will yield the change in attenuation
due to the change in electron temperature. From these
data, collision frequencies for the high electron temper-
ature condition can be calculated by use of each of the
three absorption formulae of interest. Then the resulting
collision frequencies can be corrected to a standard
neutral density and electron temperature and plotted
against electron density. The collision frequencies from
the correct formula should be independent of electron
density. This procedure has been carried out but before
the results are discussed, several characteristics of the
data should be discussed.

It is apparent from Figures 20, 21, 22 that
refractive defocussing is an important effect in inter-
preting the low pressure attenuation data obtained. Further-
more, one would expect that it should be, since the pro-
file should be quite peaked (the discharge is diffusion
controlled in the low pressure range) and the effective
collision frequency is much smaller than in the high
pressure discharge.

Figure 27 gives the most obvious indication of
the effect of refractive defocussing. It will be noted
that as the diameter of the diaphragm on the primary horn
is reduced, the "effective collision frequency" is reduced
proportionately until the 2 inch diameter diaphragm is
reached, and then the drop off is even more dramatic.
The dramatic drop off for diaphragms smaller than 2 inches
is again taken to be an indication of diffraction effects
as in Figure 19. The reduction of "the effective colli-
sion frequency" is approximately linear with diaphragm
diameter in agreement with the simple refractive defocussing
theory given previously, and the line extrapolates to
zero "collision frequency." Thus there is some evidence
that none of the attenuation used to calculate the
"effective collision frequency" was due to collisions
but was instead due entirely to refractive defocussing.

A calculation of the attenuation due to collisions expected

from neon at the pressure and electron density used for

these measurements indicates that it is indeed negligible.

Similar curves are observed for helium for pressures less

than 200 cc Hg.

Another strong indication of refractive defocussing

is the fact that attenuation-density plots for Helium

pressures of less than 200 cc Hg are identical to within

error bars for both steady-state and transient operation

of the RF discharge. Since transient operation represents

a reduction of electron temperature of about two orders

of magnitude from steady-state operation, the attenuation

observed must be independent of electron temperature and

cannot be due to collisions.

Finally, the collision frequencies calculated

from low pressure attenuation values are much too large

to be caused by collisions. Furthermore, they are almost

independent of pressure; which is certainly not collision-

like behavior.

It is of critical importance to understand how

the density profile changes as the ionized gas decays.

This problem will now be considered. The density-attenu-

ation behavior for 200 cc Hg helium pressure provides clear

evidence of what happens at least to the diffusion limited

ionized gas. The attenuation is the same for a given elec-
tron density for either the steady-state or the transient
ionized gas, so the density profiles must be the same
since the attenuation in each case is due to refractive
defocussing. Recombination is not very important in
ionization decay even for the maximum pressure of interest
in this discussion (.79 mm Hg), but it is enlightening
to indicate what would happen if it were. If the recom-
bination were proportional to the square of the electron
density, one would expect the profile to flatten out as
the decay process progressed. Such a process would tend
to make the values of v_{eff}'' calculated too high at high
electron densities. There is at least some evidence, how-
ever, that the recombination term for helium is proportional
to the first power of the electron density (20). For this
case, the density profile should remain the same as for the
case when diffusion controls.

The curves of Figures 20, 21, 22 show oscillations
which, as noted before, are due to interference of incident
and reflected waves in the ionized gas. Note that the
oscillations in the attenuation-density curve for steady-
state operation closely follow those in the transient
operation curves. This behavior is expected, since the
maxima in these curves are determined by the path length

of the reflected wave in the ionized gas which is deter-
mined (for these low neutral densities) almost entirely
by the electron density. Also, comparison of Figure 21
with Figure 23 for the same operating pressure shows that
maxima in the reflection coefficient of the ionized gas
closely follow maxima in the attenuation as predicted
by theory. Even a small unexpected bump in the reflection
coefficient at $n_e = 66 \times 10^{10}$/cm is matched by an unex-
pected bump in the attenuation coefficient at the same
density.

It is now possible to consider in detail how the
low pressure data was treated. A sketch of the procedure
was given at the beginning of this section. Sample cal-
culations are given in detail in Appendix E-2.

The first problem encountered in the procedure
was how to draw a mean line through the oscillations
visible in Figures 20, 21, 22. Analysis previously given
indicates that for a linear attenuation versus electron
density plot, the mean attenuation curve should be approxi-
mately equidistant between the maxima and minima of the
oscillations. Thus, if the oscillations are small enough,
the mean attenuation curve should also be equidistant be-
tween maxima and minima for a log (attenuation in db)
plot. The mean lines of Figures 20, 21, 22 were constructed

equidistant between the maxima and minima of the oscil-
lations insofar as was possible. To check the error in
this procedure, a "center of gravity" line was drawn
through the oscillations and values of ν_{eff} were re-
calculated. The difference between these values and the
values obtained by the mean line was only a few per cent,
so the error from this cause is thought to be small.

Again, as with the high pressure discharge re-
sults, the electron-ion and electron-wall collision fre-
quencies were found to be small compared to the electron-
neutral collision frequency.

Since there is some variation in electron-neutral
cross section over the electron energy range of interest,
the collision frequencies were corrected for electron
temperature with the factor $\sqrt{\dfrac{T_{eo}}{T_e}} \dfrac{\sigma(T_{eo})}{\sigma(T_e)}$. The temper-
ature dependence of the cross section was obtained from
(4). The ratio of the collision cross sections did not
change the result more than a few per cent, however.

The results of the calculation of ν_{eff} for each
theory are given in Figures 29, 30, 31, 32. The error
bars shown require some explanation. The bars in Figures
30, 31, 32 represent _relative_ error. That is, it repre-
sents random error in determination of density, attenu-
ation, and electron temperature only. The error in neutral

density determination is not included since it would

apply equally to all data points. The probable error in

determination of attenuation includes two factors. First,

the error in repeating a data point on a given data run.

Second, the scatter observed in repeating a data point

for different data runs under idential temperature and

pressure conditions. In every case, different data runs

were taken on separate days. The probable error from these

effects was taken as the maximum scatter in the data.

The error in electron density represents only repeatability

error since separate-run data scatter for electron density

appears in the attenuation scatter due to the method

used to obtain attenuation scatter. The error in elec-

tron temperature has already been discussed.

The error bars in Figure 29 include all the

errors indicated above plus the error in neutral density

determination. In connection with neutral density deter-

mination, the value of v_{eff}'' determined for a pressure of

.56 mm Hg will be seen to be quite high. This discrepancy

is thought to be due to inaccuracies in pressure measure-

ment. This pressure is just between the most accurate

range for the thermocouple gauge and the oil manometer.

Finally, the results of this portion of the

experiment are believed to be quite free from systematic

errors such as calibration errors, etc., since the results
are obtained from a difference process. Thus systematic
error would tend to cancel when the low temperature attenu-
ation is subtracted from the high temperature attenuation.

CHAPTER VII

CONCLUSIONS

Since v''_{eff} has been defined in such a manner
as to correct the measured collision frequencies
to a given neutral density and electron temperature, it
should be independent of the electron density existant
when it was measured. It will be seen from Figures 30
through 32 that only those values of v''_{eff} calculated by
use of the K.O. absorption formula are within an error
bar of being independent of electron density. The average
value of the K.O. v''_{eff} at a given pressure is the value
plotted in Figure 29.

It is convenient to discuss the values of
obtained in terms of their equivalent collision proba-
bilities ($P_C (cm^{-1}mm\ Hg^{-1})$). From the high pressure
afterglow results, an average value of P_C of 20 ($cm^{-1}mm\ Hg^{-1}$)
was obtained for an electron temperature of .0381 ev.
The low pressure results give an average value of
22($cm^{-1}mm\ Hg^{-1}$) for an electron temperature of 1.30 ev.
The high pressure steady-state results yield a value of
5.4($cm^{-1}mm\ Hg^{-1}$) for an electron temperature of 7.00 ev.
All electron temperatures indicated were determined by
Langmuir probes except for the one given for the after-
glow results. These values for P_C may be compared with
the values from scattering experiments (4) where P_C is

18 $cm^{-1}mm$ Hg^{-1} @ kT_C = .0381 ev; 20 @ kT_C = 1.30 ev;

15 @ kT_C = 7.00 ev.

Agreement between observed values P_C from this

experiment and those from (4) is good except for those

measured in the high pressure RF discharge which are

very low. It is almost certain that this discrepancy

is due to error in the electron temperature measurement.

It has already been noted that electron temperatures in

the high pressure range may be expected to be too high for

several reasons. Lower electron temperatures would give

higher values of P_C.

The poor agreement of the classic absorption

formula with the electron density dependence of the data

is thought to be an indication that the classic transport

equation may not account properly for dispersive effects

of the medium. So many approximations were required to

obtain an absorption formula from the Maxwell-Lorentz

theory, however, the poor agreement of the ML formula

is thought to cast doubt only on the approximations, not

the theory itself. The results of this experiment are not

believed to be conclusive evidence of the validity of the

K.O. theory or the invalidity of the classic transport

theory or the Maxwell-Lorentz absorption formula pre-

sented here. Before a final statement can be made,

another experiment should be done which uses a different ionization technique and preferrably one which may be operated under conditions that make refractive defocussing effects negligible.
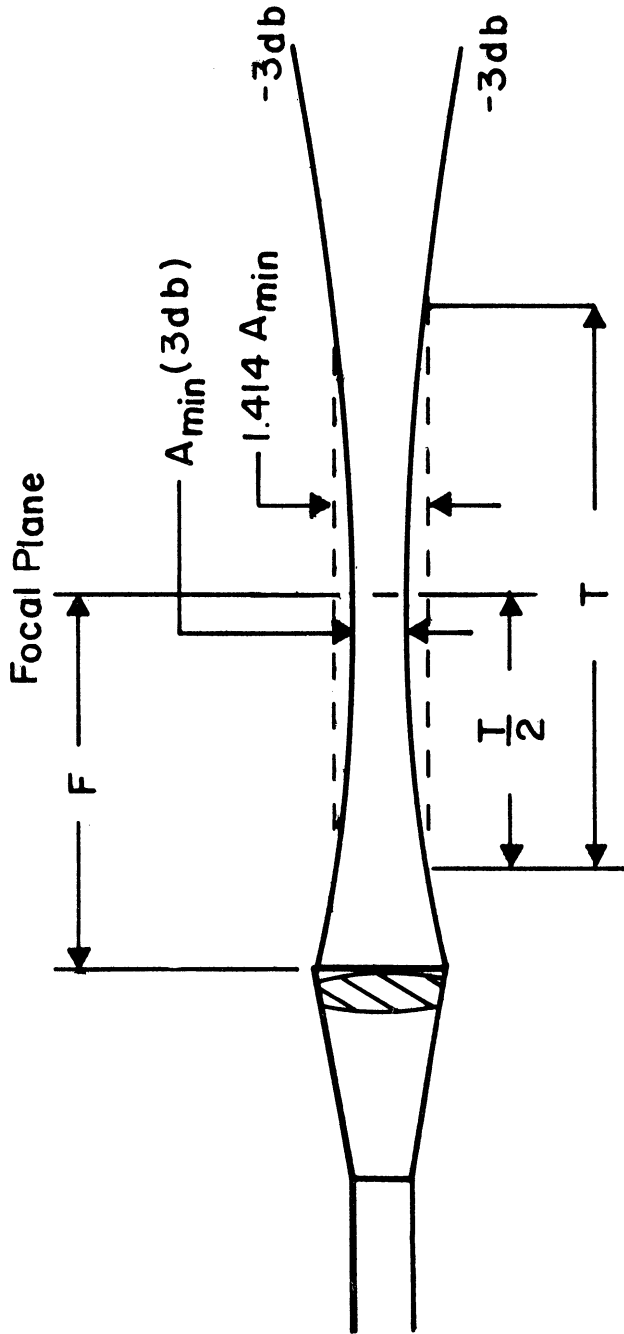
For the horns used in this experiment:

A = 2-1/2 in.

F = 8 in. (Horns can be as much as 22 in apart if necessary.)

T > 9 1/2 in.

Frequency - 12×10^9 cps $\pm .3 \times 10^9$ cps

Figure 1. Design specifications of the lens corrected microwave horns.
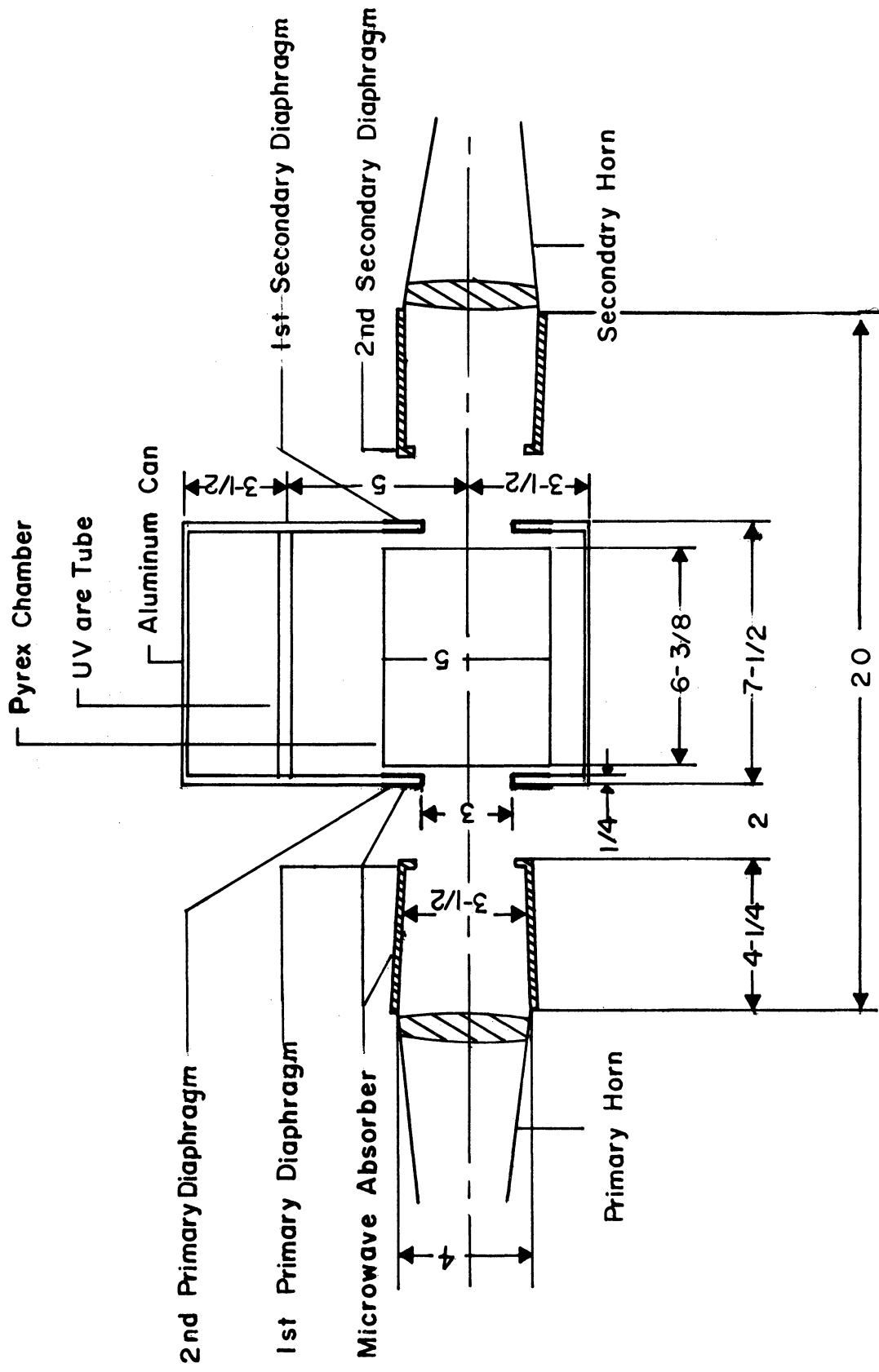
Figure 2. The Complete Experimental Assembly.
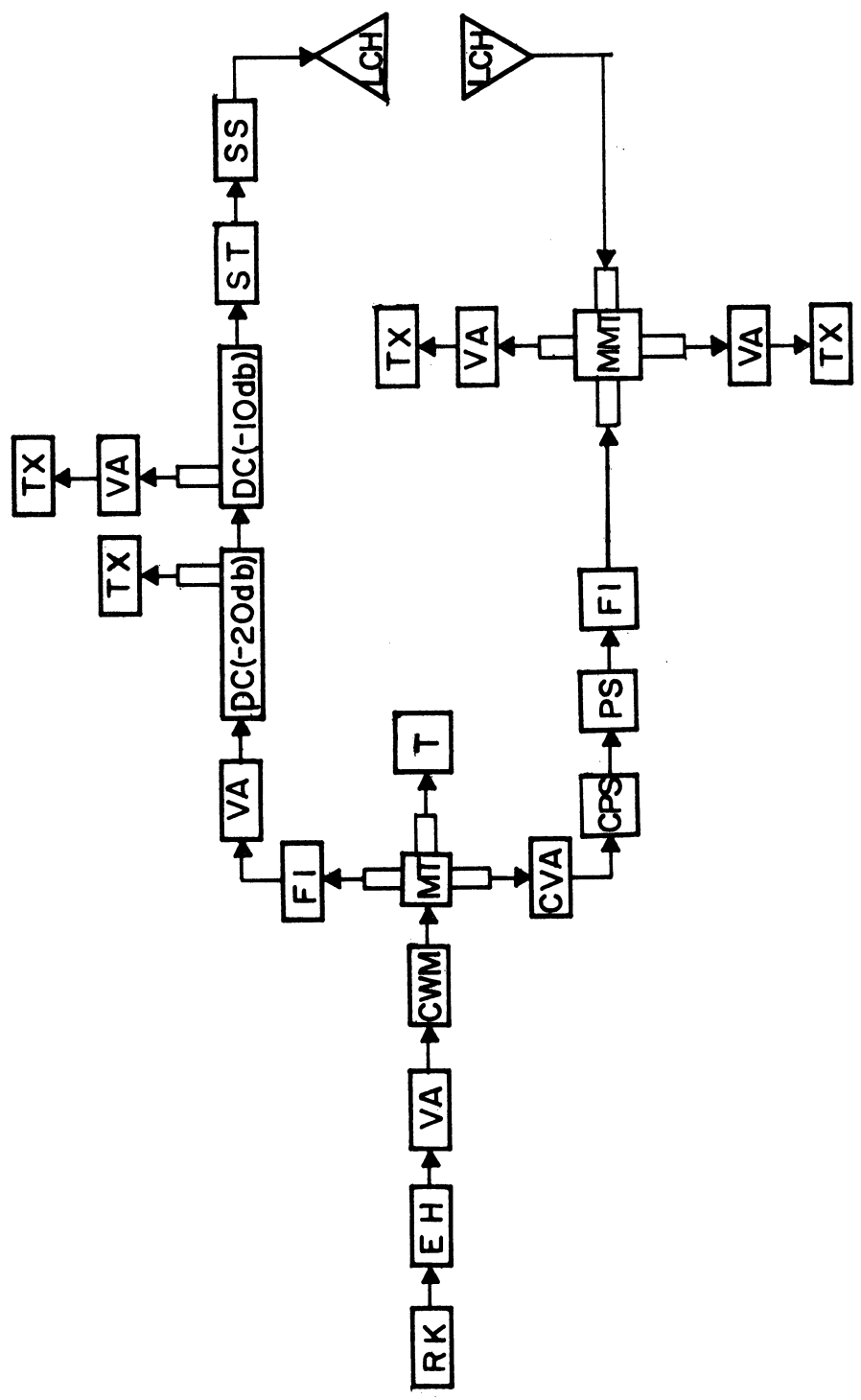
Figure 3. The microwave bridge system.
Notation: RK, reflex klystron; EH, E and H planetuner; VA, variable attenuator; CWM, cavity wavemeter (absorption type); MT, magic tee; T, termination; CVA, calibrated variable attenuator; FI, Ferrite isolator; CPS, calibrated phase shifter; PS, phase shifter; DC( ), directional coupler with coupling attenuation in parenthesis; Tx, tunable crystal mount; ST, variable stub tuner; SS, shorting switch; LCH, lens corrected horn; MMT, matched magic tee.
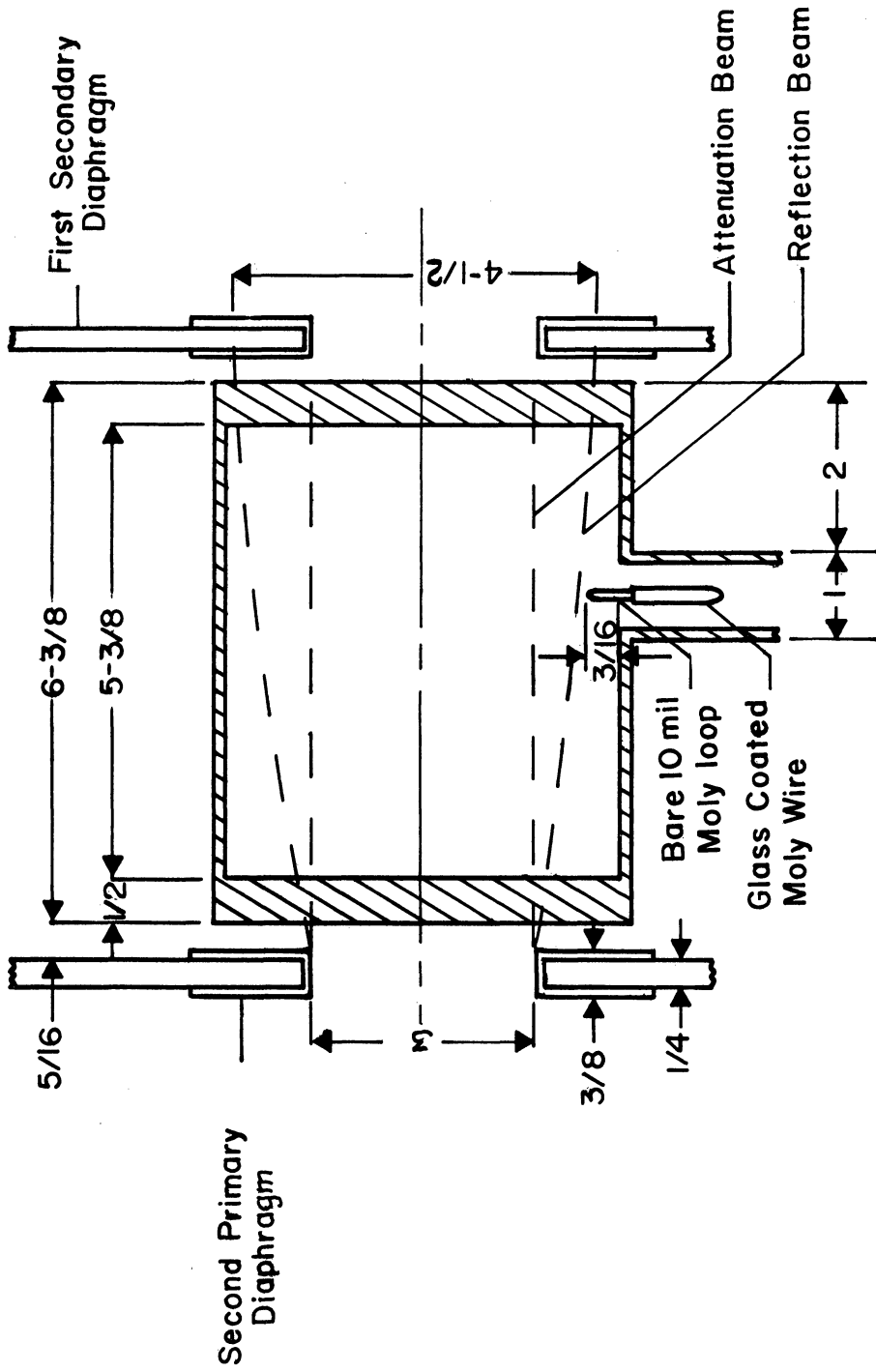
all dimensions in inches

Figure 4. The relation between the pyrex chamber, the Langmuir probes, and the microwave beam.
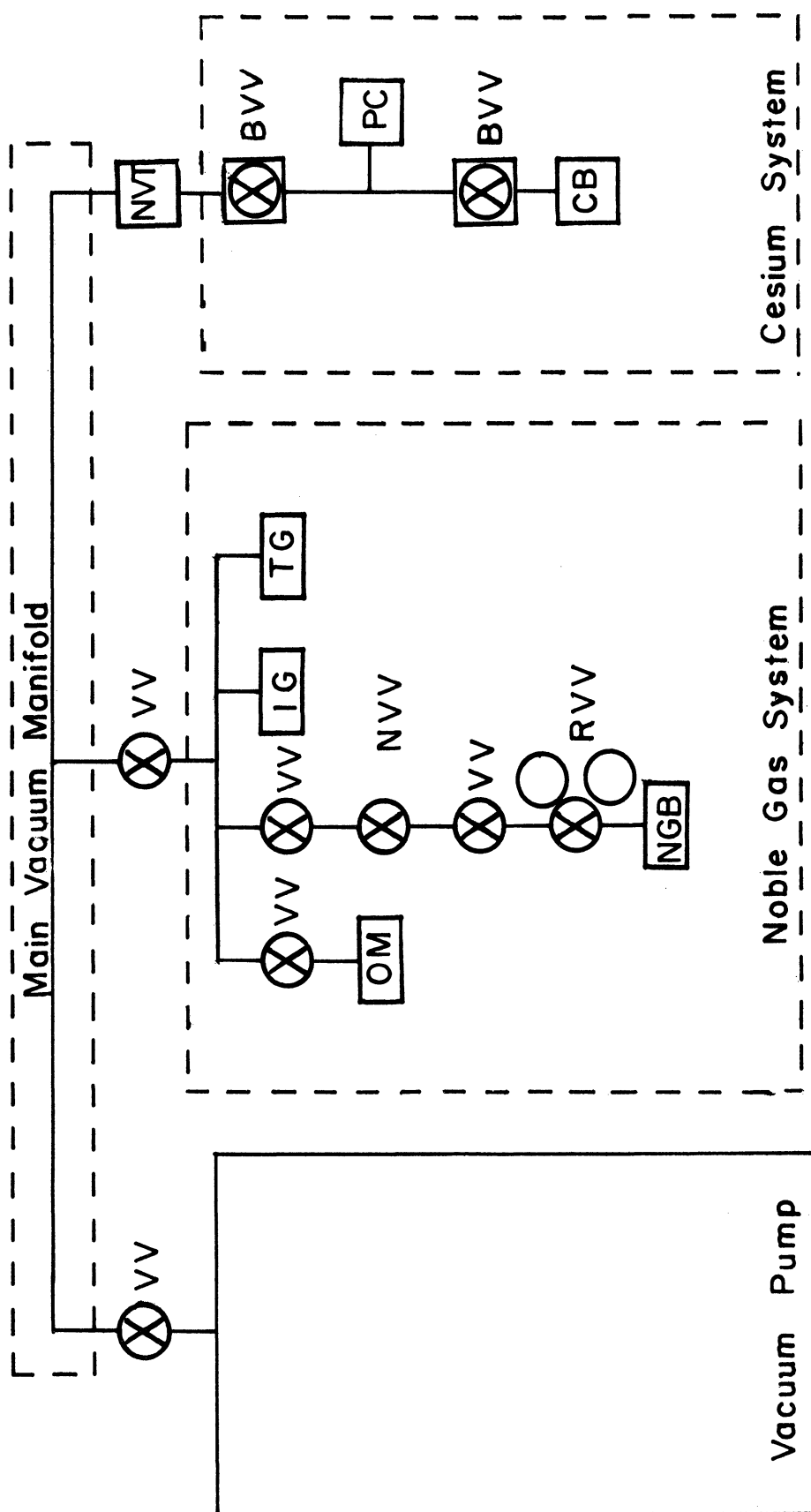
Figure 5. The vacuum system.
Notation: PC, pyrex chamber; CB, cesium bottle; NVT, liquid nitrogen-cooled
vapor trap; IG, ion gauge; TCG, thermocouple gauge; OM, oil manometer; NGB,
noble gas bottle; VV, vacuum valve; NVV, needle vacuum valve; RVV, regulator
type vacuum valve; BVV, bakable vacuum valve.
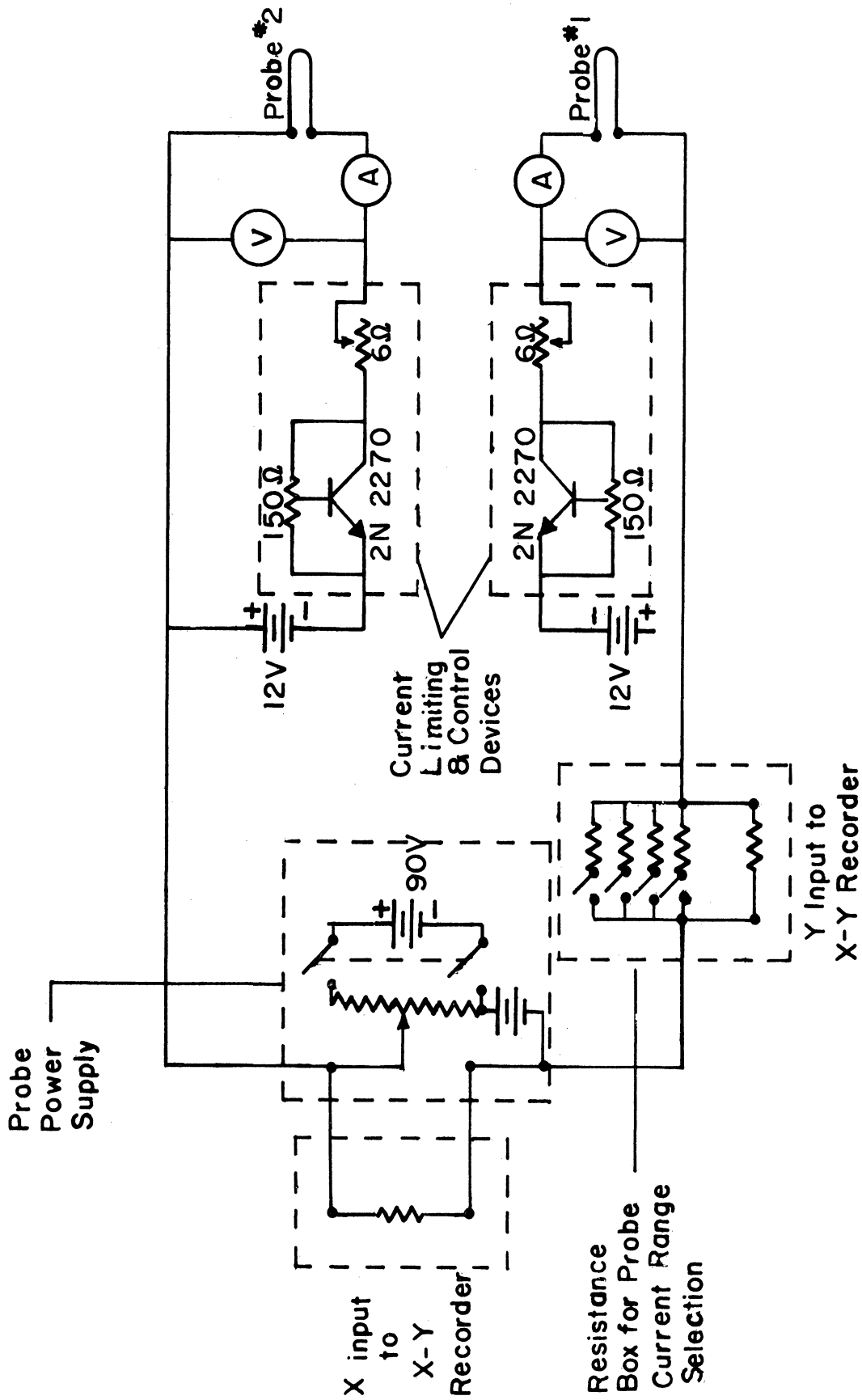
Figure 6. The probe circuit.

Tank circuit and steady-state control mechanism

B&W IOOW Transmitter

Vacuum Chamber
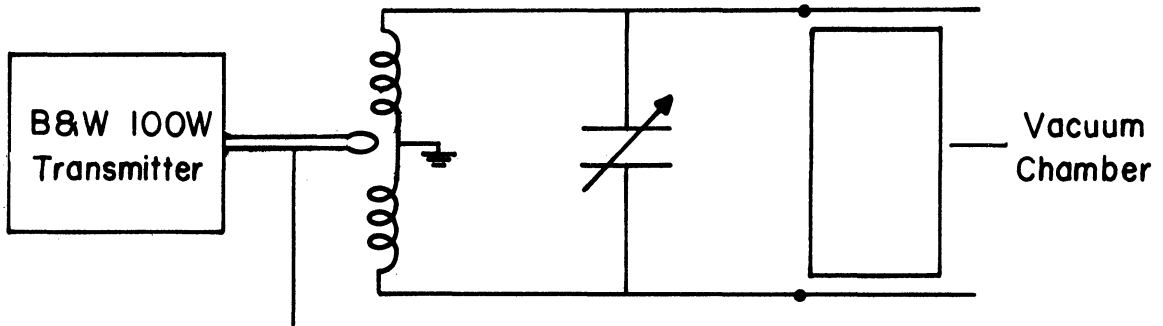
Mechanically movable link controls
RF field and thus electron density.

Switching circuit for control of transmitter
under transient operation

b

c

2N1893

e

4.7K

4.7K

Transmitter
Key Equivalent
Circuit

Square wave
Input
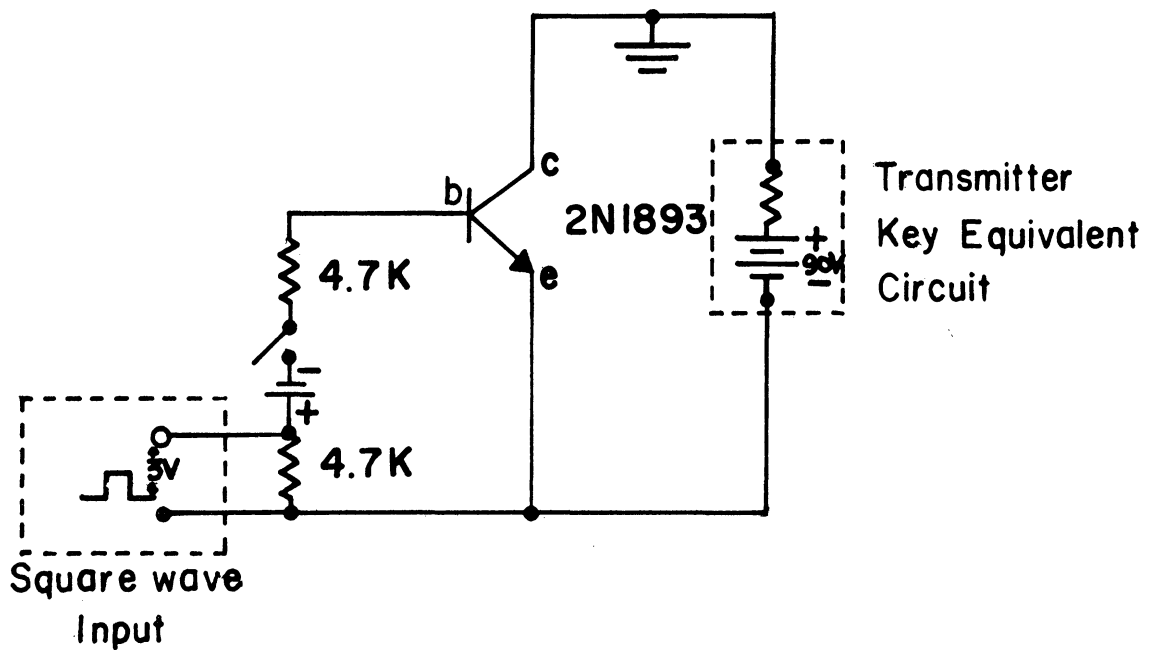
Figure 7. The RF control equipment.
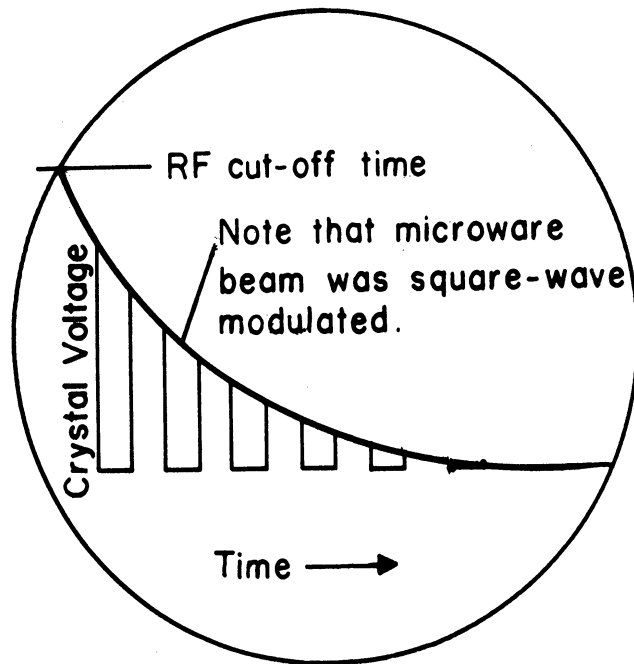
Oscilloscope display with the microwave bridge nulled
at the zero electron density condition (RF off)
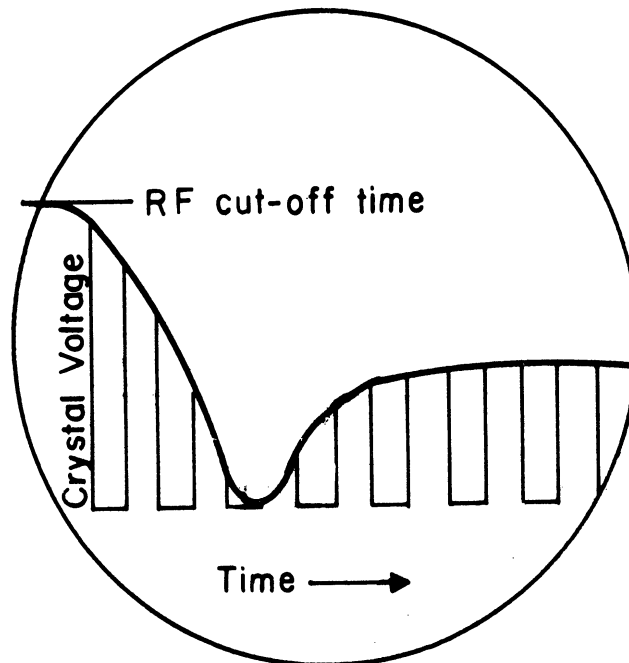
Oscilloscope display with the microwave bridge
nulled for a non-zero density and attenuation condition

Figure 8. The oscilloscope display for the discharge
operating under transient conditions.
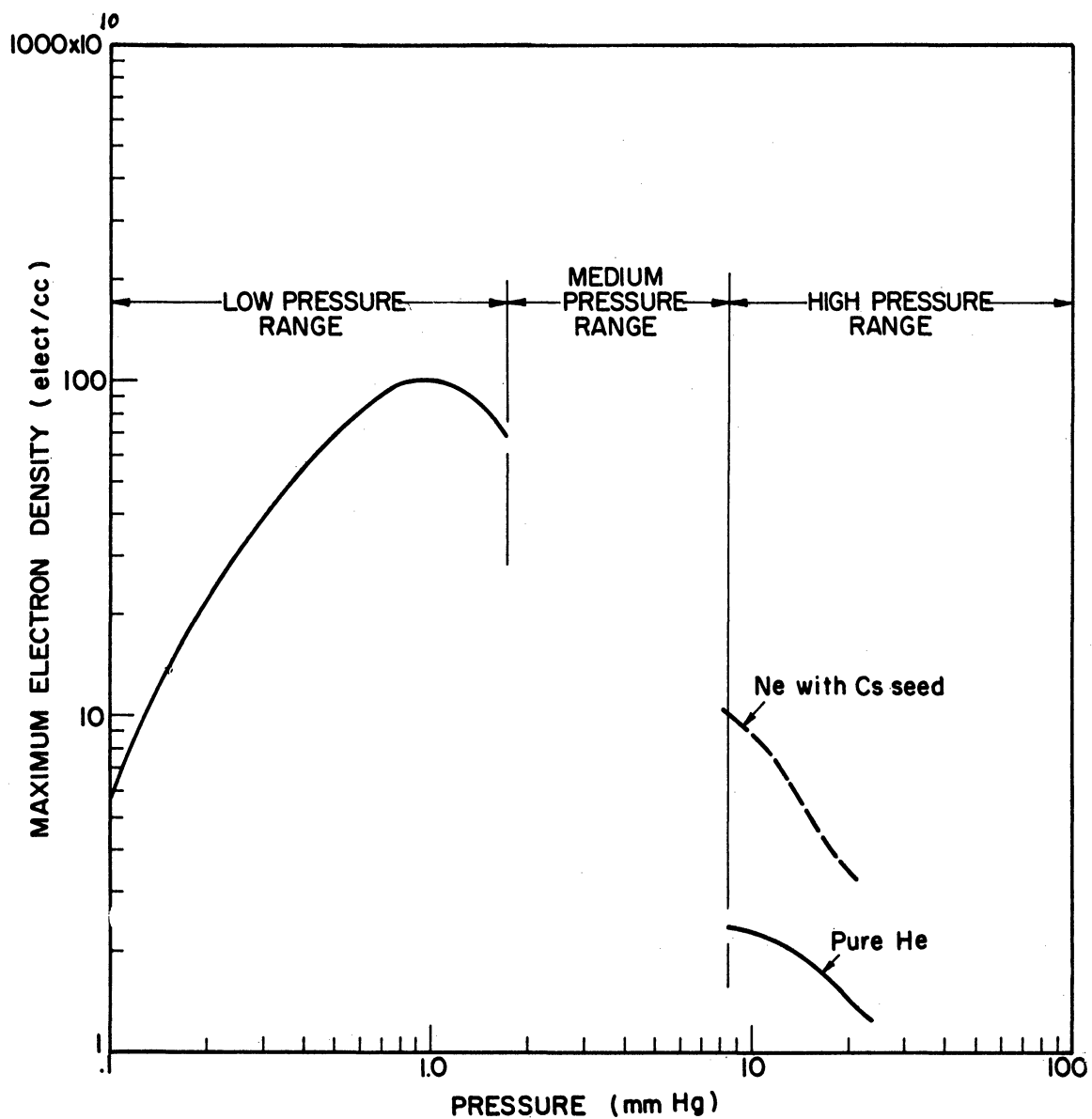
Figure 9. Maximum electron density vs. pressure for helium and for cesium seeded helium.
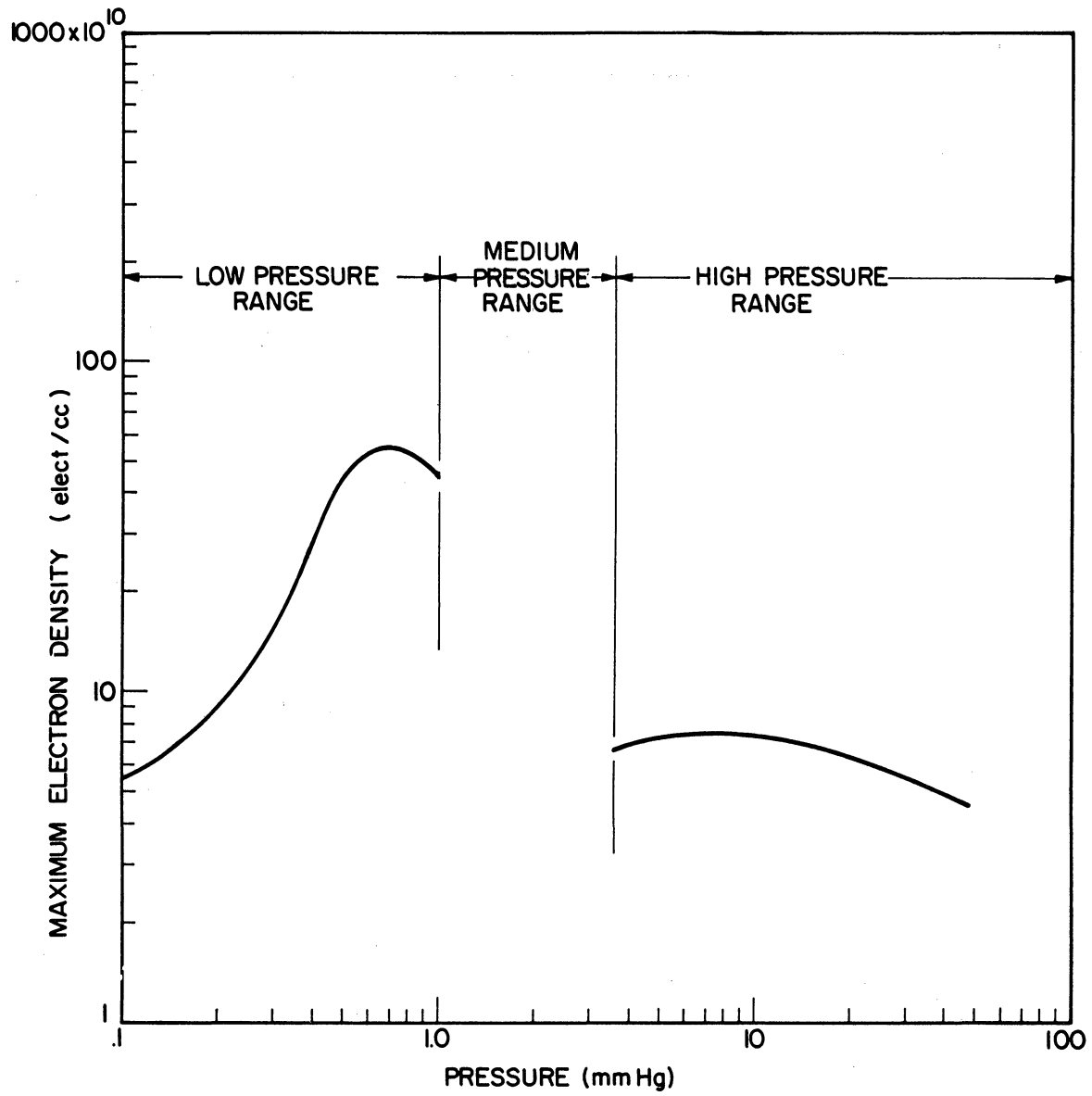
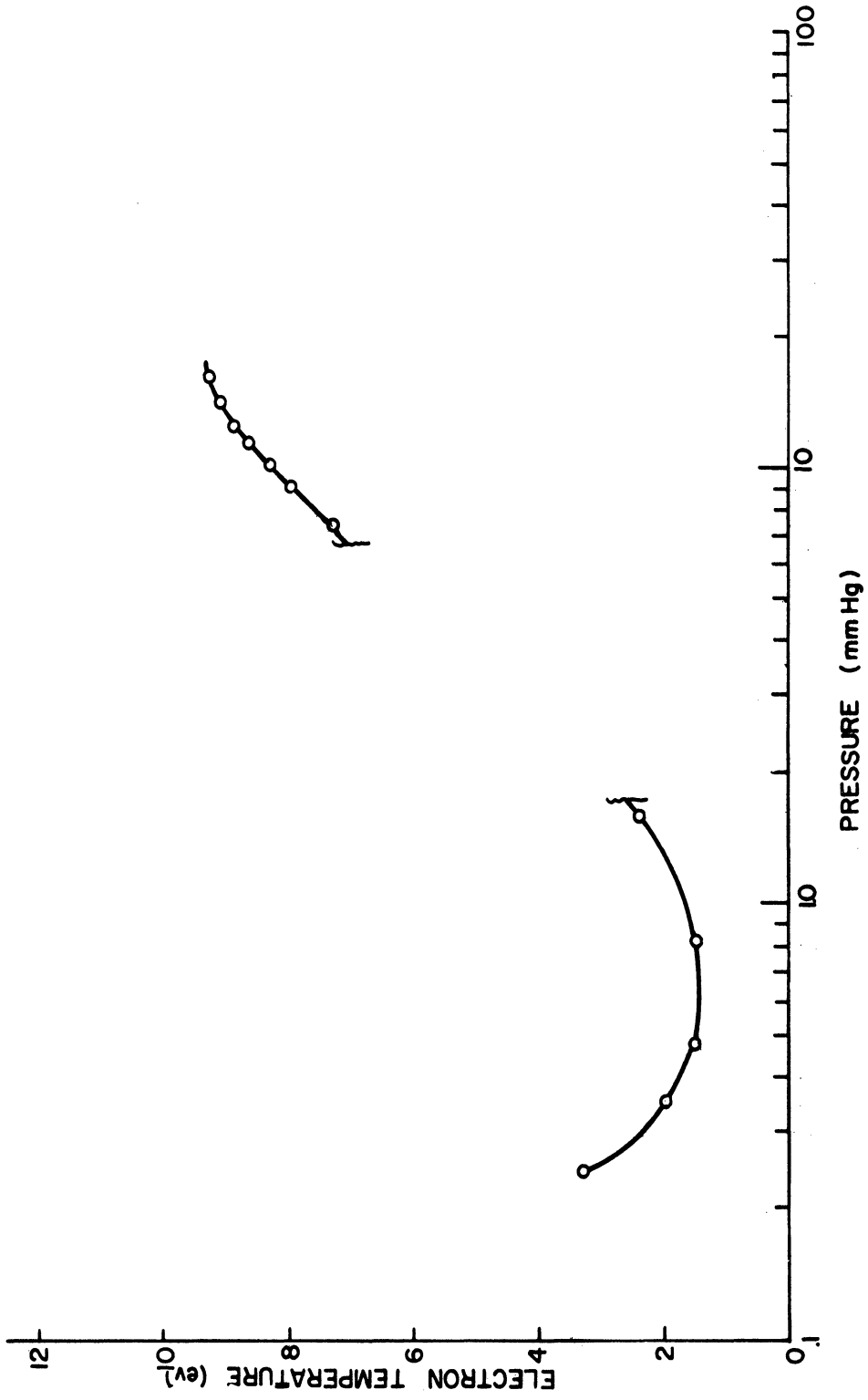Figure 10. Maximum electron density vs. pressure for neon.

Figure 11. Average value of electron temperature vs. helium pressure; temperatures calculated from Langmuir probe curves.
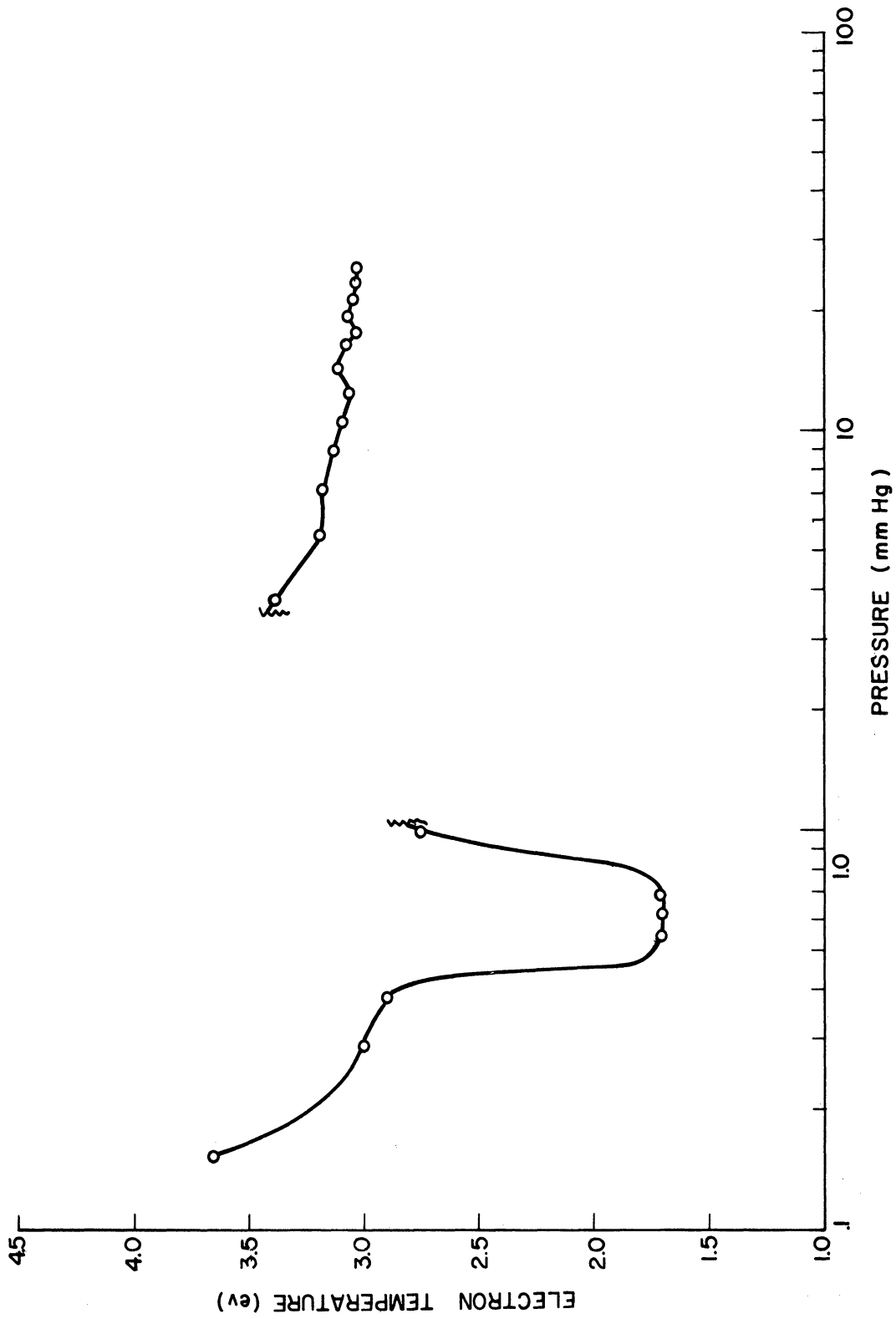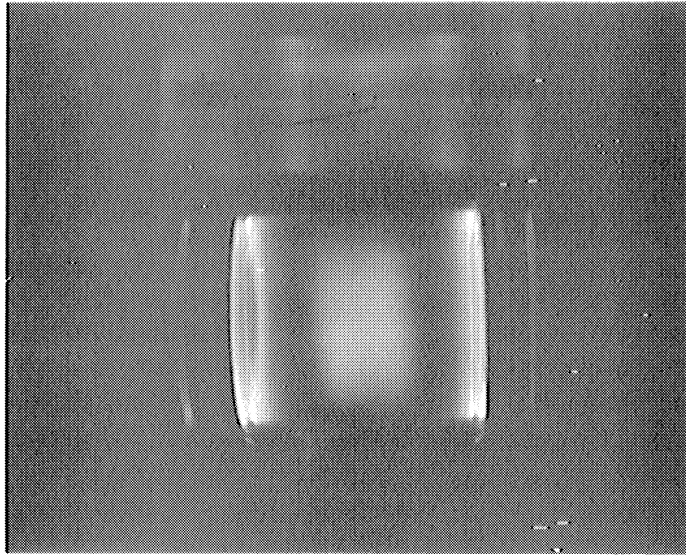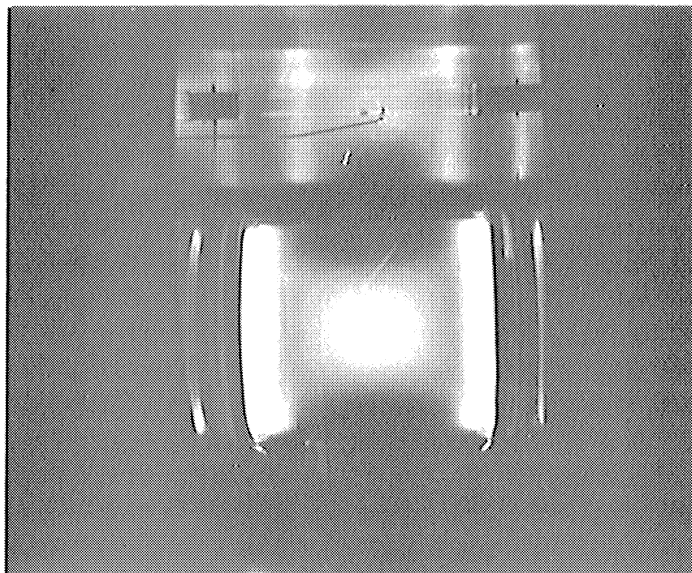
Figure 12. Average value of electron temperature vs. neon pressure;
temperatures calculated from Langmuir probe curves.

RF Discharge in Helium

$p \sim 5$ mm Hg $\qquad n_e \sim 6 \times 10^{10}$/cc $\qquad$ attenuation $\sim -.5$db

RF Discharge in Neon

$p \sim 2$ mm Hg $\qquad n_e \sim 5 \times 10^{10}$/cc $\qquad$ attenuation $\sim -.3$db

Figure 13. Photographs of the RF discharge in the medium pressure range.

Pressure -12.8 mm
Temperature $-340°K$
Electron Density $-1.77 \times 10^{10} / cc \left(\begin{array}{l} \text{from} \\ \text{phase} \end{array}\right)$
Electron Temperature -8.85 eV $\left.\begin{array}{l} \\ \end{array}\right\}$ $\left(\begin{array}{l} \text{from} \\ \text{probes} \end{array}\right)$
Electron Density $-5.9 \times 10^{8} / cc$

$$^i e_2 \mid_{V_d = 0} \quad = 30.3 \pm .4 \, \mu A$$

$$[\Sigma i_p]_{V_d = 0} = 64.6 \pm .6 \, \mu A$$

$$i_{p_1} = 37.5 \pm .4 \, \mu A$$

$$\Delta i_{p_1} \mid_{V_d = 0} \quad = 42.5 \pm .4 \mu A$$

$$\Delta V \mid_{V_d = 0} \quad = 22.0 \pm .4 \text{ Volt}$$

$$\Sigma i_p = 71.6 \pm .7 \, \mu A$$
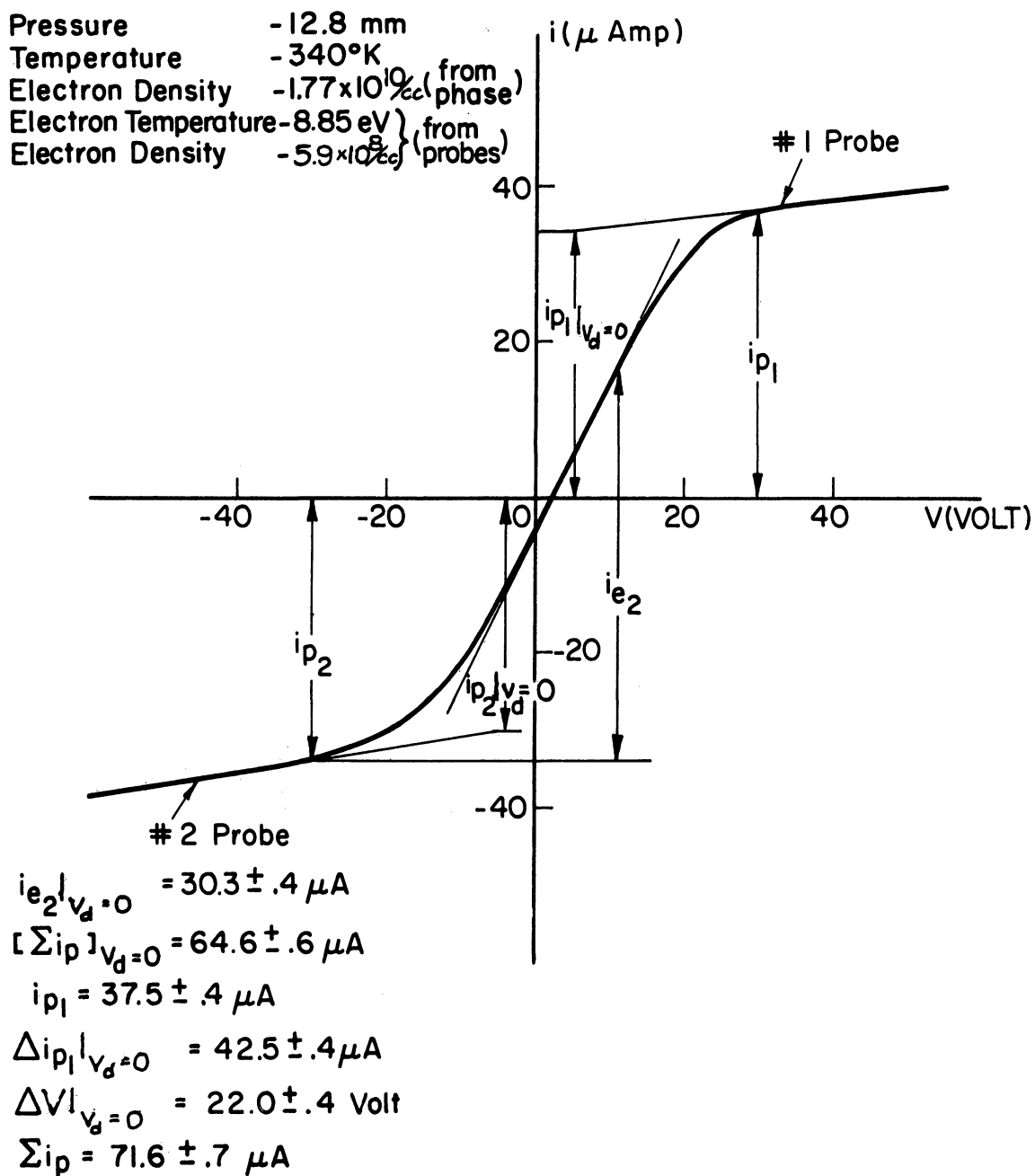
Figure 14. Typical Langmuir probe curve for helium in the high pressure range.

Pressure   -.562 mm Hg
Temperature - 319° K
Electron Density -60.9x10^{10}/cc (from phase)
Electron Temperature- 2.58 eV
Electron Density - 1.1×10^{10}/cc (from probes)

$i_{e_2}|_{V_d=0}$ = 123 ± 2 μA

$[\Sigma i_p]_{V_d=0}$ = 255 ± 3μA

i_{p_1} = 151 ± 2 μA

$\Delta i_{p_1}|_{V_d=0}$ = 151 ± 2μA

$\Delta V|_{V_d=0}$ = 5.4 ± .1 V

Σi_p = 288 ± 3 μA
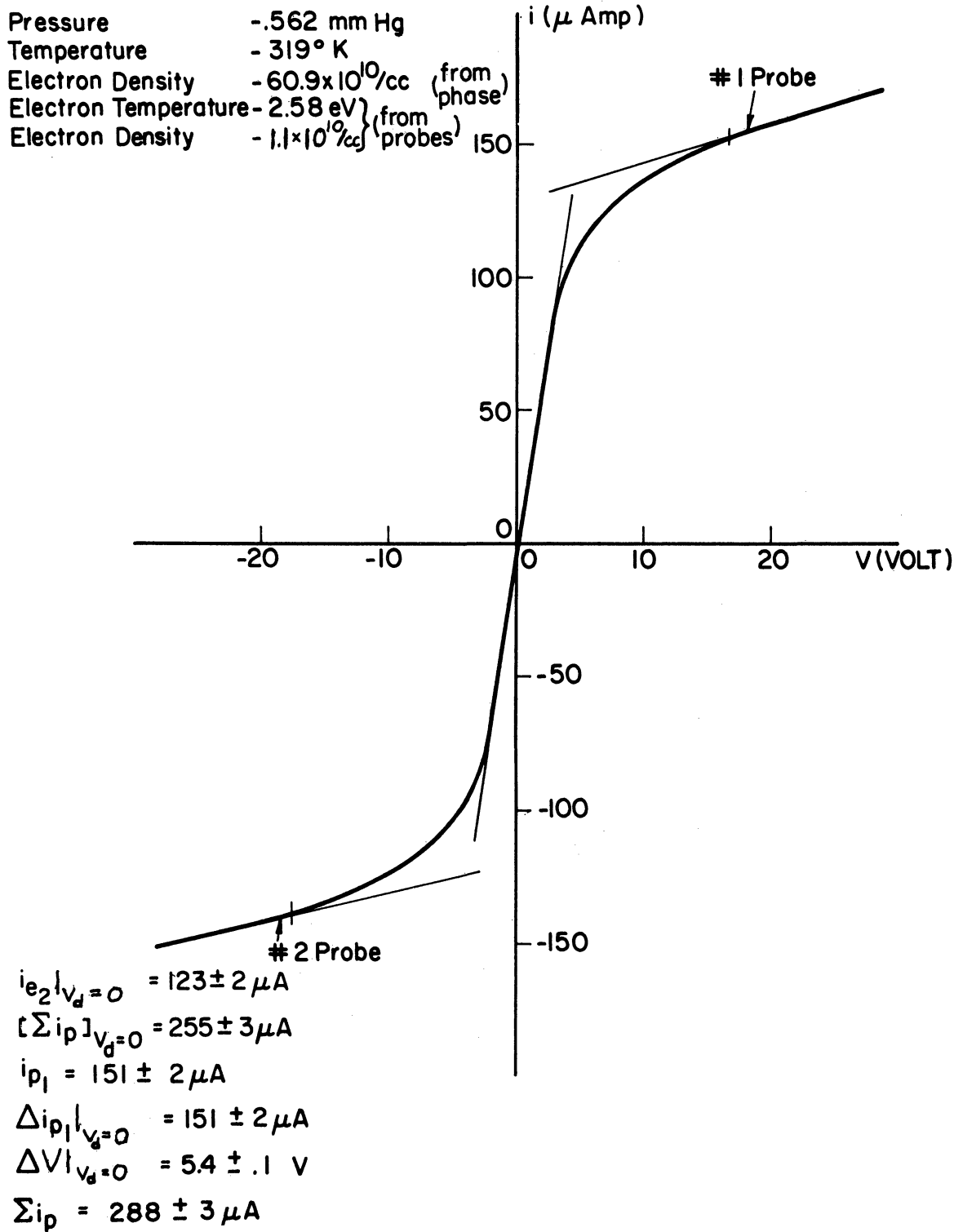
Figure 15. Typical Langmuir probe curve for helium in the low pressure range.
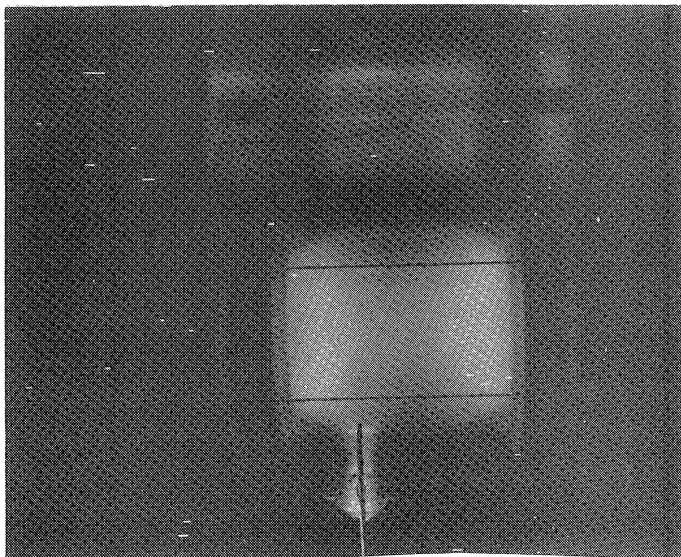
RF discharge in neon (p ~ .15 mm Hg, n_e ~ 16 x 10^{10}/cc); configuration is typical of both He and Ne discharges in the low pressure region. Note that probes (in bottleneck) do enter the glowing region but are completely clear of the microwave beam (inked lines).
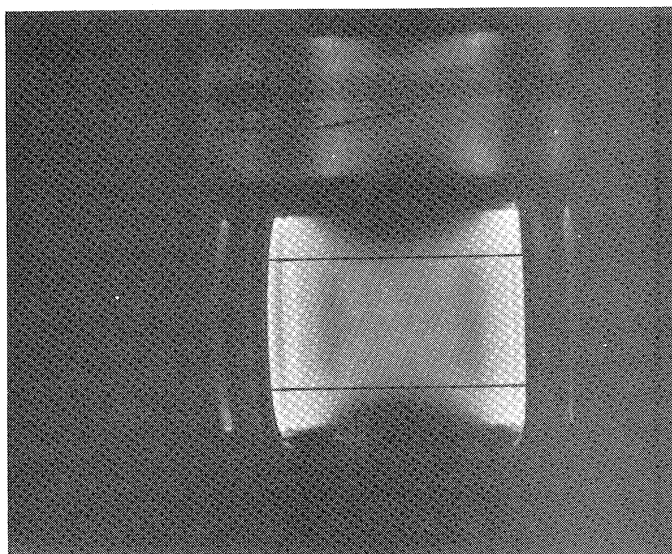
RF discharge in helium (p ~ 17 mm Hg, n_e ~ 2 x 10^{10}/cc); configuration is typical of both helium and neon discharges in the high pressure region. Note that probes (not visible in bottle neck) do not enter the glowing region but the microwave beam (inked lines) lies entirely within it.

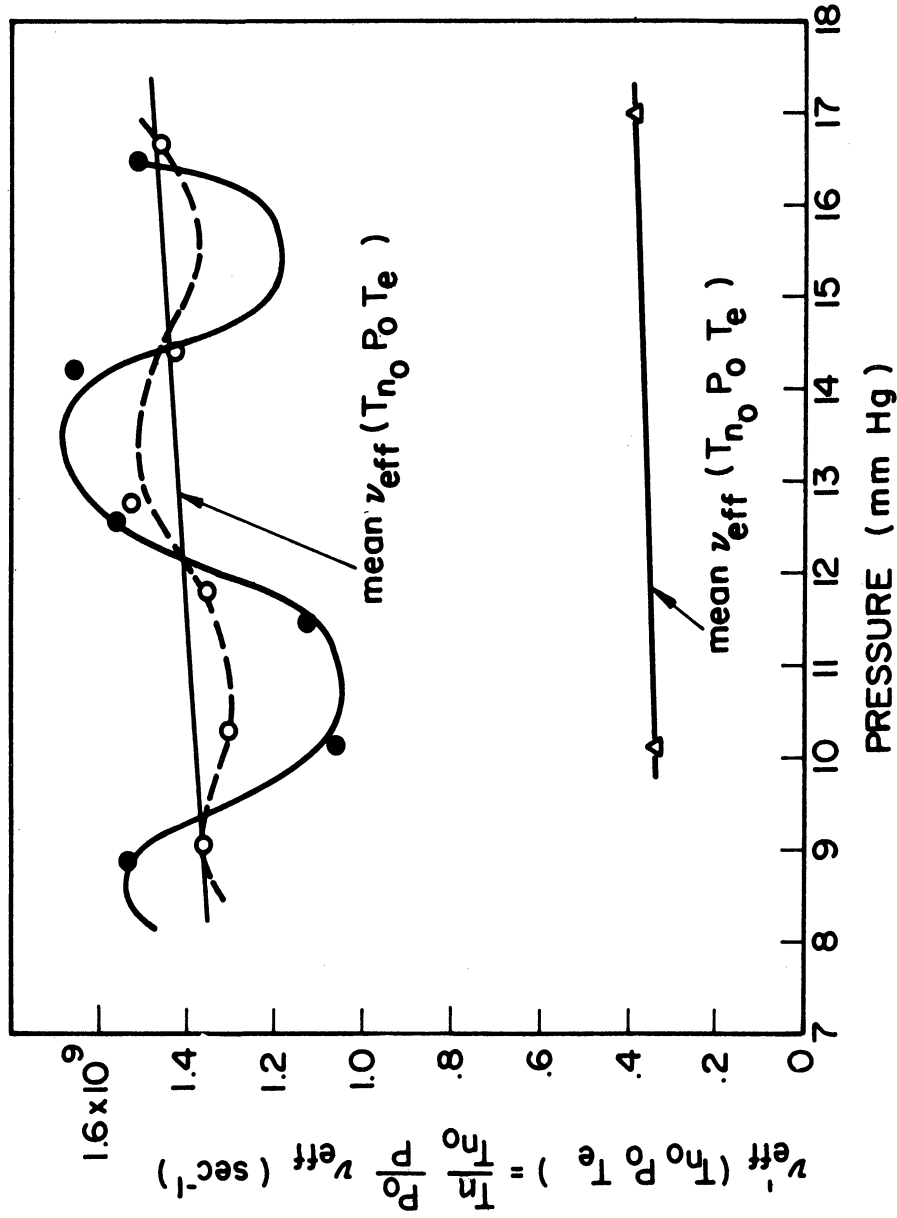Figure 16. Photographs of the RF discharge in the high and low pressure ranges.

Figure 17. Effective collision frequency $\nu'_{eff}(T_{n_0} P_0 T_e)$ versus helium pressure for both steady-state and decaying ionized gasses.
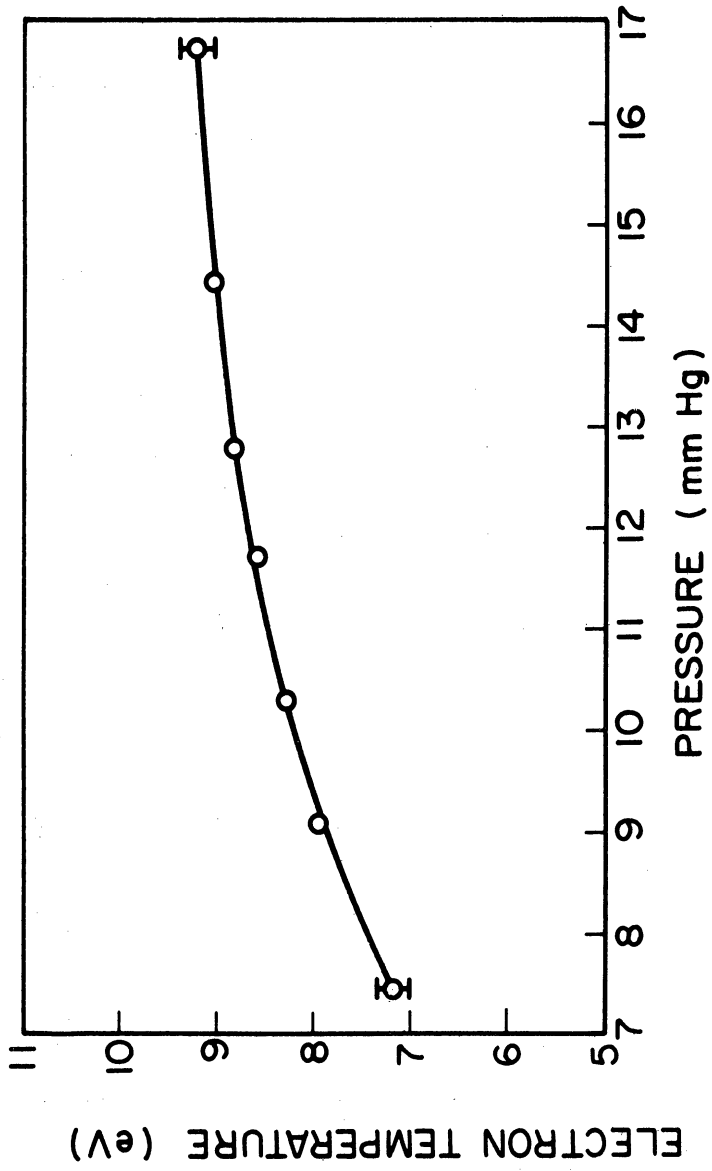
Figure 18. Average electron temperature vs. helium pressure for the steady-state RF discharge temperatures calculated from Langmuir probe curves.
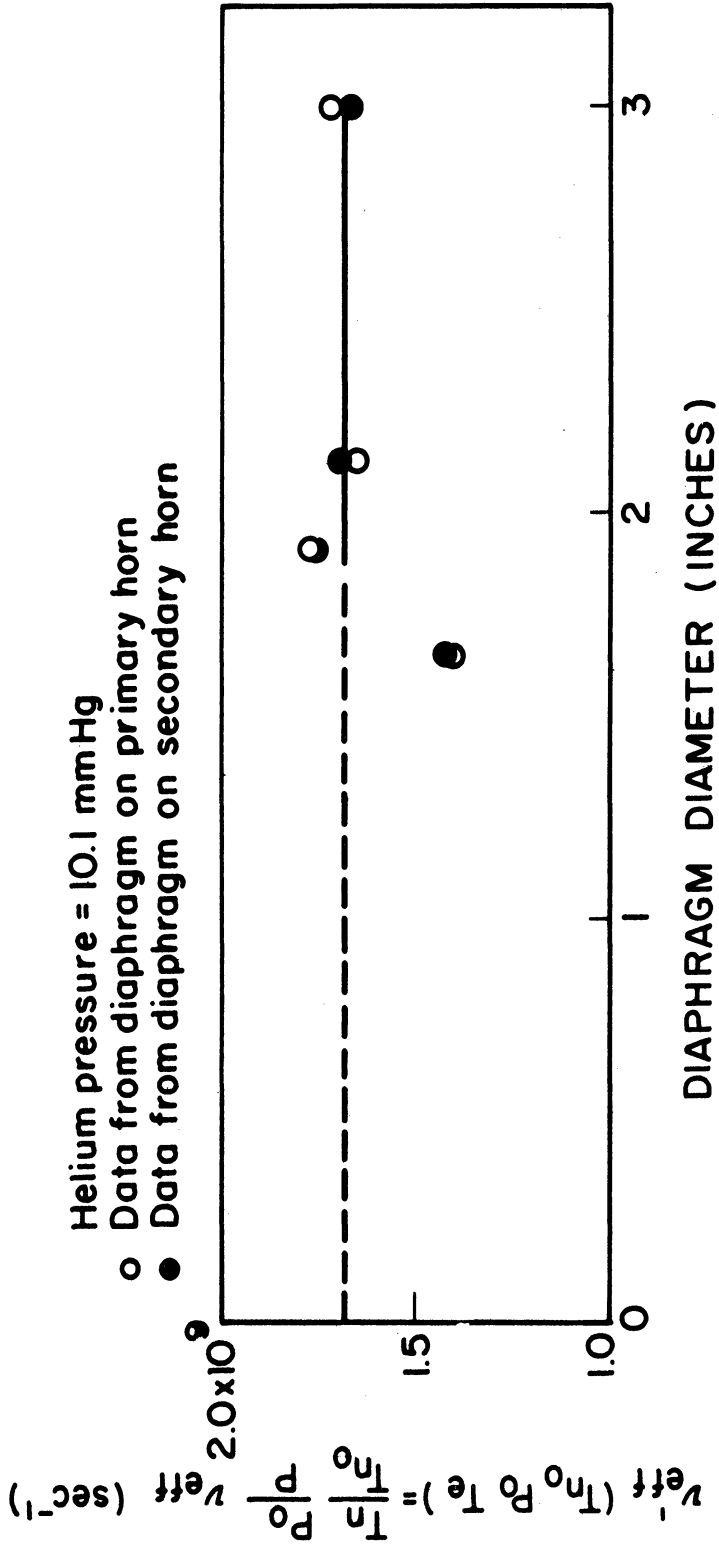
Figure 19. Effective collision frequency of helium ν'_{eff} $(T_{n_o} P_o T_e)$ versus diaphragm diameter.
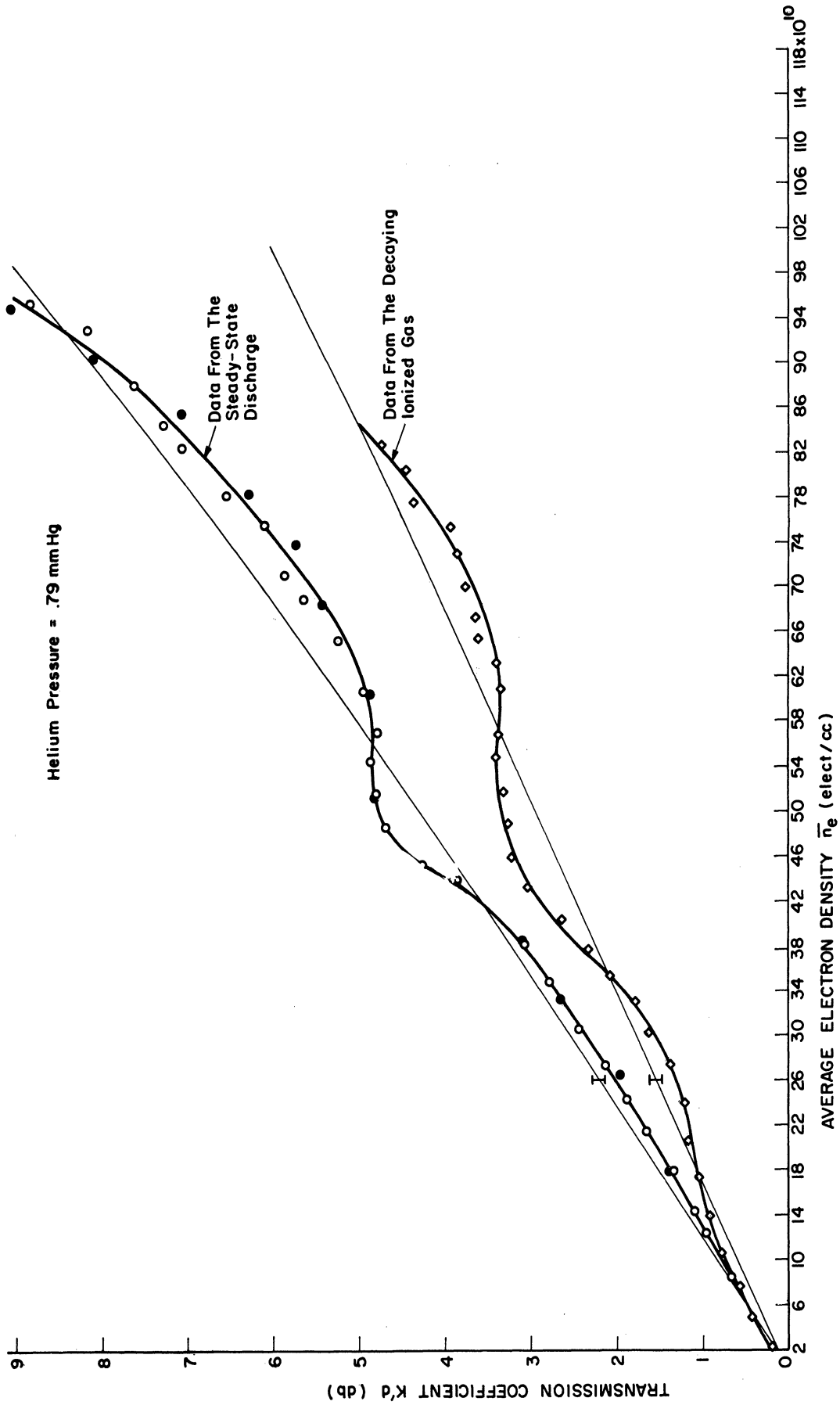
Figure 20. Transmission coefficient vs. average electron density.

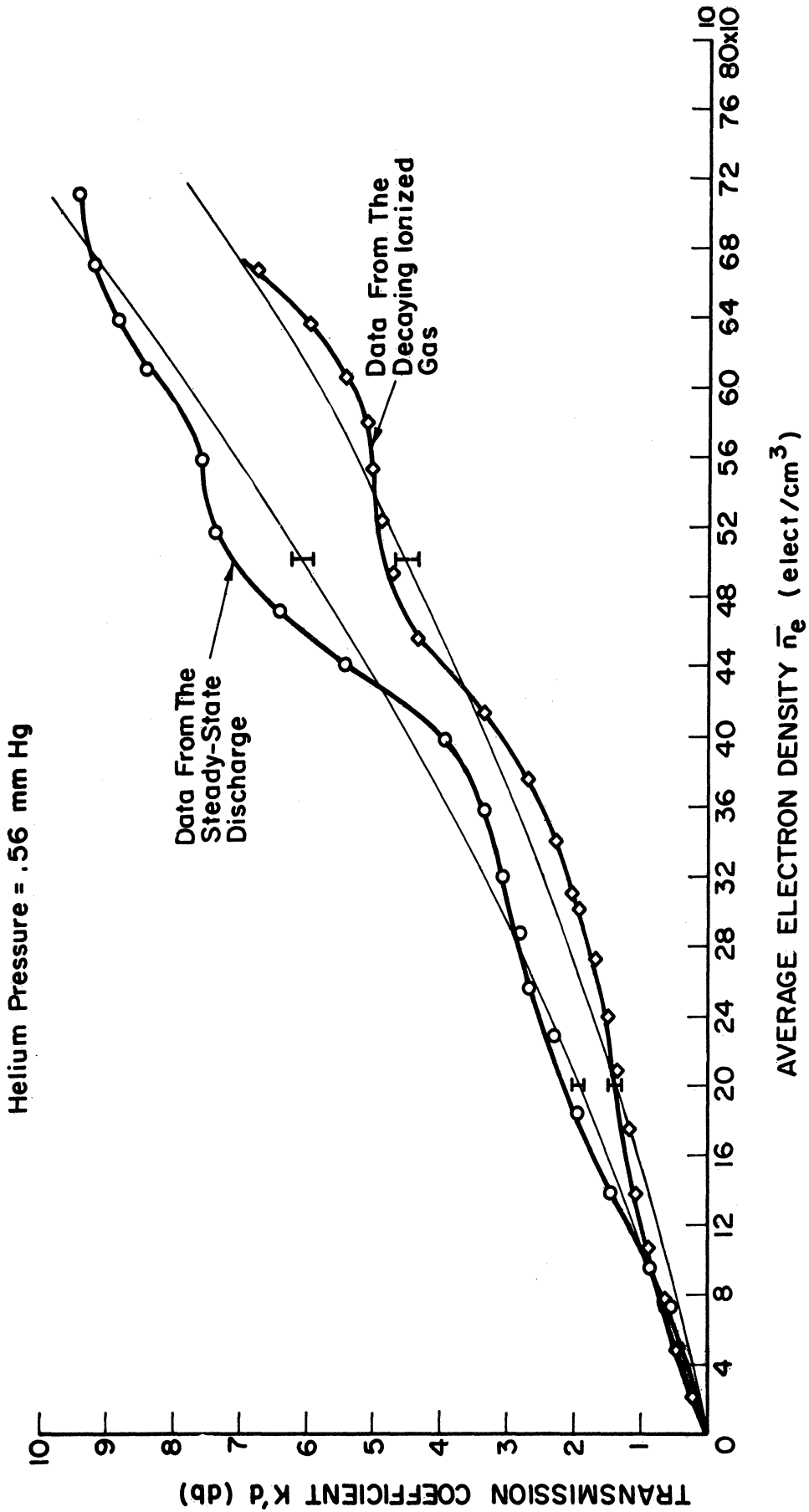Figure 21. Transmission coefficient vs. average electron density.
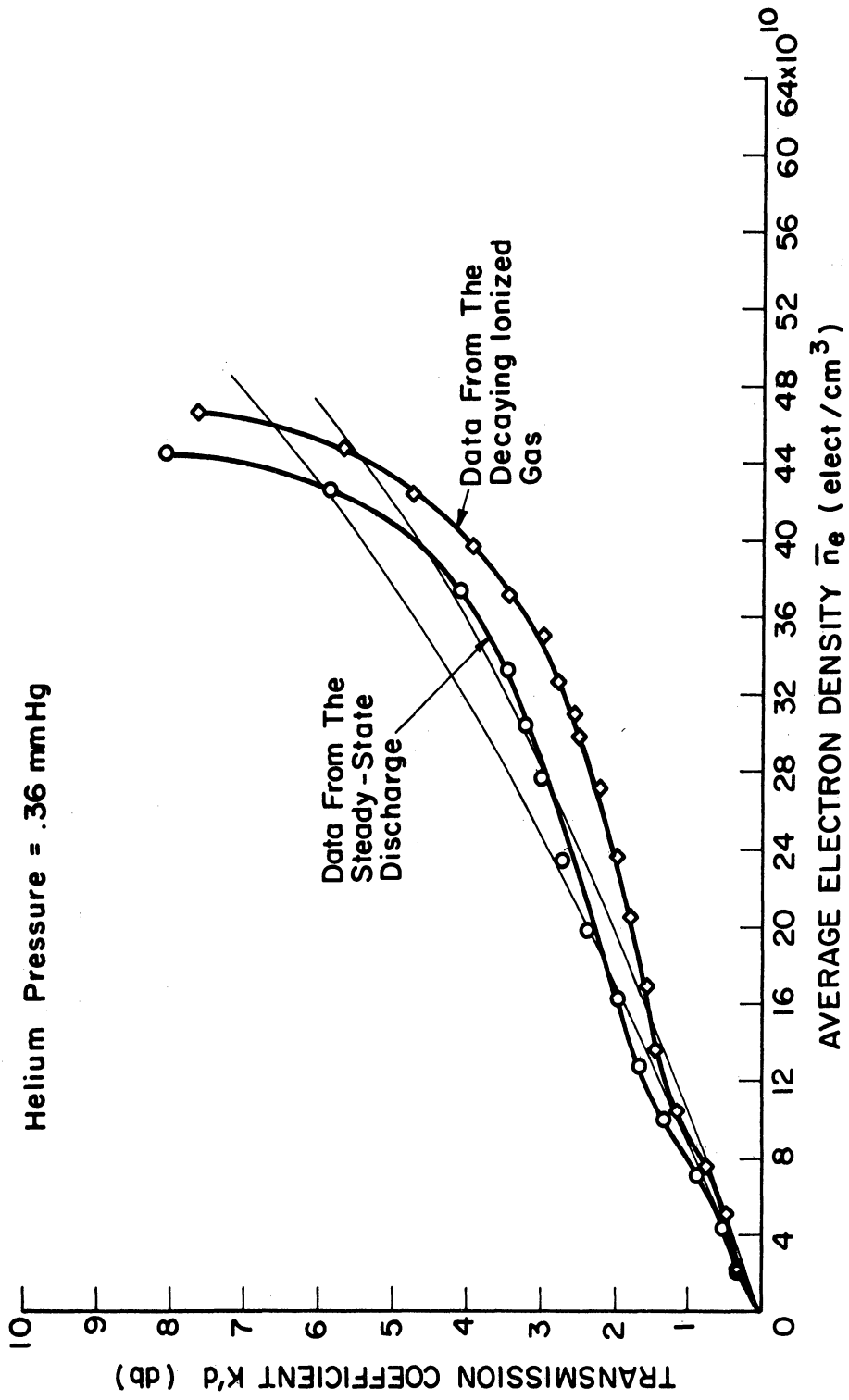
Figure 22. Transmission coefficient vs. average electron density.

Helium Pressure = .56 mm Hg

db meter could not make measurements above this line
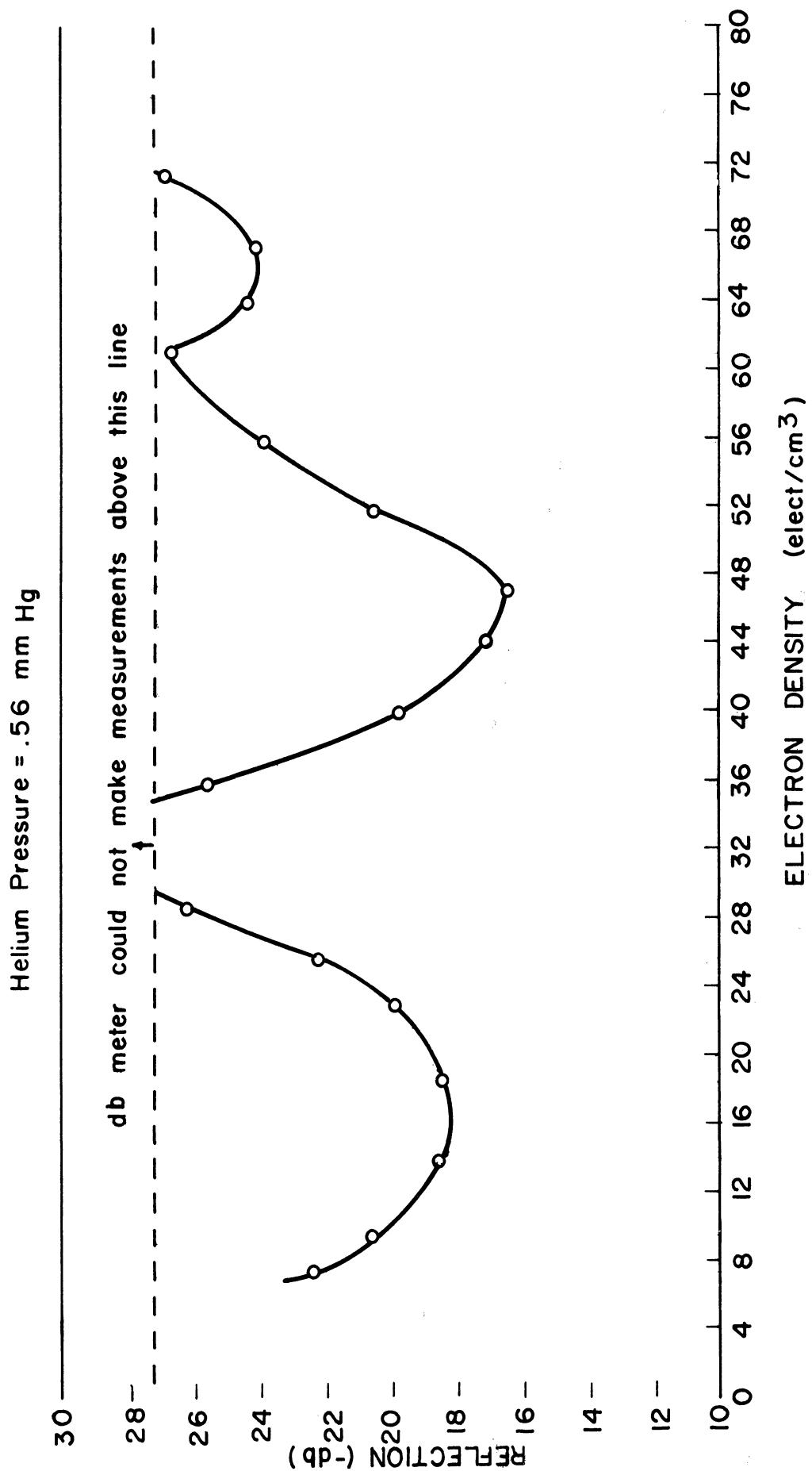
Figure 23. Reflection vs. electron density.

Helium Pressure = .79 mm Hg

ELECTRON DENSITY (elect/cm^3)

ELECTRON TEMPERATURE (ev)
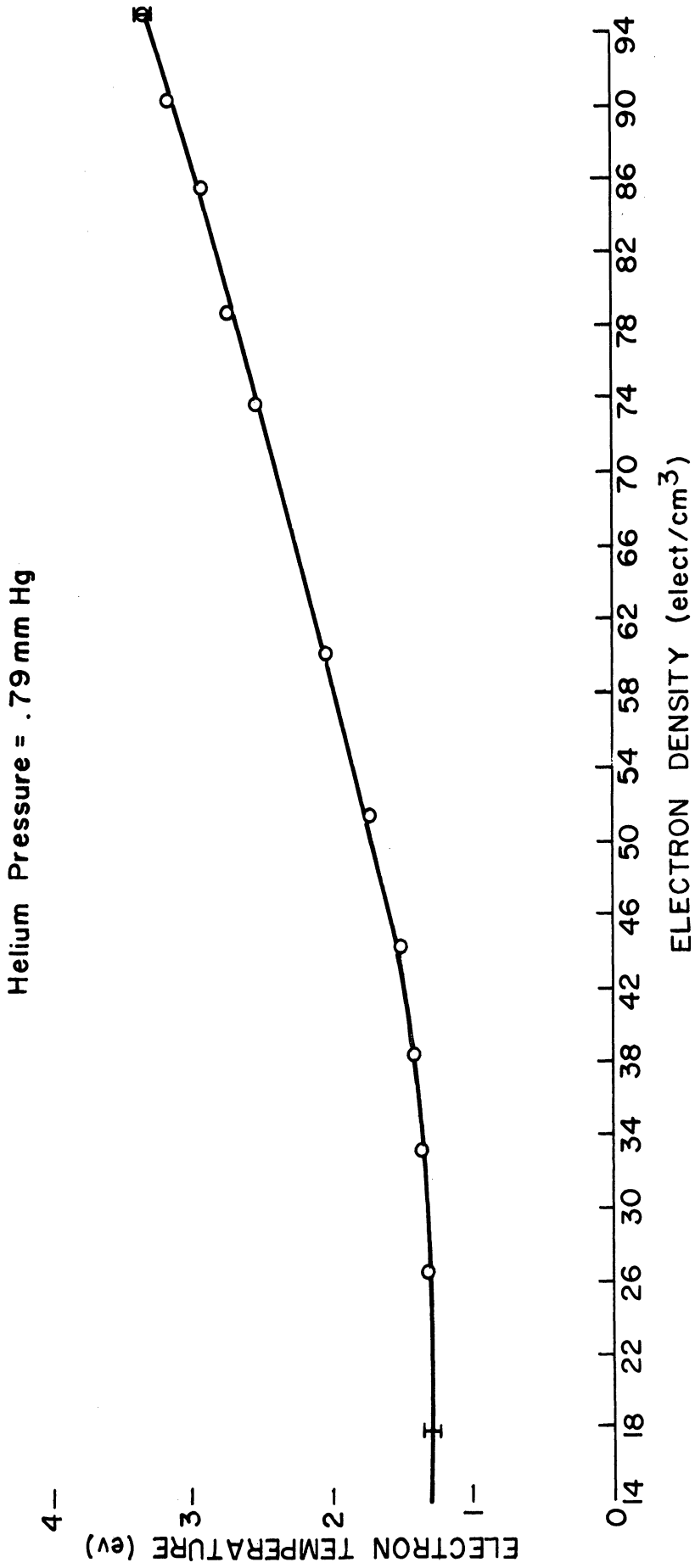
Figure 24. Electron temperature vs. electron density.

Helium Pressure = .56 mm Hg

ELECTRON DENSITY (elect/cm^3)
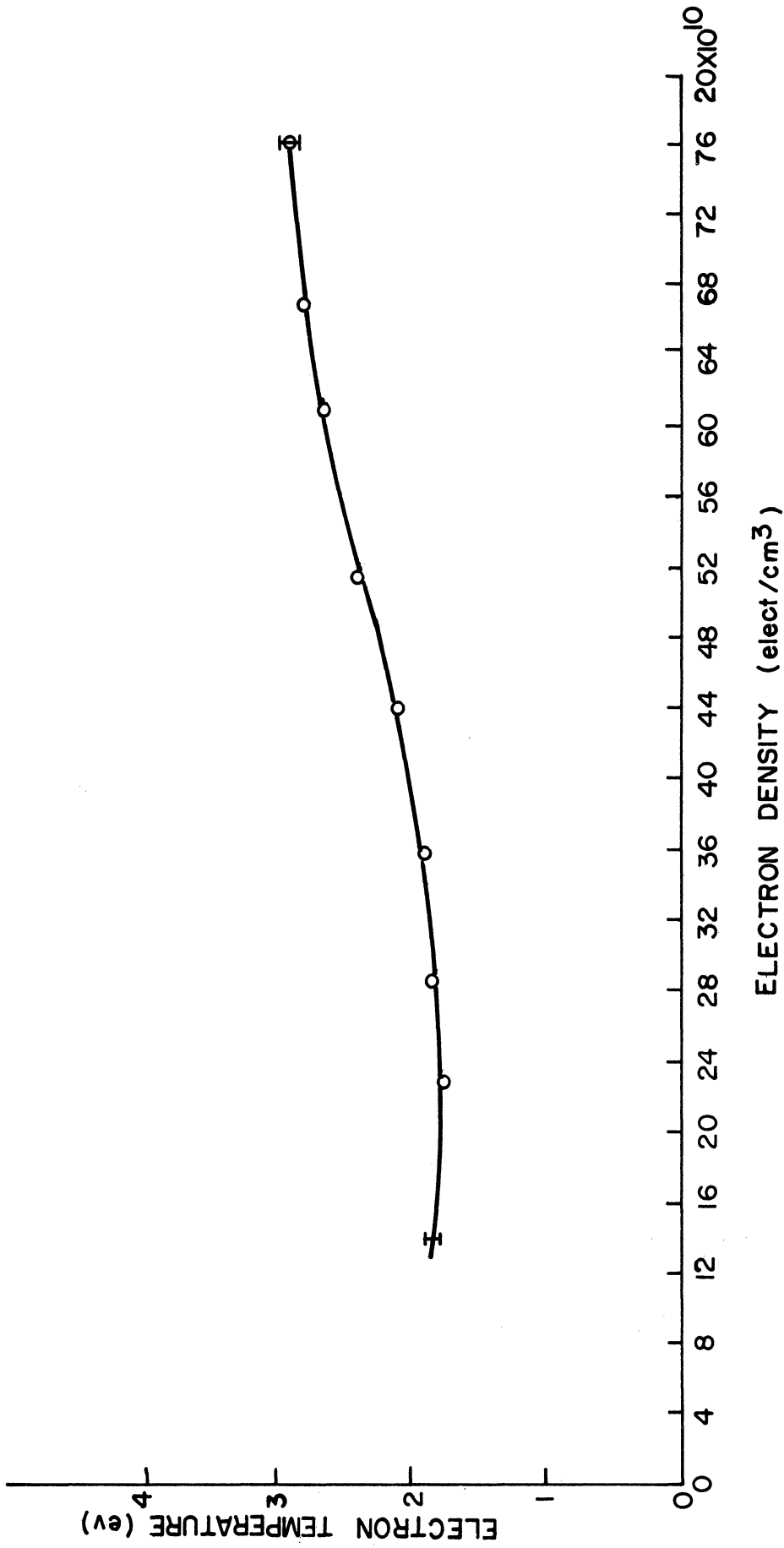
Figure 25. Electron temperature vs. electron density.
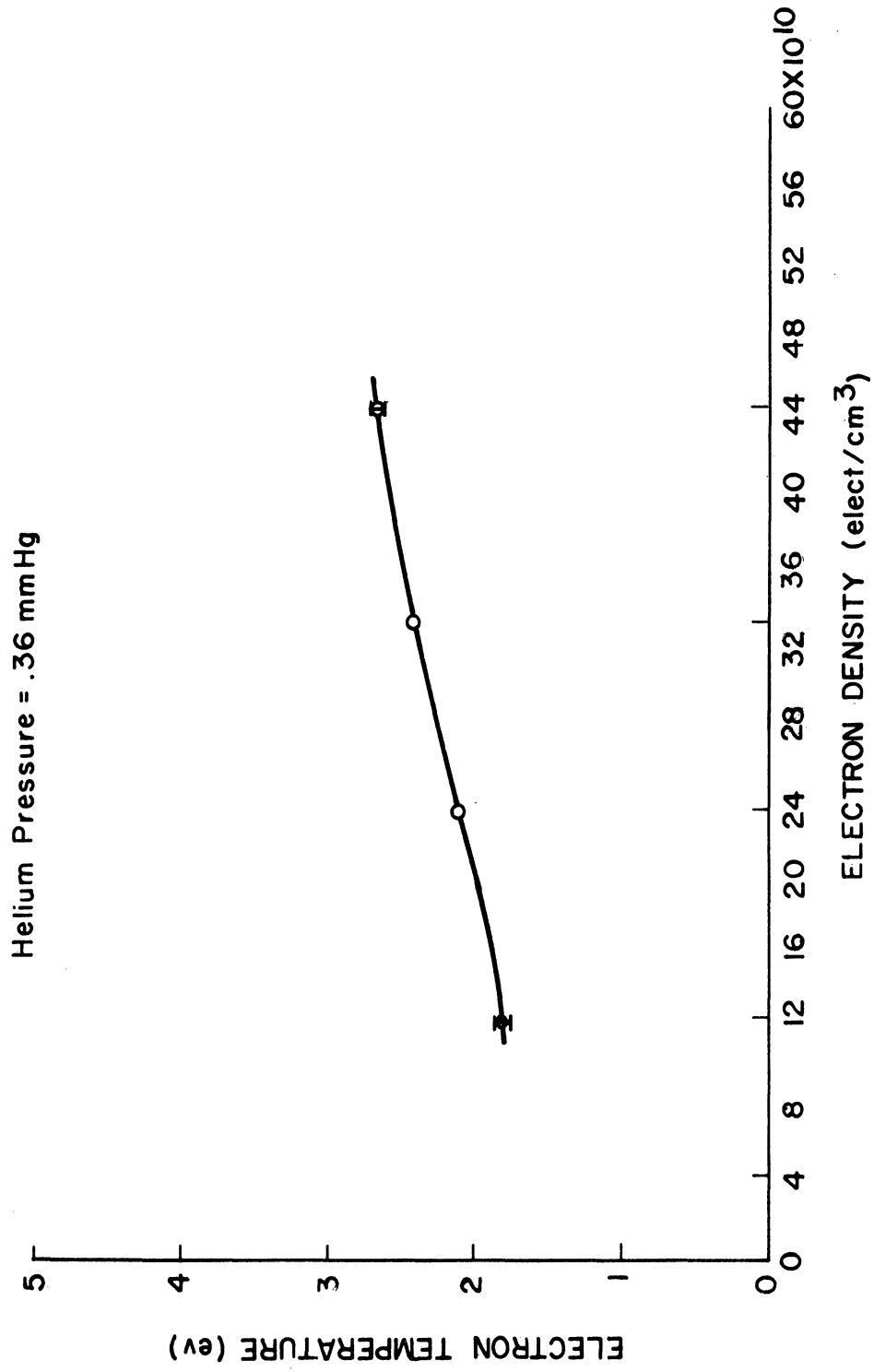
Figure 26. Electron temperature vs. electron density.
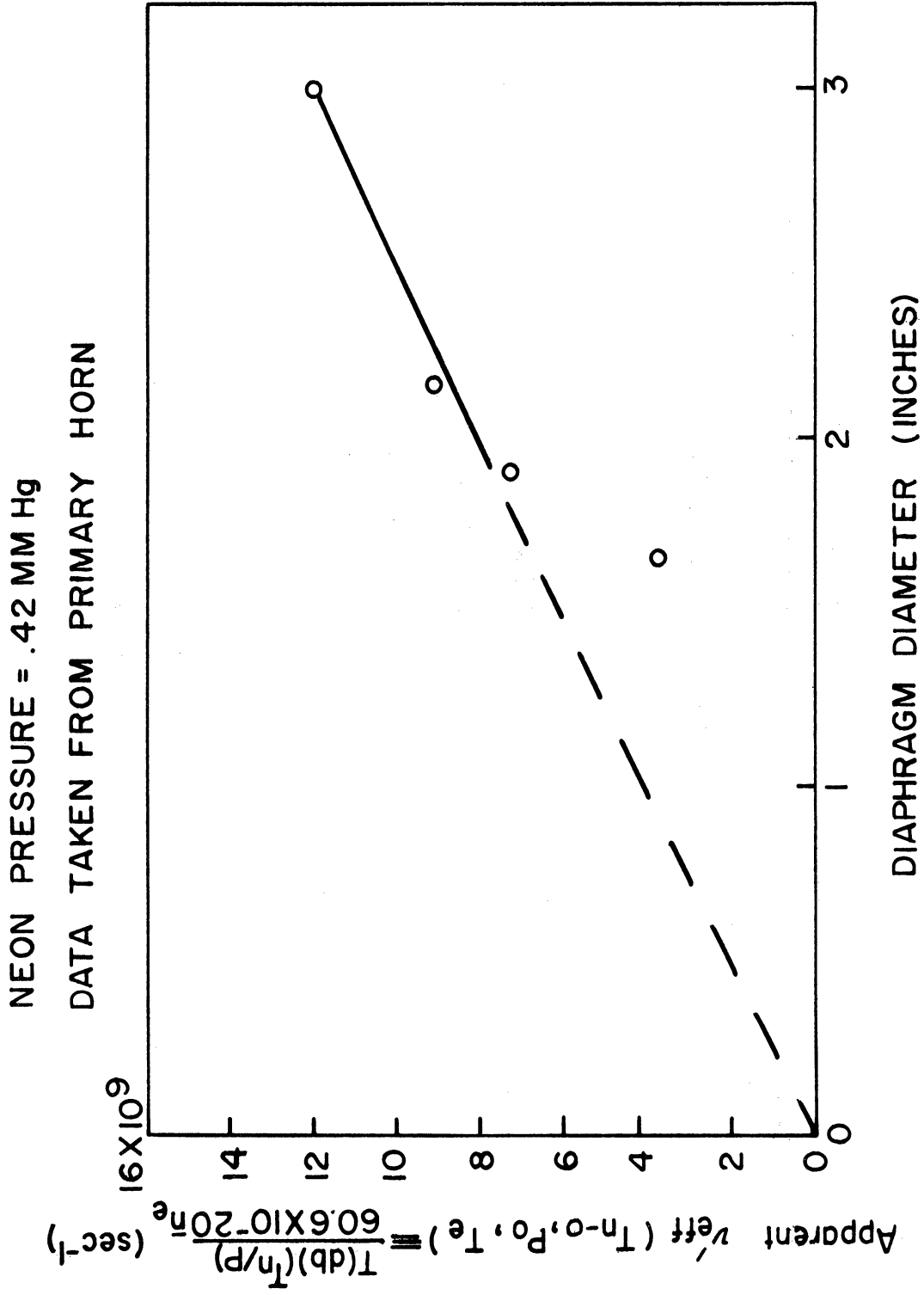
Figure 27. Apparent effective collision frequency of neon vs. diaphragm diameter.

$$\nu_{eff}''(T_{n-o}P_o T_{e-o}) = \frac{T_n}{T_{n-o}} \frac{P_o}{P_o} \sqrt{\frac{T_{e-o}}{T_e}} \frac{\sigma_{sc}(T_{e-o})}{\sigma_{sc}(T_e)} \quad (sec^{-1})$$
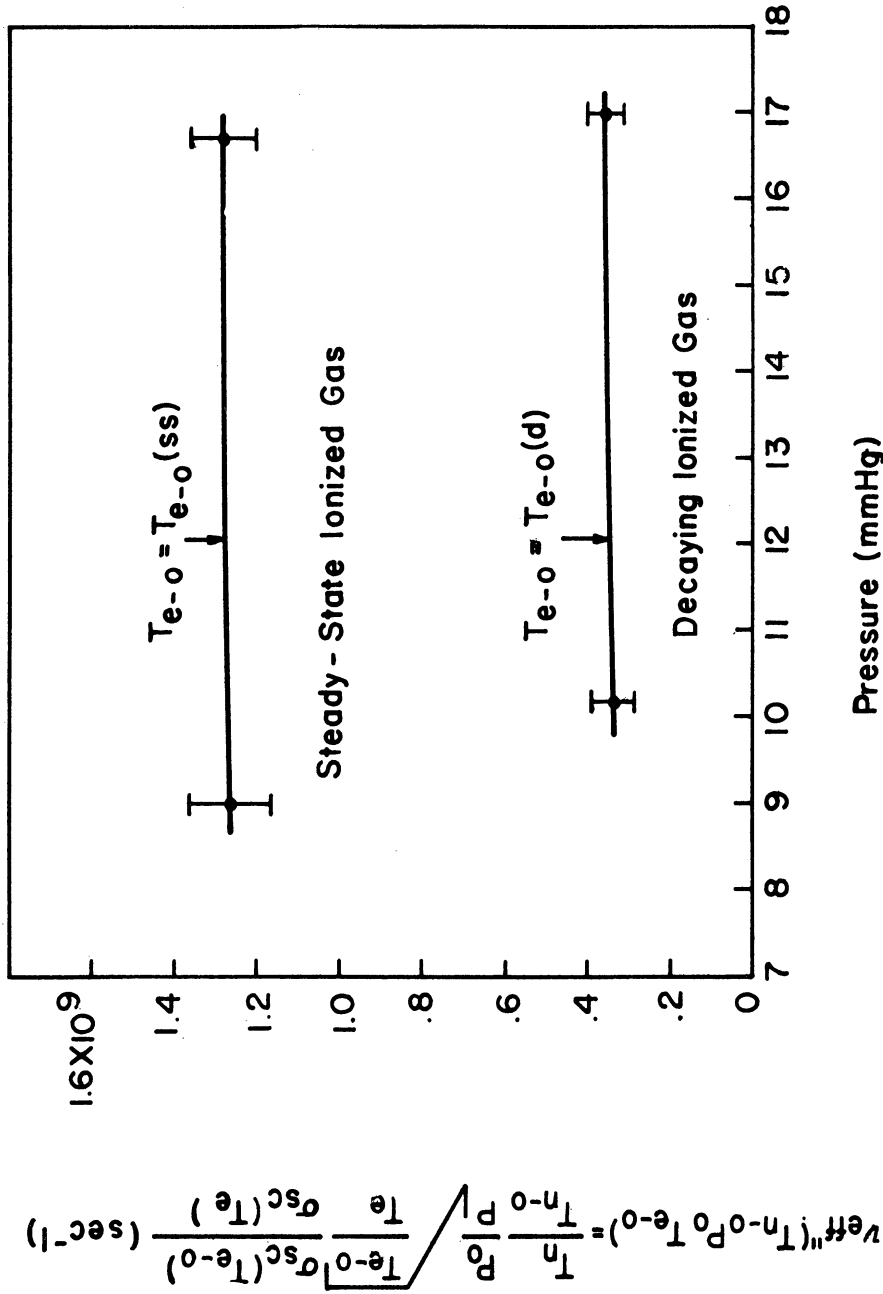
Figure 28. Effective collision frequency ν_{eff}'' $(T_{n_o} P_o T_{e_o})$ versus helium pressure for both steady-state and decaying ionized gas in the high perssure range.

$$\nu_{eff}''(T_{n-o}P_o T_{e-o}) = \left(\frac{T_n}{T_{n-o}}\right)\frac{P_o}{P_o}\sqrt{\frac{T_{e-o}}{T_e}}\frac{\sigma_{sc}(T_{e-o})}{\sigma_{sc}(T_e)}\nu_{eff}\ (\text{sec}^{-1})$$
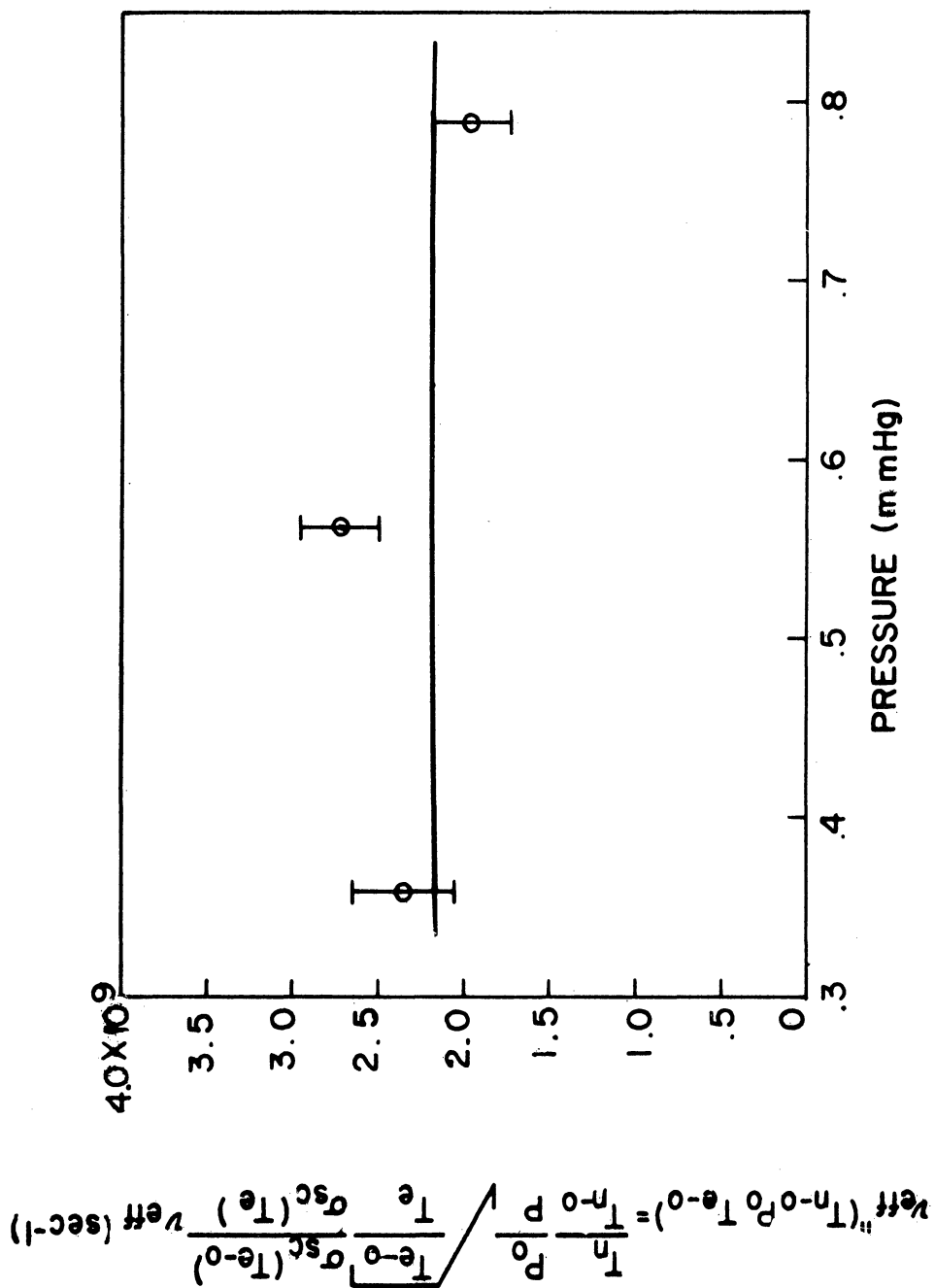
Figure 29. Effective collision frequency ν_{eff}'' $(T_{no}P_o T_{eo})$ versus helium pressure in the low pressure range (calculated with the KO absorption equation).
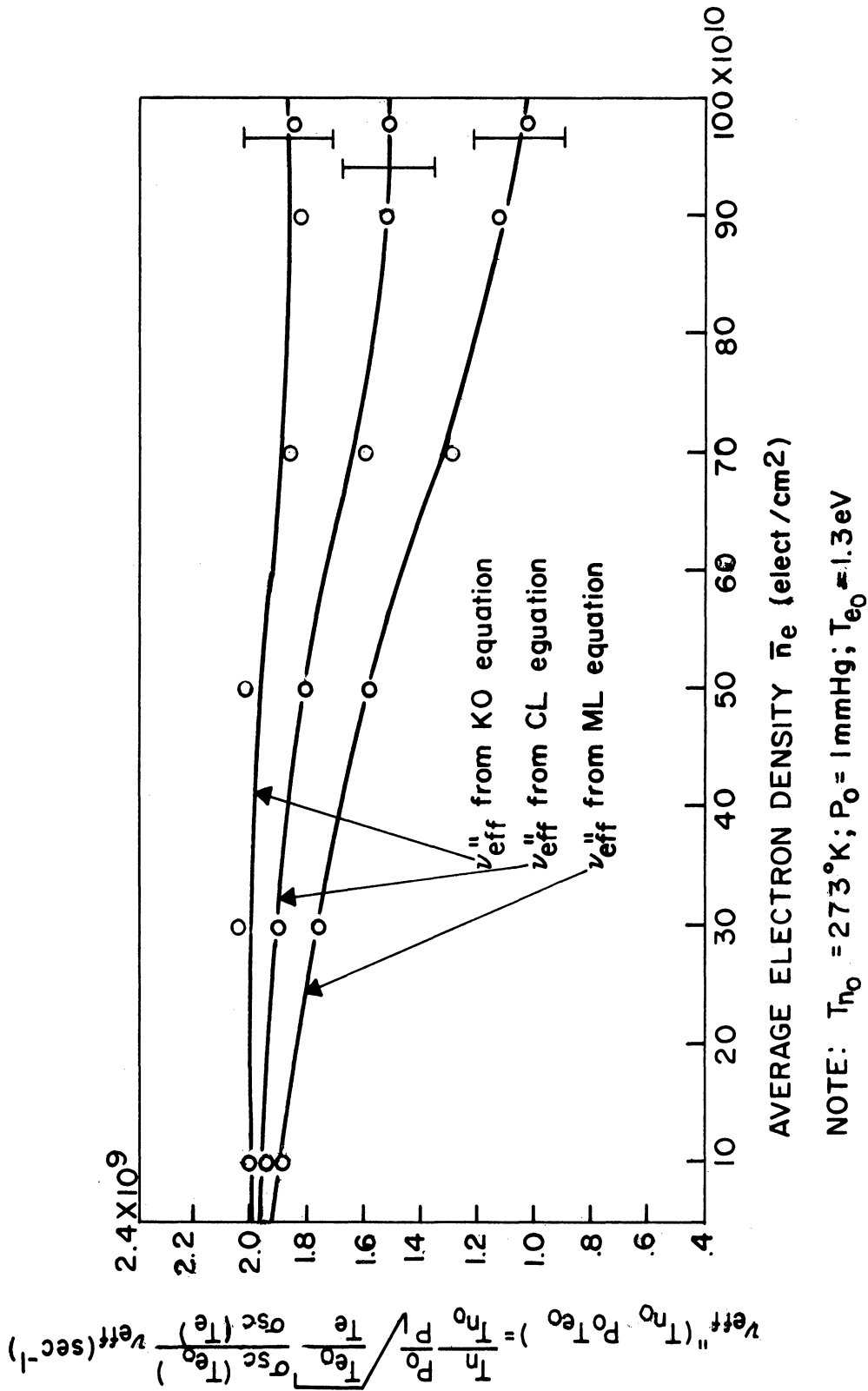
Figure 30. The effective collision frequency $\nu_{eff}''(T_{n_o}P_oT_{e_o})$ versus average electron density.
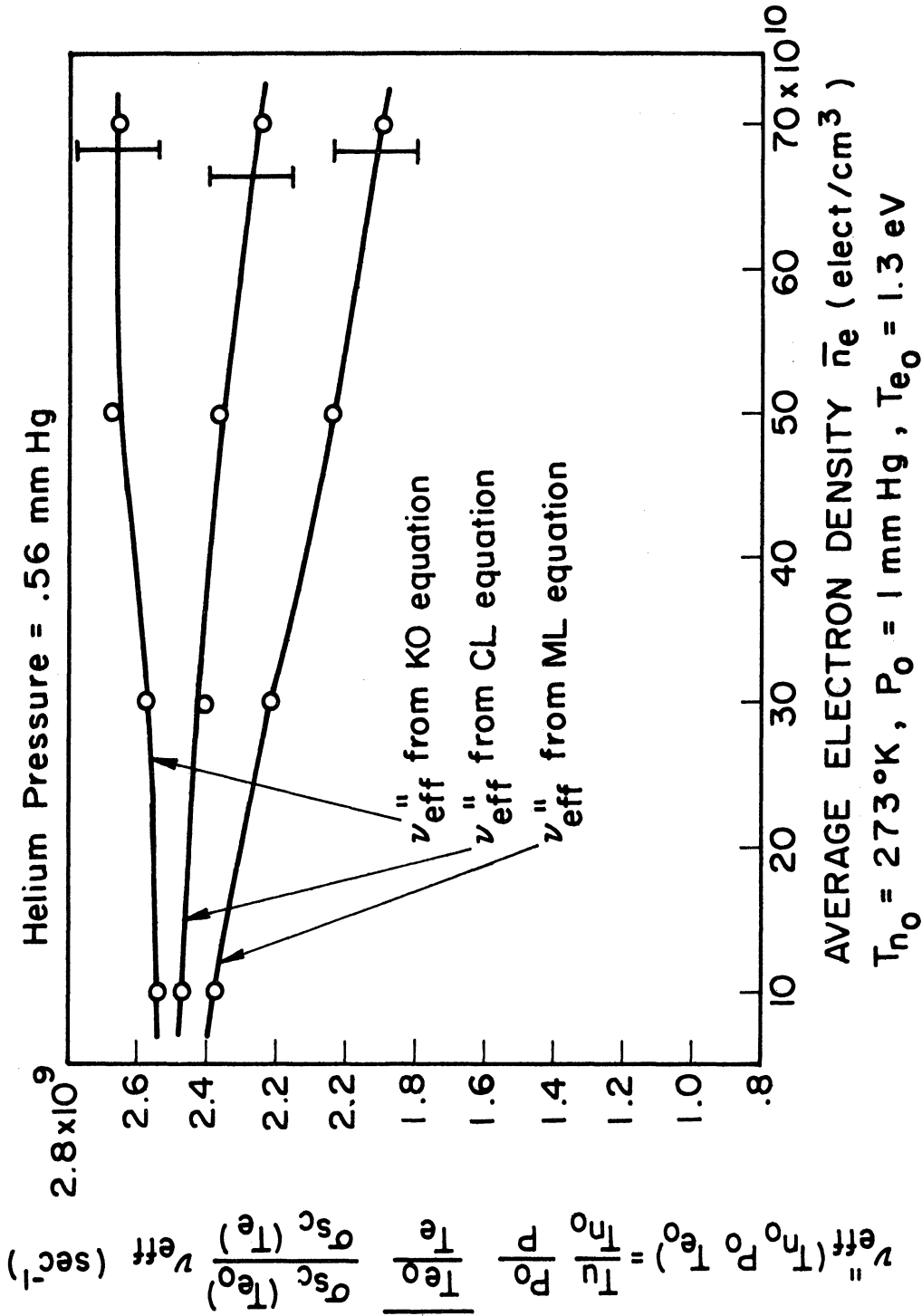
Figure 31. The effective collision frequency ν'_{eff} $(T_{n_o} P_o T_{e_o})$ versus average electron density.
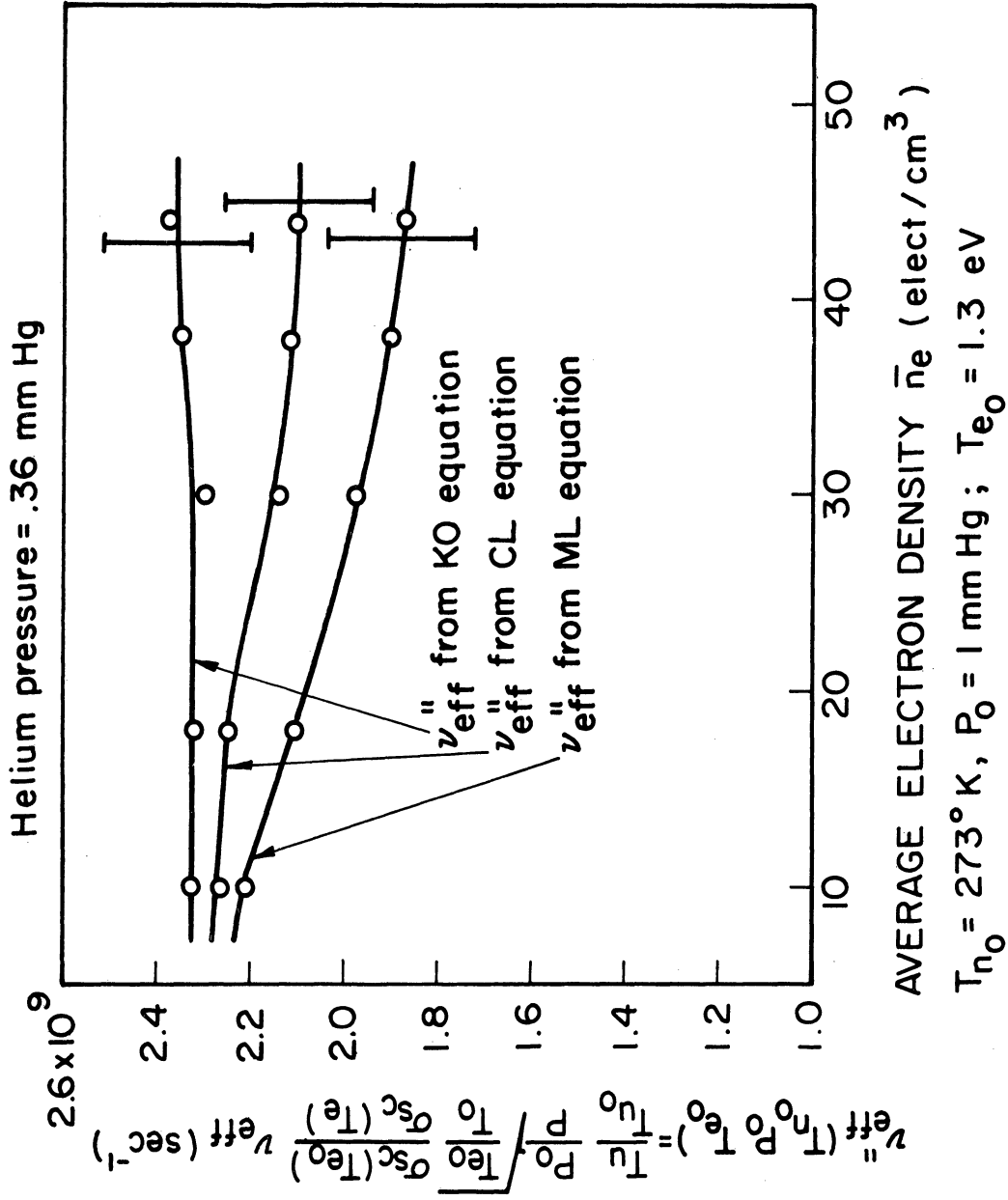
Figure 32. The effective collision frequency ν''_{eff} $(T_{n_o}P_oT_{e_o})$ versus average electron density.

APPENDIX A

DEVELOPMENT OF THE TRANSPORT EQUATIONS

1. The Classic Theory

The classic transport theory for non-dispersive media is presented in (9). The theorems required to obtain the classic transport equation for dispersive media will be cited from (9). No attempt at proof will be made for these theorems.

Before starting any derivation, it is convenient to make the following definitions. Consider the following diagram.
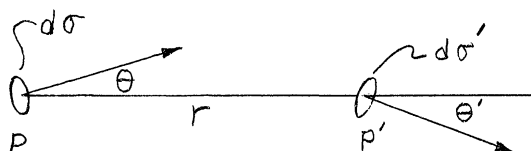
Now let

$d\sigma$ = a differential element of area with normal at an angle θ from the line pp'

$d\sigma'$ = a differential element of area with normal at an angle θ' from the line pp'

r = distance pp'

$d\Omega$ = solid angle subtended at p by $d\sigma'$

$d\Omega'$ = solid angle subtended at p' by $d\sigma$

E_{ν} = energy passing through $d\sigma$ in time dt in direction θ with frequency in $d\nu$ about ν

109

Define

I_ν ≡ specific intensity of ν radiation at p along line pp´

$$\equiv \lim_{dt d\Omega d\sigma d\nu \to 0} \frac{E_\nu}{dt d\Omega d\sigma \cos\theta d\nu}$$

It is necessary to define the Einstein "A" and "B" coefficients. Consider an assembly containing atoms of a given species capable of only 2 stationary states. The assembly may contain any number of ions and electrons and atoms of other species. The state of lower energy (state 1) is the normal state and the state of higher energy (state 2) is the excited state. Then let:

n_1 = number of atoms per cubic centimeter in the normal state

n_2 = number of atoms per cubic centimeter in the excited state

$A_{21}dt$ = probability an excited atom emits a quantum of energy $h\nu$ of frequency ν in time dt

$B_{12}I_\nu dt$ = probability a normal atom absorbs a quantum of energy $h\nu$ of frequency ν in dt

$B_{21}I_\nu dt$ = probability an excited atom is stimulated by external isotropic radiation to emit a quantum of energy $h\nu$ in time dt

$n_1(\nu)d\nu$ = number of atoms which will actually absorb radiation of frequency between ν & $\nu + d\nu$

It is now necessary to define the emission and absorption coefficients of the classic transport equation. Let:

$n_\nu d\Omega dt d\sigma dl d\nu$ = the amount of energy emitted inside solid angle $d\Omega$ through surface $d\sigma$ along a differential element of path length dl at frequency ν in time dt

Now consider a pencil of radiation of intensity I_ν. After traversing a path of length dl in the medium, let its intensity be $I_\nu + dI_\nu$. Then the absorption coefficient is defined by the equation

$$K_\nu = - \frac{1}{I_\nu} \frac{dI_\nu}{dl}$$

The writer has no knowledge of a general derivation of the classic transport equation including dispersive effects in which the absorption and emission coefficients are defined in terms of Einstein coefficients. However, (9) has the coefficients well defined, and (10) includes dispersive effects. A synthesis of the two results will be attempted here with the use of the following theorem from (9).

Theorem I: If μ is the refractive index at any point I_ν/μ^2 is constant along the path of a ray, provided the coefficient of reflection at each interface is zero. Also $\mu^2 d\Omega d\sigma = \mu'^2 d\Omega' d\sigma'$

The derivation itself may be seen by considering a small cylinder in the medium of cross section dS and length dl. It is seen that:

$$\frac{\dfrac{I_\nu}{\mu^2}\,\mu^2 d\nu d\Omega dS}{h\nu} = \text{number of quanta of } \nu \text{ radiation}$$

entering the cylinder in $d\Omega$ about $\underline{\Omega}$

$$\frac{\left(\dfrac{I_\nu}{\mu^2} + d\,\dfrac{I_\nu}{\mu^2}\right)\mu'^2 d\nu d\Omega' dS'}{h\nu} = \text{number of quanta of}$$

radiation leaving the cylinder

Also, it is noted that

$$n_2 \mu^2 dl dS \left[\frac{A_{21}}{\mu^2} + \frac{I_\nu}{\mu^2} B_{21}\right] \frac{d\Omega}{4\pi} d\nu$$

= Number of quanta of ν radiation emitted within $d\Omega$ if emission is isotropic.

$$n_1 \mu^2 dl dS \ B_{12} \frac{I_\nu}{\mu_\nu^2} \frac{d\Omega}{4\pi} d$$

= Number of quanta of ν radiation absorbed within $d\Omega$ if emission is isotropic.

Then by summing gains and losses and using Theorem I, the following equation is obtained.

A-1 $$\frac{d}{ds}\left[\frac{I_\nu}{\mu^2}\,\frac{1}{h\nu}\right] = \frac{1}{4\pi}\left[n_2\left(\frac{A_{21}}{\mu^2} + \frac{I_\nu}{\mu^2}B_{21}\right) - N_1 B_{12}\frac{I_\nu}{\mu^2}\right]$$

Equation A-1 is a transport equation for dispersive media. Scattering and polarization effects do not appear in this equation because they are not of interest in the class

of experiments treated in this paper. The derivation
is based upon the following conditions.

1) The greatest dimension of the medium is much smaller
   than the mean free path of the photons.

2) Photon wavelength is smaller than distances over which
   the intensity is expected to vary rapidly. This
   assumption implies

   a) Photon wavelength is much smaller than the mean
      free path of the photons.

   b) The refractive index must vary little over dis-
      tances of the order of a wavelength.

3) Effects which would tend to show the wave nature of
   the radiation must be small. Thus:

   a) Wave front radius of curvature must be large.

   b) Diffraction effects must be small.

Condition 2-b is required to insure that the reflections
will be small as the photon moves in the medium. A large
refractive index change in a wavelength distance would
create large reflections. The reasons for the other
conditions are obvious.

2. The Theory of Klevans and Osborn

The theory of photon transport in dispersive
media as developed by Klevans and Osborn is clearly

stated in (8). No attempt at derivation will be made here. The results will be stated and the limitations implied in the derivation will be given.

The K.O. photon transport equation may be written as follows

A-2 $\dfrac{dG_k(s)}{ds} = -\sigma G + S$

where

$G_k(s)dkd\Omega = v_g f(s,k)dkd\Omega$

$f(s,k)dkd\Omega$ = the number of photons at s traveling in a direction in $d\Omega$ about $\underline{\Omega}$ and with wave number in dk about k

$x_j \qquad = \Omega_j s + x_{jo}$

$v_g \qquad = c^2 k/\omega$ = the photon group speed.

$\sigma \qquad = (\alpha - \epsilon)/v_g$ = the absorption coefficient

$\epsilon \qquad$ = probability per unit time for emission of a photon with direction in $d\Omega$ about $\underline{\Omega}$ and wave number in dk about k.

$\alpha \qquad$ = probability per unit time for absorption of a photon traveling in a direction in $d\Omega$ about $\underline{\Omega}$ and with wave number in dk about k.

$S \qquad = \epsilon\rho$ = source term

$\rho \qquad = k^2/(2\pi)^3$ = density of states.

Equation A-2 is a simplified version of the K.O. transport equation. In writing this equation, the scattering terms

have been omitted. The derivation that produced this equation was based upon the same assumptions indicated for the classic theory.

The major part of the contribution of the K.O. theory is in the inclusion of the dispersive effects of the medium. Dispersion enters in the K.O. theory through the v_g term as

$$v_g = \frac{c^2 k}{\omega_k}$$

where

$$\omega_k^2 = \omega_p^2 + c^2 k^2$$

For non-dispersive media $(\omega_k^2 = c^2 k^2)$ the classic and KO theories may easily be compared and we find

a) $G = I_\nu / 2\pi h\nu$

b) $\alpha = h\nu \dfrac{c}{4\pi} n_1 B_{12}$

c) $\epsilon = h\nu \dfrac{c}{4\pi} n_2 B_{21}$

d) $\rho = \dfrac{1}{2\pi} \dfrac{A_{21}}{B_{21}}$

e) $v_g = C$

For dispersive media, however, the equations are different. The difference is more easily seen in the solutions for the respective equations which are examined in Chapter II.

APPENDIX B

CALCULATION OF THE COMPLEX CONDUCTIVITY

In this development, the gas will be assumed
to be made up mostly of neutrals so that electron-electron
and electron-ion interactions can be ignored. The neutrals
will be assumed to form an ideal gas.

This gas will be described by the Boltzman
equation

B-1 $\quad \dfrac{\partial f(\underline{v},t)}{\partial t} - \dfrac{e}{m} E_j \dfrac{\partial f}{\partial v_j} = -vfN\sigma_S(\underline{v},T_n) + \int d^3v' f(v',t)N$

$$(x)\sigma(\underline{v}',\ \underline{v},\ T_n)$$

where

$f(\underline{v},\ t)$ = electron distribution function

$\sigma_S(\underline{v},\ T_n)$ = total cross section for scattering of
electrons by neutrals

$\sigma(v,\ v',\ T_n)d^3v$ = cross section for scattering
of electrons by neutrals in which
electrons are scattered from v'
into d^3v about $\underline{v}$.

N = density of neutrals.

T_n = temperature of neutral atoms

To solve equation B-1, f is expanded as follows (p_1 approxi-
mation)

116

$$f(\underline{v}, t) \cong \frac{1}{4\pi} f_0(v, t) + \frac{3}{4\pi v^2} \underline{v} \cdot \underline{J}(v, t)$$

where

$$f_0(v, t) = \int d\Omega f(\underline{v}, t)$$

$$n(t) = \int_0^\infty v^2 dv f_0(v, t)$$

$$\underline{J}(v, t) = \int d\Omega \underline{\Omega} v f(\underline{v}, t)$$

It is then assumed that

$$\sigma(\underline{v}', \underline{v}, T_n) = \sigma(v', v, \underline{\Omega} \cdot \underline{\Omega}', T_n)$$

and the cross-section is expanded in Legendre polynomials

to get

$$\sigma(\underline{v}', \underline{v}, T_n) = \frac{1}{4\pi} \sigma_0(v', v, T_n) + \frac{3}{4\pi} \underline{\Omega} \cdot \underline{\Omega}' \sigma_1(v', v, T_n)$$

It is also assumed that J' is slowly varying enough so that

$$\int v'^2 dv' N \sigma_1(v', v, T) J' \cong \underline{J} N \sigma_S(v, T) \int v'^2 dv' \frac{\sigma_1(v', v, T)}{\sigma_S(v, T)}$$

The use of these expansions and assumptions makes it possi-

ble to solve equation B-1. The solution is

B-2 $$\underline{J}(v, t) = e^{-\nu(v)t} \underline{J}(v, 0) + \int_0^t dt' e^{-(t-t')\nu(v)}$$

$$(x) \frac{ev}{3m} \frac{\partial f_0(v, t')}{\partial v} (\underline{E}(t'))$$

where

$$\nu(v) \equiv v N \sigma_S(v, T) \left[1 - \int_0^\infty v'^2 dv' \frac{\sigma_1(v', v, t)}{\sigma_S(v, T)} \right]$$

Collective effects are assumed small and harmonic fields

of the type $\underline{E}(t) = \underline{E}_0 e^{i\omega t}$ are postulated. It is also

assumed that:

1) $\partial f_0/\partial v$ is not a function of time

2) $\nu t >> 1$

Under these conditions, equation B-2 may be solved for the

conductivity to give

B-3 $\quad \dfrac{\underline{E}}{\underline{J}} = \rho = -\dfrac{e^2}{3m} \int_0^\infty v^3 dv \; \dfrac{\partial f_0}{\partial v} \; \dfrac{\nu(v) - i\omega}{\nu^2(v) + \omega^2}$

For a Maxwellian electron energy distribution, equation

B-3 reduces to

B-4 $\quad \rho = \dfrac{8}{3\sqrt{\pi}} \dfrac{ne^2}{m} \int_0^\infty \dfrac{(\nu(u) - i\omega)}{\omega^2 + \nu^2(u)} u^4 e^{-u^2} du$

where

$u = \sqrt{\dfrac{m}{2\Theta_e}} \; v$

If the collision frequency is independent of electron

velocity, equation B-4 reduces to

B-5 $\quad \rho = \dfrac{1}{4\pi} \omega_p^2 \; \dfrac{\nu - i\omega}{\nu^2 + \omega^2}$

where $\omega_p^2 = 4\pi\dfrac{nc^2}{m}$

If ν is not independent of velocity, but $\omega^2 >> \nu^2$, then

equation B-5 is still valid except

B-6 $\quad \nu \rightarrow \nu_{eff} \cong \dfrac{8}{3\sqrt{\pi}} \int_0^\infty \nu(u) u^4 e^{-u^2} du$

If ν is not independent of electron velocity but $\nu^2 >> \omega^2$, then B-5 is again valid but

B-7 $\quad \dfrac{1}{\nu} \rightarrow \dfrac{1}{\nu_{eff}} \cong \dfrac{8}{3\sqrt{\pi}} \int_0^\infty \dfrac{u^4 e^{-u^2} du}{\nu(u)}$

If scattering is hard sphere type and isotropic in CMCS and if $\omega^2 >> \nu^2$, then one can easily show that

B-8 $\quad \nu \equiv \nu_{eff} = \dfrac{8}{3\sqrt{\pi}} \sigma_m N \sqrt{\dfrac{2\Theta e}{m}} = \dfrac{4}{3} \sigma_m N v_0$

where

$$v_0 = \sqrt{\dfrac{8 \Theta e}{\pi m}}$$

$$\sigma_m = \sigma_S \int (1 - \cos \Theta) I_S(\Theta) d\Omega_{cm}$$

Θ = scattering angle in CMCS

$I_S d\Omega_{cm}$ = elastic scattering frequency

Calculations of the collision cross section for momentum transfer have been done approximately for He, Ne, and A and are listed in (13)

APPENDIX C

DEVELOPMENT OF A TRANSPORT EQUATION
FROM MAXWELL'S EQUATIONS

An equation for energy conservation of the following form may be obtained from Maxwell's equations.

$$\text{C-1} \quad \frac{1}{8\pi} \frac{\partial}{\partial t} (E^2 + H^2) + \frac{C}{4\pi} \nabla \cdot (\underline{E} \times \underline{H}) = -\underline{J} \cdot \underline{E}$$

The details of this derivation are given on page 206 of (21). The terms of equation C-1 are usually given an interpretation in terms of energy loss and power flow. For example, $\frac{1}{8n} (E^2 + H^2)$ is interpreted as the density of the energy stored in the electric and magnetic fields, $- \underline{J} \cdot \underline{E}$ is interpreted as the power loss per unit volume due to Joulean heating, and $\underline{E} \times \underline{H} \cdot \underline{ds}$ is interpreted as the power flow across an element of area $\underline{ds}$. The form of equation C-1 is reminiscent of a transport equation as it now stands, but a much better form may be obtained without undue difficulty.

Consider a field with an harmonic time dependence. Make the assumption that

$$\underline{J} = \sigma \underline{E}$$

Then make the following definitions.

$$\underline{J}(t) = A(t)\underline{J}'(t)$$

$$\underline{E}(t) = A(t)\underline{E}'(t)$$

$$\underline{H}(t) = A(t)\underline{H}'(t)$$

$\underline{J}'(t)$ = slowly varying time dependence of $\underline{J}(t)$

$\underline{E}'(t)$ = slowly varying time dependence of $\underline{E}(t)$

$\underline{H}'(t)$ = slowly varying time dependence of $\underline{H}(t)$

$A(t)$ = rapidly varying time dependence of

$\underline{E}$, $\underline{H}$, $\underline{J}$ with period τ

If equation C-1 is time averaged over the period of

oscillation of $A(t)$, the result is

C-2 $\quad \dfrac{1}{8\pi} \dfrac{\partial}{\partial t} (\langle E^2 \rangle + \langle H^2 \rangle) + \dfrac{c}{4\pi} \nabla \cdot \langle \underline{E} \rangle \times \langle \underline{H} \rangle = -\rho_c \langle E^2 \rangle$

Now for plane waves propagating in an ionized gas, it may

be shown that

C-3 $\quad \langle H^2 \rangle = \left| \dfrac{c^2 k^2}{\omega^2} \right| \langle E^2 \rangle$

where

$$k^2 = \dfrac{\omega^2}{c^2} (1 - i(\dfrac{4\pi}{\omega}) \rho_c)$$

The time averaged energy density in the electric and magnetic

fields may be written as follows

C-4 $\quad U = \dfrac{1}{8\pi} (\langle E^2 \rangle + \langle H^2 \rangle)$

The use of equations C-4 and C-3 in C-2 yields for the

steady-state case

$$\hat{\underline{k}} \cdot \nabla \frac{2c\mu}{(1 + \left|\frac{c^2k^2}{\omega^2}\right|)} U = 2\frac{\omega}{c}\chi \left(\frac{2c\mu}{1 + \left|\frac{c^2k^2}{\omega^2}\right|}\right) U$$

where

$\hat{\underline{k}}$ = unit vector in the direction of propagation

of the waves.

Now let

$$H = \underline{v}U$$

where $\underline{v}$ has been identified as

$$\underline{v} = \hat{\underline{k}} \frac{2c\mu}{(1 + \left|\frac{c^2k^2}{\omega^2}\right|)} =$$ velocity of energy propagation in the medium

and then C-4 reduces to

C-5 $$\frac{d}{ds} H(s, \nu) = 2\frac{\omega}{c}\chi H$$

The solution to this equation is exactly the same as the

Maxwell-Lorentz solution of equation 18.

APPENDIX D

TEST OF THE UV-CESIUM SOURCE

Three things were necessary in the design of
a system capable of testing the UV-cesium souce. First,
it was necessary to obtain a system that would both with-
stand the cesium atmosphere on the inside and pass UV
radiation energetic enough to ionize the cesium. Second,
it was necessary to insure that a sufficient amount of
cesium was in the chamber to be ionized. Third, a sensi-
tive and reliable means of detecting electron density
was required.

Cesium compatability in the system was not
a serious problem. The probes were made of molybdenum.
The cesium manifold was made of 321 stainless-steel and
"heli-arc" welded. The cesium isolation valve was a
Varian 1-1/2" bakable valve made of stainless steel and
OFHC copper. A regular Kovar type metal to glass seal was
used to connect the manifold to the chamber. Although
this is known to be incompatible with high cesium vapor-
pressures at high temperatures, it proved to be compatible
at the low vapor pressures (100 μ Hg or less) and the
low temperatures (250° c or less) used in this test.

123

The cesium vapor source used was a small, high purity quantity (99.99%) in a stainless steel bottle that could be isolated from the rest of the system with the use of a stainless-steel high vacuum valve. The whole assembly was purchased from the Dow Chemical Company.

The cesium system was operated at a temperature at least 30° c higher than the cesium pool temperature to avoid forming cesium films cooler than the cesium pool and thus reducing the cesium vapor pressure. It was also necessary to keep the chamber as hot as possible to hold down cesium coating on the pyrex plates with resulting increase in reflection coefficient for microwaves. No problems due to cesium coatings were experienced during operation.

Pyrex was found to satisfy the chamber requirements. Cobine indicates (22) that the prime absorption line for ionization of cesium is at approximately 3100-3200A. Data from Corning and tests made here at the University of Michigan indicate that transmission through pyrex is 80% or greater for wavelengths longer than 3200A, 70% @ 3100A, and 35% @ 2900A.

Two methods were used to insure that sufficient cesium was in the chamber. First, the RF was applied to the cesium to see if a discharge could be supported

by the cesium present. A dense electron gas resulted.
Then, the temperature of one of the plates of pyrex
chamber was lowered below the cesium pool temperature.
A coating of cesium appeared on the plate. This result
was assumed to mean that the chamber contained a cesium
vapor in equilibrium with the cesium pool at its
temperature.

Two methods were used to test for ionization,
the microwave phase shift and the Langmuir probes.

Operation of the chamber and UV arc at several
cesium vapor pressures up to the maximum the system could
stand (80μ Hg) showed no measurable electron cloud as
measured by the phase of the microwaves. However, con-
siderable probe current was measured. Since the probe
current could also be produced by photo-electric effect
of the UV light on the cesium coated probes, it was assumed
that the probe current was due mostly to this effect
and very few electrons were present as an electron gas.
This assumption was supported by the results observed
when noble gas was let into the system. After about 8 mm Hg
of noble gas was mixed with the cesium, no more probe
current was observed. Apparently the noble gas inter-
fered with the flow of electrons between probes by
increasing the collision probability. This interference
reduced the current flow below a measurable value.

From the lack of measurable phase shift and
the known sensitivity of the microwave bridge, it may
be said that the electron density in the chamber due to
ionization was less than $.4 \times 10^{10}$ elect/cc.

APPENDIX E

DATA CALCULATION METHODS

1. Sample Calculations of Electron Temperatures and Densities from the Langmuir Probe Curves of Figures 14, 15.

Dimensions of the Langmuir probes used

Probe Number	Length	Diameter
1	2.54 ± .03 cm	.0254 cm
2	2.31 ± .03 cm	.0254 cm

A. Calculations of electron temperature and density for the high pressure range. See (18) for the method used.

Electron Temperature

$$T_e(ev) = (G_0 - G_0^2) R_0 {}^{\Sigma}i_p$$

where

$$G_0 = \left[i_{e_2} / {}^{\Sigma}i_p \right] v_d = 0$$

$${}^{\Sigma}i_p = i_{p_1} + i_{p_2}$$

$$R_0 = \left[\frac{dv_d}{di_{p_1}} \right]_{v_d = 0} \cong \left[\frac{\Delta v_d}{\Delta i_p} \right]_{v_d = 0}$$

All required currents and voltages are shown on Figure 14.

$$T_e(ev) = 8.84 \ ev$$

127

The probable error in the temperature is:

$$\Delta T_e (ev) = \sqrt{\left(\frac{\partial T_e}{\partial (\Sigma i_p)} \delta (\Sigma i_p)\right)^2 + \left(\frac{\partial T_e}{\partial i_{e_2}} \delta i_{e_2}\right)^2 + \left(\frac{\partial T_e}{\partial (\Delta i_p)} \delta (\Delta i_p)\right)^2}$$

$$\overline{+ \left(\frac{\partial T_e}{\partial (\Delta v)} \delta (\Delta v)\right)^2}$$

$$= .18 \; ev$$

$$\frac{\Delta T_e}{T_e} \times 100 = 2\%$$

Electron Density

For the case where $T_e \gg T_i$, the equations valid are

1) $$\frac{i_{p_1}}{n_e \gamma} = 1.15 \times 10^{-27} \sqrt{\frac{T_e}{M}} \quad (2\pi a l)$$

2) $$(i_{p_1})(-\beta^2) = 14.66 \times 10^{-6} \left(\frac{m}{M}\right)^{1/2} \left(\frac{1}{a}\right) V_{S2}^{3/2}$$

3) $$V_{S2} = V_f - 5.97 \times 10^{-5} T_e$$

4) $$V_f = 300 \frac{k T_e}{2e} \ln \left(\frac{T_e}{T_p} \frac{M}{m}\right)$$

where

a = probe radius (cm)

l = probe length (cm)

T_e = electron temperature (°K)

m = electron mass

M = mass of ion

$(-\beta^2)$ = geometric constant defined in Ref. (Cobine)

pg. 126.

i_{p_1} = defined on Figure 14.

γ = ratio of the sheath radius to the probe radius.

For the case of helium, equations 1-4 reduce to

5) $\qquad n_e = \dfrac{i_{p_1}}{\gamma} \; 1.79 \times 10^{15} \left(\dfrac{300}{T_e}\right)^{1/2}$

6) $\qquad (-\beta^2) \cong 2.96 \times 10^{-7} \left(\dfrac{T_e}{300}\right)^{3/2} \dfrac{1}{i_{p_1}}$

The use of the graph on page 126 of (22) relating $(-\beta^2)$

with γ makes the solution of these equations possible

and the answer is

$\qquad n_e = 5.9 \times 10^8 /cc$

Note that the average electron density obtained from phase

measurements is

$\qquad \overline{n}_e = 1.77 \times 10^{10}/cc$

In order to judge whether the theory used to analyze the

probe results is correct, it is necessary to calculate the

average number of collisions which take place within the

probe sheath. From the definition of γ it is seen that

the sheath thickness t is

$$t = a(\gamma - 1)$$

$$= .065 \text{ cm}$$

The mean-free-path λ for 8.84 ev electrons in helium at a pressure of 12.8 mm Hg is approximately

$$\lambda = \frac{1}{p_c(8.8 \text{ ev})} \frac{1}{12.8} = \frac{1}{4 \times 12.8} = .02 \text{ cm}$$

where $p_c(8.8)$ is the probability for collision at 1 mm Hg press and 8.8 ev electron temperature.

Thus, approximately 3 collisions will take place within the probe sheath according to the theory used.

B. Calculations of electron temperature and density for the low pressure range

Electron Temperature

$$T_e(\text{ev}) = (G_0 - G_0^2) \, R_0{}^{\Sigma}{}_{ip}$$

All required currents and voltages are shown on fig. 15.

$$T_e(\text{ev}) = 2.58 \text{ ev}$$

The probable error in the temperature is

$$\Delta T_e(\text{ev}) = .065$$

$$\frac{\Delta T_e}{T_e} \times 100 = 2.5\%$$

Electron Density

Use of equations (5, 6), the graph on page 126 of (22), and the data from Figure 15 yields for

the electron density

$$n_e = 1.1 \times 10^{10}/cc$$

Note that the average electron density obtained from

phase measurements is

$$\bar{n}_e = 60.9 \times 10^{10}/cc$$

To check the applicability of the theory at this pressure,

it is again necessary to check the average number of

collisions within the sheath. Use of the same methods

as those given on page 3 yield an answer of

$$t = .82 \times \frac{.0254}{2} = .010 \text{ cm}$$

$$\lambda = \frac{1}{20 \times .5} = .010 \text{ cm}$$

Thus approximately 1 collision will take place within

the probe sheath according to the theory used.

2. Sample calculations of ν_{eff}

Equation 29 was used to calculate ν_{eff} from the

absorption and phase data obtained in the experiment.

The absorption coefficient was calculated by the use

of all three theories and labeled according to which

theory was used. For convenience, the equations are

repeated here.

29 $\quad T = t'(0+) \exp\left[-K(\bar{n}_e)d\right]$

where

19 $\quad K_{cl} = \dfrac{\nu_{eff\ tr}}{c}\ \dfrac{\omega_p^2}{\omega^2}$

20 $\quad K_{KO} = \dfrac{\nu_{eff\ tr}}{c}\ \dfrac{\omega_p^2}{ck\omega_k}$

21 $\quad K_{ML} = \dfrac{\nu_{eff}}{c}\ \dfrac{\omega_p^2}{\omega ck_\omega}$

22a $\quad \omega_k = ck\left(1 + \dfrac{\omega_p^2}{c^2k^2}\right)^{1/2}$

22b $\quad ck_\omega = \omega\left(1 - \dfrac{\omega_p^2}{\omega^2}\right)^{1/2}$

The transmission coefficient which accounts for the effects of medium interfaces $t'(0+)$ is unimportant in this experiment. For the high pressure data, it is unimportant because it is small compared to attenuation due to collisions for the small electron densities obtainable at high pressures.

For the low pressure data, $t'(0+)$ cancels out when the attentuation at low electron temperatures is eliminated from the attenuation at high electron temperatures. The $t'(0+)$ factor is the same for each temperature condition because it depends almost entirely on electron density for the range of values of ν_{eff}^2/ω^2 and ω_p/ω which obtain in the low pressure region.

The electron density is calculated from equation

23 $\quad (1 - \dfrac{\omega_p^2}{\omega^2})^{1/2} = - \dfrac{\Delta\phi\lambda}{2\pi d} + 1$

A. Sample calculation of ν_{eff} for the high pressure region.

The experimental system used has the following values for parameters in the equations of interest.

$f = 12.00 \times 10^9 \pm .005 \times 10^9$ cps

$d = 13.65 \pm .13$ cm

It is convenient to present the data in terms of a standard neutral density. For this purpose, we define standard values of neutral temperature and pressure as follows

$T_{n_o} = 273° K$

$P_o = 1$ mm Hg

Then the effective collision frequency is

$\nu_{eff}(T_n P_o T_e) = \dfrac{K'(db)}{2.22 \times 10^{-21}\bar{n}_e} \quad (\dfrac{1}{sec})$

$\nu'_{eff}(T_{n_o} P_o T_e) = \dfrac{T_n}{T_{n_o}} \dfrac{P_o}{P} \nu_{eff}(T_n P T_e) = - \dfrac{K'(db)(T_n/p)}{60.6 \times 10^{-20}\bar{n}_e}$

$\nu''_{eff}(T_{n_o} P_o T_{e_o}) = \dfrac{T_n}{T_{n_o}} \dfrac{P_o}{P} \sqrt{\dfrac{T_{e_o}}{T_e}} \dfrac{\sigma_{sc}(T_{e_o})}{\sigma_{sc}(T_e)} \nu_{eff}(T_n P T_e) =$

$- \sqrt{\dfrac{T_{e_o}}{T_e}} \dfrac{K'(db)(T_n/p)}{60.6 \times 10^{-20}\bar{n}_e}$

where

K´ (db)   = transmission coefficient in decibels

T_n = observed neutral temperature in °K

p   = observed neutral pressure in mm Hg

$\bar{n}_e$ = average electron density

$\sigma_{sc}(T_e)$ = total electron-neutral scattering cross

            section for electrons with temperature T_e.

The average electron density for the system was cal-

culated with the formula

$$(1 - 5.59 \times 10^{12}\bar{n}_e)^{1/2} = -.000509\Delta\phi° + 1$$

as an example, the following data were taken

    p = 11.7 ± .04 mm Hg ± 5% uncertainty (see
        Chapter V)

    T_n = 346 ± 2 °K

    $\Delta\phi°$ = 13.5° ± .4° uncorrected

K´(db) = - .62 ± .03 db uncorrected

    $\Delta\phi°$ = 12.3° ± .4° corrected for phase of attenu-
                ation

    T(db) = - .62 ± .03 db corrected for attenuation
                of phase shifter.

The resulting values of $\bar{n}_e$ and ν_{eff} are

    $\bar{n}_e$ = 2.24 × 10^{10}/cc

    $\nu´_{eff}(T_{n_o}, P_o, T_e)$ = 1.36 × 10^9/sec   (T_e = 8.60 ev)

    $\nu´´_{eff}(T_{n_o}, P_o, T_{e_o})$ = 1.23 × 10^9/sec   (T_{e_o} = 7.00 ev)

The probable error in the results is as follows

$$\Delta \bar{n}_e = \sqrt{\left(\frac{\partial \bar{n}_e}{\partial(\Delta\phi)} \delta(\Delta\phi)\right)^2 + \left(\frac{\partial \bar{n}_e}{\partial d} \delta d\right)^2 + \left(\frac{\partial \bar{n}_e}{\partial w} \delta w\right)^2}$$

$$= .07 \times 10^{10}/cc$$

$$\frac{\Delta \bar{n}_e}{\bar{n}_e} \times 100 = 3.1\%$$

$$\Delta \nu_{eff}(T_{n_o}, P_o, T_e) = \sqrt{\left(\frac{\partial \nu_{eff}}{\partial K}\delta K\right)^2 + \left(\frac{\partial \nu_{eff}}{\partial n_e} \delta n_e\right)^2}$$
$$\overline{+ \left(\frac{\partial \nu_{eff}}{\partial T_n} \delta T_n\right)^2 + \left(\frac{\partial \nu_{eff}}{\partial P} \delta P\right)^2 + \left(\frac{\partial \nu_{eff}}{\partial \omega} \delta \omega\right)^2}$$
$$\overline{+ \left(\frac{\partial \nu_{eff}}{\partial d} \delta d\right)^2}$$

$$= .105 \times 10^{10}/sec$$

$$\frac{\Delta \nu_{eff}}{\nu_{eff}} \times 100 = 7.7\%$$

$$\Delta \nu_{eff}(T_{n_o}, P_o, T_{e_o}) = \sqrt{\left(\Delta \nu_{eff}(T_{n_o}, P_o, T_e)\right)^2 + \left(\frac{\partial \nu_{eff}}{\partial T_e} \delta T_e\right)^2}$$

$$= .106 \times 10^{10}/sec$$

$$\frac{\Delta \nu_{eff}}{\nu_{eff}} \times 100 = 7.8\%$$

b. Sample Calculation of ν_{eff} for the low pressure region. The phase data from the low pressure discharge was used to calculate $\bar{n}_e$ exactly as was done in the sample calculation previously given. These values

of $\bar{n}_e$ were then used to make the attenuation versus $\bar{n}_e$ plots shown in figures 20, 21, 22. A mean line was drawn through the oscillations, and the effective collision frequency was calculated with the following formula

$$\nu_{eff}''(T_{n_o}P_oT_{e_o}) = -(K_{mss}'-K_{md}'+K_{mo}') \sqrt{\frac{T_{e_o}}{T_e}} \quad \frac{\sigma_{sc}(T_{e_o})}{\sigma_{sc}(T_e)}$$

$$\frac{T_n/p}{60.6 \times 10^{-20}\bar{n}_e} \quad \frac{\omega^2}{ck\omega}$$

where $(\omega^2/ck\omega)$ is determined by equations 22 for the three absorption equations of interest and

K_{md}' = transmission coefficient from the mean curve for the decaying ionized gas of Figures 20, 21, 22.

K_{mss}' = transmission coefficient from the mean curve for the steady-state ionized gas of Figures 20, 21, 22.

K_{mo}' = transmission coefficient calculated in db by equations 19, 20, 21, 22 for electrons with temperature the same as the vacuum chamber temperature.

The neutral gas conditions for this ionized gas are

$$T_n = 310° \pm 2°K$$

$$P = .790 \pm .05 \text{ mm Hg}$$

For $\bar{n}_e = 70 \times 10^{10}$ elect/cm, Figure 20 gives

$$K'_{mss} = -6.11 \text{ db} \pm .15 \text{ db}$$

$$K'_{md} = -4.11 \text{ db} \pm .13 \text{ db}$$

The resulting values of ν_{eff} are as follows.

Classic absorption equation

$$\nu''_{eff}(T_{n_o}, P_o, T_{e_o}) = 1.60 \times 10^9/\text{sec}$$

KO absorption equation

$$\nu''_{eff}(T_{n_o}, P_o, T_{e_o}) = 1.86 \times 10^9/\text{sec}$$

Maxwell-Lorentz absorption equation

$$\nu''_{eff}(T_{n_o}, P_o, T_{e_o}) = 1.29 \times 10^9/\text{sec}$$

where $T_{e_o} = 1.30$ ev

$$T_{n_o} = 273° \text{ K}$$

$$P_o = 1 \text{ mm Hg}$$

Two probable errors are of interest for these data. First, a "relative error" is important in Figures 30, 31, 32 where the comparison of the different absorption equations is made. The relative error includes only errors in $\bar{n}_e$, K, and T_e, since these are the only quantities which vary.

Second, a "total error" is important in figures 28,

29 since the effective collision frequencies from

figures 28, 29 will be compared with other values

in the literature. The total error includes all

of the factors of the relative error plus the error

in d, T_n, P_n and ω. For the example calculated

above, the relative and absolute errors are as follows.

$$
\Delta\nu_{eff}(rel) = \sqrt{\left(\frac{\partial\nu_{eff}}{\partial K_{mss}}\,\delta K_{mss}\right)^2 + \left(\frac{\partial\nu_{eff}}{\partial K_{md}}\,\delta K_{md}\right)^2}
$$

$$
\overline{+ \left(\frac{\partial\nu_{eff}}{\partial\bar{n}_e}\,\delta\bar{n}_e\right)^2 + \left(\frac{\partial\nu_{eff}}{\partial T_e}\,\delta T_e\right)^2}
$$

$$
= .16 \times 10^9
$$

$$
\frac{\Delta\nu_{eff}(rel)}{\nu_{eff}} \times 100 = 10\%
$$

$$
\nu_{eff}(tot) = \sqrt{\left(\Delta\nu_{eff}\,(rel)\right)^2 + \left(\frac{\partial\nu_{eff}}{\partial T_n}\,\delta T_n\right)^2 + \left(\frac{\partial\nu_{eff}}{\partial p}\,\delta p\right)^2}
$$

$$
\overline{+\left(\frac{\partial\nu_{eff}}{\partial\omega}\,\delta\omega\right)^2 + \left(\frac{\partial\nu_{eff}}{\partial d}\,\delta d\right)^2}
$$

$$
= .20 \times 10^9
$$

$$
\frac{\Delta\nu_{eff}(tot)}{\nu_{eff}} \times 100 = 11\%
$$

The probable error is approximately the same for all

absorption equations.

BIBLIOGRAPHY

1. A. Olte and E.K. Miller, "A Study of Plasma Applications in Microwave Circuits," University of Michigan Radiation Lab Report No. 4915-1-F (1963).

2. M.B. Bachynski, C.G. Cloutier and K.A. Graf, "Microwave Measurements in a Finite Plasma," Defense Document AD 415324 Defense Documentation Center for Scientific and Technological Information. Cameron Station, Alexandria, Va.

3. J.M. Anderson and L. Goldstein, Phys. Rev. 100, 1037 (1955).

4. D.F. Golden and H.W. Bandel, Phys. Rev. 138, A-14 (5 April 1965).

5. A.V. Phelps, O.T. Fundingsland and S.C. Brown, Phys. Rev. 84, 559 (1951)

6. A.V. Phelps, J.L. Pack, and L.S. Frost, Phys. Rev. 117, 470 (1960).

7. J.C. Bowe, Phys. Rev. 117, 1411 and 1416 (1960).

8. E.K. Klevans, "A Theory of Photon Transport in Dispersive Media" The University of Michigan Radiation Lab. Report No. 2764-12-T. (1962).

9. Milne, Handbuch der Astrophysick Hälfte 1, Teil 3 pg. 72 ff.

10. Woolley, RvdR "The Solar Corona" Australian Journal of Science, Suppl. 10, No. 2, (1947).

11. Z. Akcasa and L. Wald, "Bremsstrahlung of Slow Electrons in Neutral Gasses and Free-Free Absorption of Microwaves" (to be published).

12. F.A. Albini and R.G. Jahn, J. Appl. Phys. 32, 75 (1961).

13. H.S.W. Massey and E.H.S. Burhop, Electronic and Ionic Impact Phenomena, Clarendon Press, Oxford (1952), pg. 92.

14. M.A. Heald and C.B. Wharton, Plasma Diagnostics With Microwaves, John Wifey and Sons, Inc., New York (1965) pg. 127 ff.

15. R.G. Jahn, "Interaction of Electromagnetic Waves With Slightly Ionized Gasses," I. Uniform Media. Technical Note No. 2. Daniel and Florence Guggenheim Jet Propulsion Center, California Institute of Technology, Pasadena, California (1960).

16. "Microwave Equipment Catalog, 1963/1964" The DeMornay-Bonardi Company, 780 S. Arroyo Parkway, Pasadena, Calif.

17. A.R. Von Hipple, Ed., Dielectric Materials and Applications; John Wiley and Sons, Inc., New York, N.Y. (1954).

18. E.O. Johnson and L. Malter, Phys. Rev. 80, 58 (1950).

19. J.H. Cahn, Phys. Rev. 75, 838 (1949).

20. L.B. Loeb, Basic Processes of Gaseous Electronics, Berkeley, University of California Press, (1955) Chapter VI.

21. R. Plonsey and R.F. Collin, Principles and Applications of Electromagnetic Fields, McGraw-Hill, Inc., New York (1961) pg. 317.

22. J.D. Cobine, Gaseous Conductors, Dover Publications, Inc., New York (1958).